Title

THERMODYNAMIC and KINETIC STUDIES OF SOME GROUP III and GROUP V ELEMENTS and ALLOYS BY SOLID STATE ELECTROCHEMICAL TECHNIQUES

Author

Anderson, Timothy J.

Publication Date

1975-10-01

LBL-4148

THERMODYNAMIC AND KINETIC STUDIES OF SOME GROUP III AND GROUP V ELEMENTS AND ALLOYS BY SOLID STATE ELECTROCHEMICAL TECHNIQUES

Timothy J. Anderson
(M. S. thesis)

October 1975

Prepared for the U. S. Energy Research and Development Administration under Contract W-7405-ENG-48

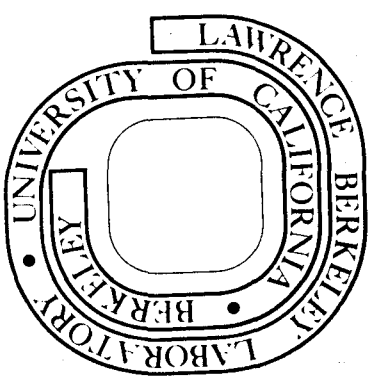

LBL-4148

DISCLAIMER

Contents

THERMODYNAMIC AND KINETIC STUDIES OF SOME GROUP III AND GROUP V ELEMENTS AND ALLOYS BY SOLID STATE ELECTROCHEMICAL TECHNIQUES

Timothy J. Anderson

Inorganic Materials Research Division, Lawrence Berkeley Laboratory and Department of Chemical Engineering; University of California Berkeley, California 94720

ABSTRACT

Solid state electrochemical methods are studied for measuring some thermodynamic and kinetic properties of Group III and V semiconducting materials. The Gibbs free energy of forming gallium sesquioxide and indium sesquioxide are measured using a CO_2-CO-O_2 gas reference electrode and calcia stabilized zirconia as the solid electrolyte. The free energies are given by

$$\Delta G_f^o(\beta\text{-}Ga_2O_3(c)) = -(265,309\pm152) + (82.47\pm0.16)(T/K)\ cal_{th}\,mol^{-1} \qquad (1)$$

and

$$\Delta G_f^o(In_2O_3(c)) = -(223,160\pm137) + (79.47\pm0.12)(T/K)\ cal_{th}\,mol^{-1}\ . \qquad (2)$$

The measured absolute free energies of formation of In_2O_3 and β-Ga_2O_3 are in excellent agreement with previous studies though discrepancies are found in the standard entropy and enthalpy changes. Comparison is made to available calorimetric results by a third law calculation with the data of this investigation proving to be the most consistent.

A solid state galvanic cell is employed to measure gallium activities in Ga-Sb liquid alloys. A survey of the available literature indicates gallium activities ranging from moderate positive to strong

negative deviations from Raoult's law. The results of this investigation show moderate negative deviations from ideality in the composition range $0.039 < x_{Ga} < 0.833$. From the temperature dependence of the measured activities, partial molar enthalpies and entropies are calculated; these are, within experimental error, in agreement with calorimetric data. The results of this work are combined with calorimetric data to calculate the liquidus temperatures of the Ga-Sb system; the results are found to be in excellent agreement with measured liquidus temperatures. The effect of short-range ordering is also investigated.

Coulometric titration techniques are used to investigate the solubility and diffusivity of oxygen in liquid indium. Dissolved atomic oxygen is found to follow Henry's law and a saturation solubility of $x_o^{sat} = 3.3 \times 10^{-3}$ is determined at 908°K. From a galvanostatic response of an indium electrode an oxygen diffusivity of 2.2×10^{-6} cm^2 sec^{-1} is found and is in good agreement with other available data.

The application of CaF_2 as a solid electrolyte for solid state electrochemical studies is investigated. A theoretical basis is given for the use of fluorine conducting CaF_2 with respect to Group III-V alloys. Experimental techniques are explored for the use of CaF_2 in an open cell arrangement. Experimental difficulties are found with several cell configurations though the emf response is in the correct direction and has the right order of magnitude.

I. GENERAL INTRODUCTION

Compounds and solid solutions formed from the Group IIIA elements gallium, indium and aluminum and the Group VA elements phosphorous, arsenic and antimony can be termed second generation semiconductor materials where the first generation materials were silicon and germanium. Today the binary Group IIIA-VA compounds are found in many solid state device applications. GaAs is used as a red light emitting diode[1] while GaP has received major interest in its use for red and green light emitting electroluminescent diodes.[2, 3] The luminescent properties of GaSb p-n junctions in the infrared region has been investigated[4,5] and InAs liquid phase epitaxial layers have been studied for the fabrication of laser diodes.[6] InP, AlAs, AlP and AlSb have also been investigated for their luminescent properties.[1] Solid solutions of the psuedobinary compound (AlGa)As have shown interesting possibilities for GaAs-base bipolar transitors[7] and high-voltage, high-temperature rectifiers.[8, 9] The ternaries In(AsP), (InGa)As, and Ga(AsSb) have received attention for fabrication of negative electron affinity devices,[10] while In(AsSb) is suitable for infrared emitting diodes and detectors.[11] The system $Ga_xIn_{1-x}Sb$ has shown the Gunn effect for the composition range $0.3 < x < 0.54$.[11]

Effective design of Group IIIA and VA materials processing equipment would be greatly aided by an accurate description of their thermodynamic properties. Though these semiconductor materials are of current practical interest, direct determinations of their

thermodynamic properties is lacking. Much of the available information is inferred from simple models using liquidus data. In this study, electrochemical techniques are investigated for determining some thermodynamic and kinetic properties. Specifically, solid state galvanic cells that employ solid electrolytes conductive to oxygen or fluorine ions are investigated with respect to their applications to Group III-V compounds.

It is well known that high temperature galvanic cells with solid electrolytes allow direct study of reaction free energies with high accuracy. The majority of electrochemical studies with solid electrolytes have utilized an oxygen conducting solid elecyrolyte (either calcia stabilized zirconia on yittria doped thoria). A fluorine conducting electrolyte, CaF_2, has received very little attention with respect to III-V semiconductor compounds, although potentially it has a larger range of applicability due to the inclusion of Al and also a lower working temperature. In this study both the common oxide electrolyte and the less investigated CaF_2 are used. Particular experimental and theoretical attention is given to CaF_2 in conjunction with Group III-V compounds, as the literature is somewhat limited.

In electrochemical cells involving coexistence electrodes such as $Ga(\ell) + Ga_2O_3(c)$, $In(\ell) + In_2O_3(c)$ or metal-metal fluoride, accurate free energies of formation of the oxides or fluorides are required. Thus accurate Gibbs free energy of formation for gallium and indium sesquioxides are needed. These compounds are also of interest for thick film resistor applications and can be

important in the processing of the elements. Galvanic cells measuring the formation free energy of the Group III metal fluorides are also reported.

Many solid compound semiconductors can be prepared by liquid phase epitaxy. Crystal growth of these compounds is facilitated by a knowledge of the liquid solution thermodynamics. In this study a detailed examination of the liquid Ga-Sb system is given with component activities directly measured. Also, a discussion of the applications of CaF_2 to study both the liquid and solid solution thermodynamics is presented.

Oxygen is important as an electrically active impurity in compound semiconductors. Consequently, one objective of this study is to develop methods to measure oxygen solubilities and diffusivities for oxygen in semiconductor materials.

REFERENCES

1. H. Kressel and H. Nelson, Physics of Thin Film, M. H. Francombe, ed., Academic Press, N. Y., 1973.

2. F. Williams, Phys. Stat. Solidi 25, 493 (1968).

3. R. N. Bhargava, C. Michel, W. L. Lupatkin, R. L. Bronnes and S. K. Kurtz, Appl. Phys. Letters 20, 227 (1972).

4. J. W. Burns, Trans. AIME 242, 432 (1968).

5. G. M. Blom, J. Appl. Phys. 42, 1057 (1971).

6. M. A. C. S. Brown and P. Porteous, Brit. J. Appl. Physics 18, 1527 (1967).

7. C. J. Nuese, J. J. Gannon, R. H. Dean, H. F. Gossenberger and R. E. Enstrom, Solid-State Electron. 15, 481 (1972).

8. Zh. I. Alferov, V. M. Andreev, V. I. Korolkov, D. N. Tretyakov and V. M. Tuchkevich, Sov. Phys. - Semicond. 1, 1313 (1968).

9. R. E.Enstrom, H. Kressel and L. Krassner in Semiconductors and Semimetals, Vol. 7, R. K. Willardson and A. C. Beer, Eds. (Adademic Press, Inc. N. Y., 1971).

10. L. W. James, G. A. Antypas, J. J. Uebbing, J. Edgecumbe and R. L. Bell 1970 Proc. 3rd. Int. Symp. on GaAs: Inst. Phys., Phys. Soc. Conf., Ser. No. 9.

11. J. C. McGroddy, Negative Differential Conductivity in Semiconductors in Proceedings of the Tenth International Conference in the Physics of Semiconductors, U. S. Atomic Energy Commission, 1970.

II. THEORY

A. Introduction

Thermodynamic equilibria and kinetic electrochemical studies can be carried out with Group III and V elements and compounds with the use of solid electrolytes. Two electrolytes are useful: fluorine conducting CaF_2 and oxygen conducting calcia stabilized zirconia (CSZ). Solid oxide electrolytes have received much attention in the measurement of free energies of formation[1-9] and of component activities in alloys.[1, 2, 10-15] Much less work has been done with CaF_2[16-24] which potentially exhibits a greater range of applicability to Group III-V compounds.

B. Thermochemical Measurements With Solid State Galvanic Cell

When the electrolyte conduction is exclusively ionic, a simple relation exists between the measured cell potential and chemical energy change,

$$\Delta G = -nFE \qquad (1)$$

where ΔG is the Gibbs free energy change for the overall cell reaction, n is the equivalents of charged passed, F is Faraday's constant and E is the reversible cell potential. Furthermore, by applying the Gibbs-Helmholtz relationships to the temperature dependence of the cell potential, ΔH and ΔS information can be extracted by

$$-nF \frac{dE}{dT} = -\Delta S = \frac{-nEF - \Delta H}{T} \tag{2}$$

If accurate E vs. temperature data are available, the constant pressure heat capacity change of the overall reaction can be determined from

$$\Delta C_p = nFT \left(\frac{\partial^2 E}{\partial T^2}\right)_p . \tag{3}$$

Finally, the chemical potential of the reaction constituents can be measured. The theoretical analysis was carried out by Wagner[1] for conduction in a crystalline binary compound $M_{Z_x} X_{Z_m}$ and the following relationship was derived

$$E = -\frac{1}{F} \int_{\mu_x''}^{\mu_x'} t_{ion} \frac{du_x}{|Z_x|} = -\frac{1}{F} \int_{\mu_m'}^{\mu_m''} t_{ion} \frac{du_m}{Z_m} \tag{4}$$

where t_{ion} is the ionic transference number, μ_x and μ_m are the chemical potentials of the nonmetal and metal, respectively, Z_x and Z_m are the cation and anion valences, and the superscripts differentiate the chemical potential at either reversible electrode. In this equation the functional dependence of t_{ion} on the chemical potential must be known. This is easiest if t_{ion} is independent of the chemical potential and equal to unity. In kinetic studies, a nonreversible electrode is intentionally polarized in a controlled manner so that the cell voltage and current used to polarize can be related to reactions or transport phenomenon in or at the electrode.

Equation 4 is usually coupled with Faraday's Law

$$j_i = I/Z_iF \qquad (5)$$

where j_i is the rate (moles/sec) at which ionic species, i, is transported through the electrolyte to the external circuit. The practical use of equations (1 - 5) requires that the galvanic cell be operated in a region where the transference number of the reacting ion in unity.

C. Solid Electrolytes

1. CaF_2

Solid compounds exhibiting exclusive ionic conduction are at present few. Past investigations have shown anionic conduction in halides and oxides and cationic conduction in various compounds of Ag^+, Cu^+, Mg^{++}, Al^{+++} and Na^+. Solid CaF_2 has been explored in this study as the electrolyte to be used in the study of III-V compound semiconductors. In 1957, Ure[25] showed that the predominant defect in CaF_2 crystals were of the anti-Frenkel type (equal concentrations of anion vacancies and anion interstitials). He found the mobility of F^- in the range of 690 to 920°C to be given by.

$$\mu = (1.34 \times 10^7)T^{-1} \exp [(-(19 \pm 4)\times 10^3/T] \text{ cm}^2\text{sec}^{-1}\text{volt}^{-1} . \qquad (6)$$

Also the defect density, n_o, was determined as a function of temperature in the same range:

$$n_o = 2.96 \times 10^{25} \exp\left[-(16.3 \times 10^3)/T\right] cm^{-3}. \quad (7)$$

Furthermore, it was demonstrated that the cation contribution to the total ionic conduction is negligble ($t_{cation} = 3 \times 10^{-8}$ at 850°C[2], 8×10^{-7} at 1000°C and 1×10^{-6} at 1100°C[26]). As a result, CaF_2 ionic conduction can be considered to be entirely due to F^- transport. As pointed out earlier, any feasible use of CaF_2 as a solid electrolyte requires operation in a region where $t_{F^-} > .99$. For anti-Frenkel defects, the following equilibrium equation can be written:

$$0 \rightleftharpoons F_i^- + V_{F^-}^+ \qquad K_F = \left[V_{F^-}^+\right][F_i^-] \quad (8)$$

where 0 represents the perfect lattice, F_i^- is an interstitial fluorine anion, and V_{F^-} is a fluorine anion vacancy. When CaF_2 solid is brought into equilibrium with its surroundings ionic defects and compensating electronic defects are introduced. If the surroundings are at high (relative to the stoichiometry of CaF_2) activities the equilibrium equation is given by

$$\frac{1}{2} F_2(v) \rightleftharpoons F_i^- + h^+ \qquad K_{HIGH} = [F_i^-]p/P_{F_2}^{1/2} \quad (9)$$

where p is the hole concentration and P_{F_2} is the fluorine partial pressure. Similarly, if the atmosphere is of low fluorine activity,

$$0 \rightleftharpoons 1/2\ F_2 + V_F^{+-} + e^- \ , \ K_{LOW} = n\left[V_F^{+-}\right] P_{F_2}^{1/2} \qquad (10)$$

where n is the free electron concentration. To maintain electrical neutrality the following equation must be observed,

$$p + \left[V_F^{+-}\right] = n + [F_i^-] \quad . \qquad (11)$$

For significant ionic transference this equation must reduce to $[V_F^{+-}] = [F_i^-]$ in a P_{F_2} range which includes the composition of exact stoichiometry. In the ionic conductivity range it can be shown that $n \alpha P_{F_2}^{-1/2}$ and $p \alpha P_F^{1/2}$, and the ionic defect concentrations are independent of P_{F_2} under the above conditions. Since conductivity is directly porportional to the V_F^{+-} concentration this leads to the useful conclusion that σ_{ion} (ionic conductivity) is P_{F_2} independent, and σ_θ (excess electron conductivity) is proportional to $P_{F_2}^{-1/2}$, and $\sigma_\oplus$ (hole conductivity) is proportional to $P_{F_2}^{1/2}$, all at constant temperature. On the other hand, at constant P_{F_2}, all conductivities exhibit an Arrhenius-type temperature dependence. Following Patterson,[27] we can write Arrhenius-type equations describing each mode of conductivity,

$$\sigma_{ion} = \sigma_{ion}^o \exp\left[-\frac{Q_{ion}}{RT}\right]$$

$$\sigma_\oplus = \sigma_\oplus^o \exp\left[-\frac{Q_\oplus}{RT}\right]$$

$$\sigma_\ominus = \sigma_\ominus^o \exp\left[-\frac{Q_\ominus}{RT}\right]$$

$$\sigma_T = \sigma_{ion} + \sigma_{\oplus} + \sigma_{\ominus} \tag{12}$$

where σ^o's are proportionality constants and Q's are activation energies, all of which are independent of temperature and P_{F_2}. To arrive at the condition of $t_{ion} > .99$ we equate σ_{ion} to $100\sigma_{\oplus}$ and $100\sigma_{\ominus}$. Upon doing so the following equations now define the ionic conduction domain limits

$$\log P_{F_2} = -2 \frac{Q_{ion} + Q_{\oplus}}{2.3R} \frac{1}{T} + 2 \log \frac{\sigma^o_{ion}}{100\sigma^o_{\oplus}}$$

$$\log P_{F_2} = +2 \frac{Q_{ion} - Q_{\ominus}}{2.3R} \frac{1}{T} - 2 \log \frac{\sigma^o_{ion}}{100\sigma^o_{\ominus}}. \tag{13}$$

It is now apparent that a plot of $\log P_{F_2}$ vs. 1/T should provide linear ionic conduction domain boundaries. Recent studies by Egan have shown that $t_{ion} \simeq 0.991$ at 1000°C.[20] A thermodynamic treatment due to Wagner has established a portion of the lower P_{F_2} boundary line.[28] An excess of Ca is dissolved in CaF_2 due to the following mechanism,

$$Ca(v) + 2F^x \rightleftharpoons CaF_2 + 2e'_F \tag{14}$$

where F^x is a fluoride ion on a regular ion site and e'_F is an electron substituted for a fluoride ion. By applying the law of mass action, the number of e'_F is proportional to the square root of the activity of Ca. In addition, excess electrons can be formed by the following reaction,

$$e_F^x \rightleftharpoons V_{F^-}^+ + e^- . \qquad (15)$$

The mobility of e_F^x is related to the mobility of the excess electrons by,

$$({}^n e_F)({}^\mu e_F) = n\mu_n . \qquad (16)$$

Using the definition of conductivity and equation (14) to (16) one can calculate the transference number of electrons, $t_\ominus$, from

$$t_\ominus = \sigma_\ominus/(\sigma_{ion} + \sigma_\ominus + \sigma_\oplus) \cong \sigma_\ominus/\sigma_{ion} = \frac{({}^n e_F)({}^\mu e_F)}{\sigma_{ion}} a_{Ca}^{1/2} \qquad (17)$$

if $\sigma_\ominus + \sigma_\oplus << \sigma_{ion}$. Utilizing equation (17) with concentration and mobility data of Ure[25], Wagner determined that $t_\ominus < 0.01$ when the activity of Ca $< 1\times10^{-5}$ at 600°C and $a_{Ca} < 6\times10^{-6}$ at 840°C. Using ΔG_F data for CaF_2 it can be shown the lower ionic conduction domain boundary corresponds to $P_{F_2} = 10^{-58.6}$ atm at 600°C and $P_{F_2} = 10^{-43}$ atm at 840°C. Shown in Fig. 1 are estimates of the Gibbs free energies of forming the various fluorides of interest to this study.[29-31] The lower boundary conservatively estimated by Wagner would be near the MgF_2 trajectory. But recent studies by Patterson and Skelton[24] have produced stable and accurate (as compared to calorimetric data) emf's for the Ca-CaF_2 electrode which indicates that the lower domain boundary lies below this line. Patterson[27] postulates that the upper boundary can be located far above 1 atm fluorine pressure as a result of the electronegativity difference

between Ca^{2+} and F^- ions and also the extreme forbidden gap for CaF_2. In view of the above discussion it is evident that CaF_2 provides a larger ionic conduction domain than the other common solid electrolytes. The major drawback of using CaF_2 appears to be its reactivity. Ure[25] showed CaF_2 conductivity changed when annealed in a oxygen atmosphere. Also, several investigators reported electrolyte-electrode reactions.

2. CSZ

Calcia stabilized zirconia is of the defect fluorite structure and conducts doubly charged oxygen ions via a vacancy mechanism. This oxygen vacancy defect density occuring in zironia has been found to increase greatly if divalent Ca is added in solid solution with tetravalent zirconia, up to a dopant level of 15 mole% Ca. As a result of this defect predominance the ionic conductivity and working P_{O_2} range ($t_{ion} > 0.99$) is enhanced. In-depth presentations of the theory of conduction of solid oxide electrolytes can be found in the literature.[32-36]

Shown in Fig. 2 are conservative and liberal lower oxygen partial pressure limits to the ionic conduction domain of CSZ as derived from the data of Schmalzreid[37] and Patterson[38, 39] and Tretyakov.[40] The conservative limit[37] places the Ga_2O_3-Ga-O_2 equilibrium outside the electrolytic domain. The more recent and liberal limit[38-40] places the most stable equilibrium of interest well within the limits of operation. The fact that the CSZ is a workable electrolyte with Ga + Ga_2O_3 electrodes can be verified by a determination of the Gibbs free energy of forming

Ga_2O_3 and a comparison of the results with data obtained using yittria doped thoria (having a lower electrolytic domain boundary). The use of CSZ over YDT was prescribed by ease of use (thermal stressing, radioactivity, etc.).

Also plotted in Fig. 2 are the Gibbs free energies of forming the various oxides of the materials investigated in these studies.[2,3,15,41] It can be concluded by inspection of Fig. 2 that Ga_2O_3 is the most stable oxide in the temperature range studied. Therefore, coexistence electrodes must contain Ga_2O_3 and a metal alloy if gallium is a component of the alloy.

REFERENCES

1. K. Kiukkola and C. Wagner, J. Electrochem. Soc. 104, 379 (1957).
2. K. A. Klinedinst and D. A. Stevenson, J. Chem. Thermo. 4, 565 (1972).
3. K. A. Klinedinst and D. A. Stevenson, J. Chem. Thermo. 5, 21 (1973).
4. R. W. Headrick, Design Criteria for Solid Electrolyte Electrochemical Cells (M.S. thesis), LBL-839, July 1972.
5. W. G. Budgen and J. N. Pratt, Trans. AIME 79, 221 (1970).
6. G. G. Charette and S. N. Flengas, J. Electrochem. Soc. 115, 796 (1968).
7. F. E. Rizzo, L. R. Bidwell and D. F. Frank, Trans. AIME 239, 593 (1967).
8. L. R. Bidwell, J. Electrochem. Soc. 114, 30 (1967).
9. R. A. Rapp, Trans. AIME 227, 371 (1963).
10. P. Chatterji and J. V. Smith, J. Electrochem. Soc. 120, 770 (1973).
11. K. A. Klinedinst, M. A. Rao and D. A. Stevenson, J. Electrochem. Soc. 119, 126 (1972).
12. W. G. Budgen and J. N. Pratt, J. Chem. Thermo., 1, 353 (1969).
13. A. Kubik and C. B. Alcock, Metal Sci. Journal 1, 19 (1967).
14. L. R. Bidwell and R. Speiser, Acta Met. 13, 61 (1965),
15. A. U. Seybolt, J. Electrochem. Soc., 111, 697 (1964).
16. N. L. Lofgren and E. J. McIver, U. K. A.E.A., A.E.R.E.R 5169, (1966).
17. J. J. Egan and R. J. Heus, Z. Phys. Chem. 49, 38 (1966).

of a few keV is $f_s = 0.9$ for clean titanium surfaces.

To sustain the plasma, dN/dt must be zero.

We will illustrate the effect of the thermal component, I_o, by means of a numerical example. For 10 keV deuterium $v = 10^8$ cm/sec. Assuming $n = 2 \times 10^{13}$ cm^{-3}, $R_p = 20$ cm, $G = 1$, $f_s = 0.9$ and taking $\langle \sigma v \rangle_{ie} = 3.6 \times 10^{-8}$, $\langle \sigma v \rangle_{ii} = 2 \times 10^{-8}$, and $\langle \sigma v \rangle_{cx} = 14 \times 10^{-8}$ for both the energetic neutral beam and thermal neutrals (i.e., average σv values for thermal neutrals are determined by the velocity distribution of the contained plasma), we find

$$\frac{nV}{\tau} \sim \frac{I}{q}\, 0.33 - \frac{I_o}{q}\, 0.71 - \frac{1}{4}\, n_o v_o A_p f_x.$$

Neglecting charge exchange with the background gas

$$\frac{nV}{\tau} = \frac{I}{q}\, 0.33 \left(1 - \frac{I_o}{I}\, \frac{0.71}{0.33}\right).$$

Obviously it is necessary that

$$\frac{I_o}{I} < \frac{0.33}{0.71} = 0.46.$$

If I^* is the current required to sustain the plasma when $I_o = 0$, then the required values of I for cases where $I_o/I = 0.1$, 0.2, and 0.3 are $I = 1.27\, I^*$, $1.75\, I^*$ and $2.8\, I^*$ respectively. The rapid escalation of the required neutral beam current with I_o/I emphasizes the importance of suppressing the thermal component.

The consequence of alterations of the angular distribution in the contained plasma by charge exchange with the beam needs further evaluation as the amplification factor in the B-C scaling law could be adversely affected.

(3.110) **2XIIB Major Project**

The scientific objectives, uncertainty, and scope of the 2XIIB Major Project were discussed in the preceding section. This physics discussion covers the entire 2XII Program Plan, providing a broader view of 2XII than is needed to describe the 2XIIB Major Project, which is defined as the new Magnet and Vacuum System. Future major project proposals may or may not contain this level of physics detail.

(3.120) ENGINEERING ASPECTS OF 2XIIB MAJOR PROJECT

Engineering Description of 2XIIB

The 2XIIB modification is fundamentally the installation of a new pulsed magnet system into the existing 2XII system (which is described in Appendix G). There are two subsystems in the 2XIIB proposal. The first is the magnet subsystem, and the second is the vacuum chamber subsystem.

The magnet subsystem which will convert 2XII into 2XIIB is composed of four parts. They will be described in the time sequence of operation during the experiment.

First are the dc magnets, which are turned on and stabilized very early in the experimental sequence. Their function is to provide the magnetic field to guide the injected plasma into the compression chamber. Two new dc magnets will be needed due to dimensional changes in the pulsed magnet that were made to accommodate intense neutral injection.

The pulsed magnet as shown in Fig. 3 comprises the other three parts of the magnet subsystem. The second magnet to operate is the barrier (or slow gate) magnet. It reflects a fraction of the injected plasma. After the barrier magnet is energized a quantity of plasma is injected into the compression chamber. The next magnet in the sequence, the fast gate magnet, is energized at the proper time to trap in the compression chamber part of the plasma reflected by the barrier magnet. The compression magnet then compresses the trapped plasma. At the time of maximum current, the compression magnet is short circuited so that the field decays with the characteristic L/R decay time of the magnet. As the L/R time is presently much greater than the characteristic plasma lifetime, the magnetic field duration is sufficient for the investigation of the relevant plasma phenomena. As plasma containment is improved, it will be necessary to extend the duration of the magnetic field. The compression magnet alone is shown in Fig. 2.

The vacuum subsystem as shown in Fig. 3 is a pyroceram chamber which is inside of the magnet subsystem. Its function is to provide a clean vacuum environment for the plasma by isolating the plasma from the magnet and surrounding structures.

18. R. J. Bones, T. L. Markin and V. J. Wheller, Proc. Br. Cer. Soc. 8, 51 (1967).

19. S. Aronson, Compounds of Interest in Nuclear Reactor Technology, Boulder, Colo.: A.I.M.E. 10, 247 (1964).

20. J. J. Egan, J. Phys. Chem. 68, 978 (1964).

21. W. K. Behl and J. J. Egan, J. Electrochem. Soc. 113, 376 (1966).

22. S. Aronson and A. Auskern, In Thermodynamics (Vienna, I.A.E.A) Vol. 1, 165 (1965).

23. S. Aronson and K. A. Gingerich, Paper 6-RS-66, presented at 68th Meeting of American Ceramic Soc., 1966.

24. W. H. Skelton and J. W. Patterson, J. Less-Common Metals 31, 47 (1973).

25. R. W. Ure, J. Chem. Phys., 26, 1363 (1957).

26. H. Matzke and R. Lindner, Z. Naturf., 19a, 1178 (1964).

27. J. W. Patterson, J. Electrochem. Soc., 118, 1033 (1971).

28. C. Wagner, J. Electrochem. Soc., 115, 933 (1968).

29. W. J. Hammer, M. S. Malmberg and B. Rubin, J. Electorchem. Soc. 112, 750 (1965).

30. E. Steinmetz and H. Roth, J. Less-Common Metals 16, 295 (1968).

31. L. Brewer, In The Chemistry and Metallurgy of Miscellaneous Materials, L. L. Quill ed., paper 7, McGraw Hill Book Co, Inc. (1950).

32. N. F. Mott, R. W. Garney, Electronic Processes in Ionic Crystals (Clarmden Press, Oxford, 1948), 2nd ed.

33. R. A. Rapp and D. A. Shores, Solid Electrolyte Galvanic Cells in Physiochemical Measurements in High Temperature Systems

(Interscience Publishers, New York, 1970), pt. 2.

34. C. B. Alcock, Transport of Ions and Electrons in Ceramic Oxides in Electromotive Force Measurements in High Temperature Systems (American Elsevier Publishing Company, Inc., 1968).

35. F. A. Kröger, The Chemistry of Imperfect Crystals (North-Holland Publ., Amsterdam, 1964).

36. Motaaki Sato, Electrochemical Measurements and Control of Oxygen Fugacity and Other Gaseous Fugacities with Solid Electrolyte Sensors in Research Techniques for High Pressure and High Temperature (Springer-Verlag, N. Y., 1971).

37. H. Schmalzreid, Z. Elektrochem., 66, 572 (1962).

38. J. W. Patterson, C. C. Bogden and R. A. Rapp, J. Electrochem. Soc. 114, 752 (1967).

39. J. W. Patterson, J. Electrochem. Soc. 118, 1033 (1971).

40. J. D. Tretyakov, Neorg. Materials (USSR) 2, 501 (1966).

41. J. P. Coughlin, Contributions to the Data in Theoretical Metallurgy, XII, Heats and Free Energies of Formation of Inorganic Oxides Bulletin 542, Bureau of Mines, U.S. Government Printing Office, Washington (1954).

LIST OF FIGURES

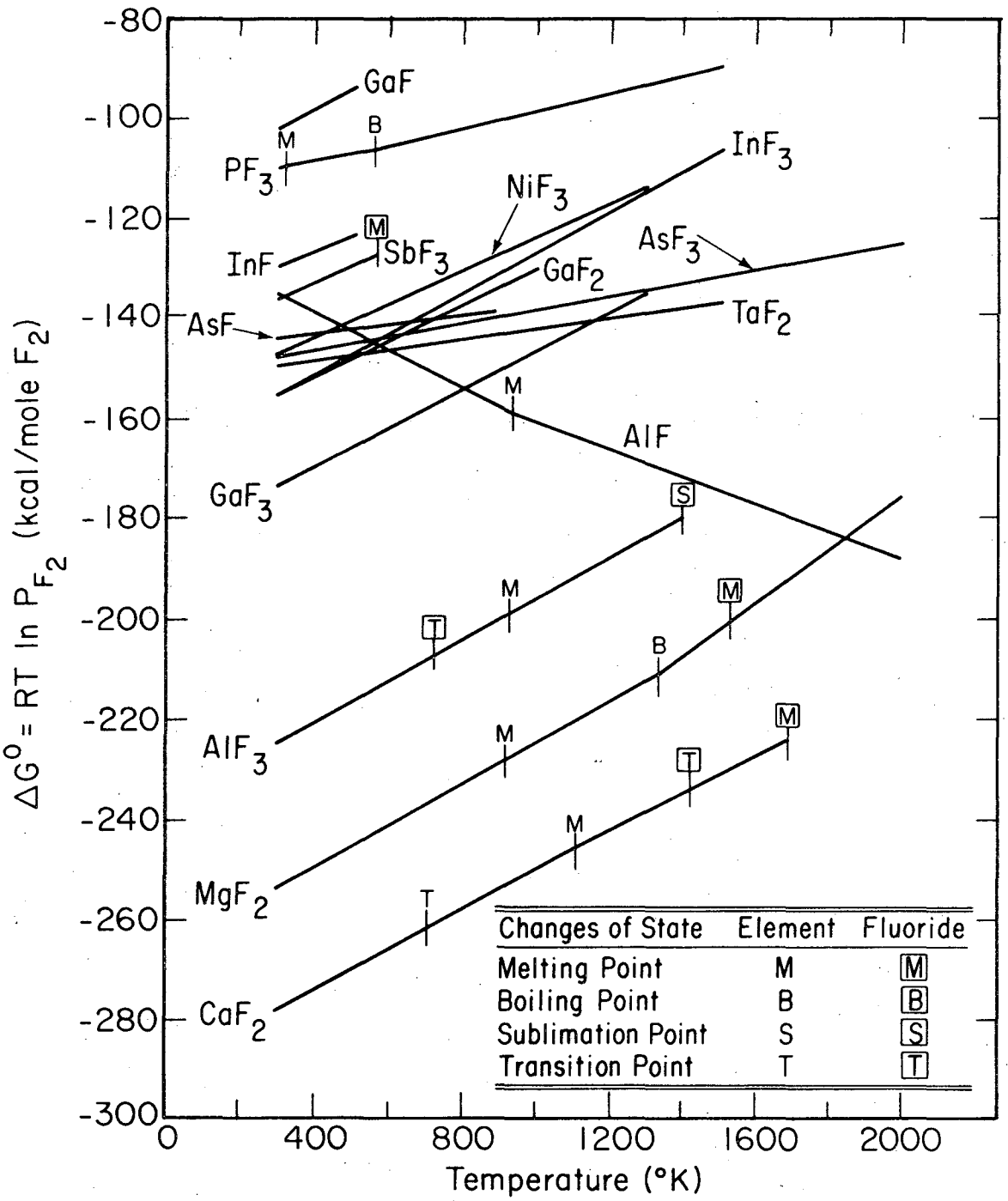
-80
-100
-120
-140
-160
-180
-200
-220
-240
-260
-280
-300
0
400
800
1200
1600
2000
Temperature (°K)
ΔG° = RT ln P_F2 (kcal/mole F2)
GaF
PF3
InF3
NiF3
InF
SbF3
AsF3
GaF2
AsF
TaF2
AlF
GaF3
AlF3
MgF2
CaF2
M
B
S
T
Changes of State
Element
Fluoride
Melting Point
Boiling Point
Sublimation Point
Transition Point
XBL 757-6776

Fig. 1.

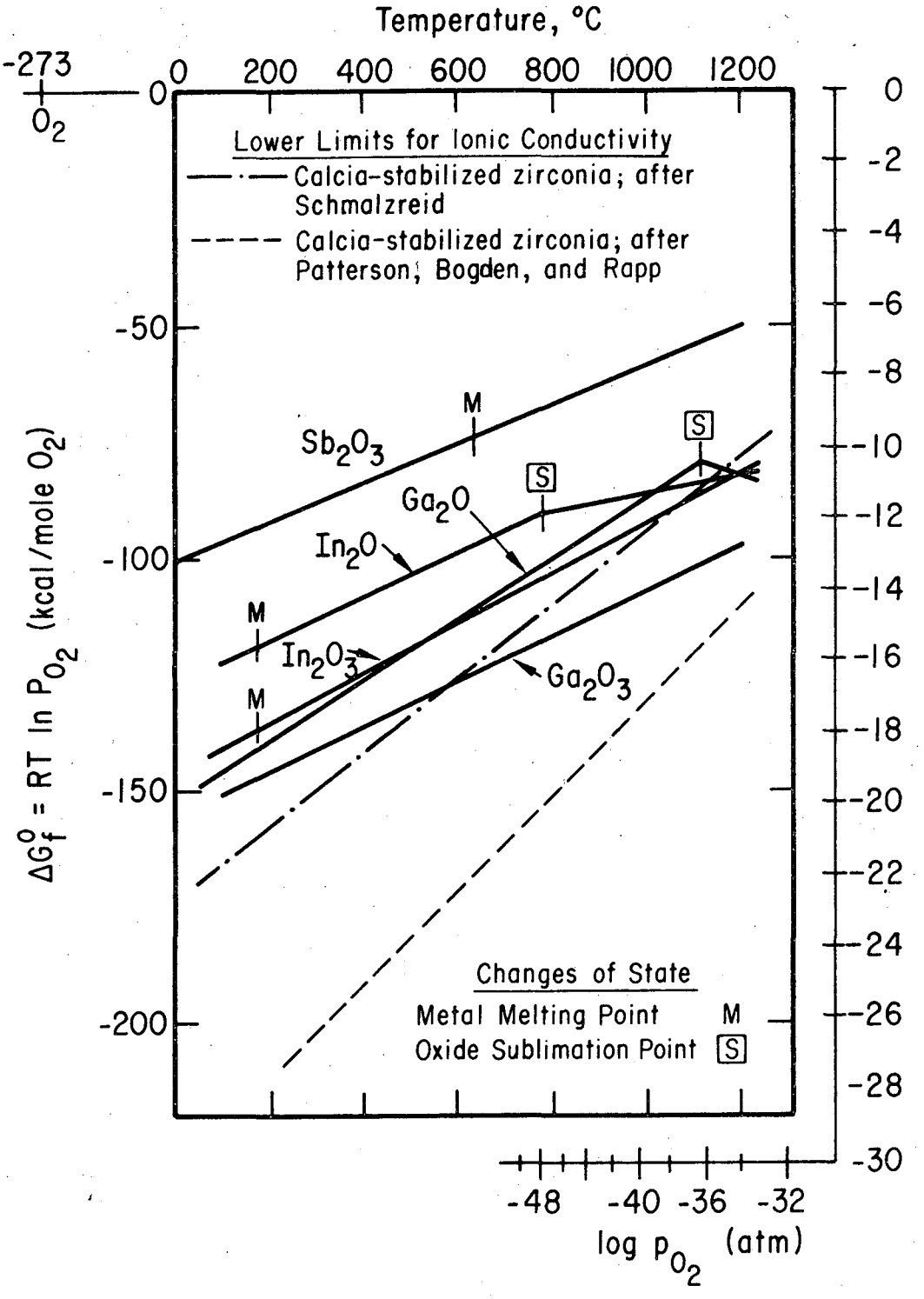

XBL 757-6780

Fig. 2.

III. SOLID-STATE ELECTROCHEMICAL STUDY OF THE FREE ENERGY OF FORMATION OF β-GALLIUM SESQUIOXIDE USING A CALCIA-STABILIZED ZIRCONIA ELECTROLYTE

A. Introduction

Gallium has become important in the semiconductor microelectronics industries as a component of compounds for electroluminescent and microwave devices. Gallium is also an important solvent for liquid-phase epitaxial crystal growth of compound semiconductors where oxygen is an electrically active impurity. Gallium sesquioxide added to Ga-GaP solutions has been used to achieve high electroluminescence efficiency in Zn-doped GaP light-emitting diodes.[1-4] Effective design of semiconductor device processes involving gallium should be aided by accurate thermodynamic data for gallium oxide.

The Gibbs free energy of formation of β-Ga_2O_3 by the reaction

$$2Ga(\ell) + \frac{3}{2} O_2(g) = \beta\text{-}Ga_2O_3(c) \qquad (1)$$

has been estimated by Coughlin[5] and measured using solid-state electrochemical methods by Klinedinst and Stevenson[6] and Smith and Chatterji.[7] Pankratz and Kelley determined the high temperature heat content of β-Ga_2O_3 by calorimetric methods.[8] More recently Mills[9] measured the enthalpy of formation of β-Ga_2O_3 by drop calorimetry. Unfortunately, the Gibbs free energies of formation as determined in the above studies show marked discrepancies, especially in the temperature dependence, i.e., the standard entropy of formation. In this study the Gibbs free energy of formation of

β-Ga_2O_3 was measured in a high-temperature, solid-state electrochemical cell under microcomputer control.

B. Experimental

1. The Experimental Cell

The basic, solid-state galvanic cell design is depicted in Fig. 1. The cell consisted of a 2-inch diameter, closed-end alumina tube 18 inch in length secured by a Viton O-ring to a water-cooled, brass cell-head. Three 1/8-inch Cajon through-bore fittings were located on the cell head symetrically around a 1/4-inch Cajon through-bore fitting. The 1/8-inch thermocouples and lead wires in ceramic sheaths were passed through the 1/8-inch fittings. The larger, centered fitting was used to seal to a 1/4-inch calcia-stabilized zirconia (CSZ) electrolyte tube, closed at the bottom.

Included in the brass head were bores for gas entrance and exit. The exit placement was such that the gas had flow downward to the experimental cell, then through an alumina pushrod. Three spring-loaded tungsten wires provided support for a graphite chamber containing liquid gallium and β-Ga_2O_3 in contact with the CSZ tube.

The electrode materials were contained in a 2-inch diameter closed graphite crucible fitted with a screw cap containing a closely fitting hole through which the CSZ tube was inserted into the gallium electrode. Powdered graphite was added to seal the CSZ tube to the graphite lid. Details of electrode compartments are shown in Fig. 2.

The cell was heated with a Marshall resistance-heated furnace 20 inch in length with a 2 1/2 inch bore. Excellent temperature

control was furnished by an integrating, temperature-regulated, power supply designed and built at the Lawrence Berkeley Laboratory. Temperature uniformity and stability was held to with ±0.5°C in the vicinity of the electrodes. Stray cell voltages induced by the temperature regulation circuit were eliminated by a metal ground shield placed around the 2-inch alumina tube. Type-K thermocouples (0.020 inch Pt - Pt 10% Rh) were calibrated in the cell under vacuum against a thermocouple calibrated at the National Bureau of Standards. The calibration was performed with the standard thermocouple occupying the position normally that of the electrode, while the unknown thermocouple was placed in their normal operating positions. Thermocouple emf's were amplified using a x100 thermocouple amplifier calibrated with a Leeds and Northrup Type K-3 potentiometer facility.

Cell emf's were measured with a Keithley 640 electrometer. High-isolation triaxial cable used to connect the experimental cell to the input head of the electrometer. The inner conductor of the triaxial cable was connected to the positive lead wire of the cell. The outer conductor was driven by the unity-gain feedback from the electrometer, thus acting as a driven guard. Leakage sources at the input head were negligible since the cable was guarded up to the sapphire insulated electrometer contact.

2. Materials

Gallium metal used in the study was semiconductor grade, 99.9999% pure, obtained from Cominco American. Gallium oxide was obtained from Alfa Products, and had a purity of 99.99%. The oxide

was confirmed to be β-Ga_2O_3 and to show no detectable second phases by X-ray diffraction analysis.

The calcia-stabilized zirconia tubes containing 7.5 weight percent calcia were obtained from the Zirconia Corporation of America. The tubes were confirmed to be leak tight both before and after the experiments. Spectroscopic-grade graphite was employed in the electrode compartment containing the liquid metal and a small amount of the oxide. Platinum lead wires were attached to the graphite compartment and to a platinum electrode made from Englehard unfluxed platinum paste (No. 6926) inside the CSZ tube end.

The CO-CO_2 reference electrode gas mixture was obtained from Matheson Gas Products. Chemical analysis showed the mixture to contain (25.29 ± 0.02) percent CO_2 and (2.45 ± 0.02) percent CO in high-purity argon.

High-purity argon was prepared by passing it over Linde 4A molecular sieve at 195°K, then through a special, alumina-lined titanium sponge purifer heated to 800°C. This gas was used as an inert purge gas for the metal-oxide electrode compartment, with the purge flow rate adjusted to 10 cm^3/min.

Reagent dibutyl phthalate was used in gas exhaust traps to prevent back-diffusion of oxygen into the experimental cell.

3. Microcomputer Control System

Operation of the electrochemical experiments and data acquisition were automated with a microcomputer system based on an Intel 8008 microprocessor. The facility is schematically shown in Fig. 3. The system had the capability of setting the cell operation

temperature and monitoring cell emfs and thermocouple outputs on a predetermined time base until equilibrium had been established, thus allowing continuous cell operation without operator assistance. A 4 1/2 digit panel meter alternately displayed the cell voltage and temperature, while a permanent record was obtained on a teletype. The microcomputer was constructed from components stocked at the Lawrence Livermore Laboratory.

4. Procedure

In each of several experiments the cell compartments were leak-checked using a high vacuum system, then purged with high purity argon. The cell temperature was programmed to rise at 100°K/hour to the lowest measurement temperature, after which the reference gas flow was initiated. The cell temperature was then sequentially incremented and decremented throughout the experimental range, with the cell voltage measured and periodically recorded at each temperature until equilibrium was reached and confirmed. Reference gas and argon flow rates did not affect the cell voltage in the ranges selected. At the conclusion of each experiment the cell compartments were again checked for leaks and the metal electrode examined for evidence of oxidation. The electrode material was then analyzed by X-ray diffraction to confirm the absence of side-reaction products.

C. Results

The solid-electrolyte galvanic cell employed in measuring the free energy of formation of β-Ga_2O_3 can be represented schematically as

$$Pt|C|Ga(\ell),\ Ga_2O_3(c)||CSZ||CO,\ CO_2|Pt. \qquad (2)$$

The equilibrium partial pressures of oxygen in the two electrodes are related to the cell potential, E, by the Nernst equation:

$$E = (RT/4F)\ \ell n\ \{P(O_2, CO + CO_2)/P(O_2, Ga(\ell)+\beta\text{-}Ga_2O_3)\} \qquad (3)$$

In this equation, $P(O_2,\ CO + CO_2)$ indicates the oxygen fugacity of the $CO + CO_2$ gas mixture, $P(O_2,\ Ga(\ell) + \beta\text{-}\ Ga_2O_3(c))$ represents the $Ga + Ga_2O_3$ mixture, R is the gas constant, T is the thermodynamic temperature and F is the Faraday constant.

The measured cell emf differs from the equilibrium cell potential by the thermal emf generated by the Pt - C couple. This thermal emf was measured by Chatterji and Smith[10] and found to vary nearly linearly with temperature in the range investigated. The measured cell voltage $E_{(m)}$ was corrected by the following equation for the equilibrium cell voltage,

$$E = (E_{(m)}/mV) - 3.7 + .007(T/K)mV. \qquad (4)$$

The Gibbs free energy of formation of β-Ga_2O_3 is related to the oxygen partial pressure over the Ga + Ga_2O_3 mixture by the equilibrium constant for the formation reaction:

$$K_f(\beta\text{-}Ga_2O_3) = a(\beta\text{-}Ga_2O_3)/a(Ga)^2 P(O_2,\ \beta\text{-}Ga_2O_3 + Ga)^{3/2}$$

or

$$K_f(\ \ \text{-}Ga_2O_3) = \exp\ \{-\Delta G_f^o(\beta\text{-}Ga_2O_3)/RT \qquad (5)$$

Equations 3 and 5 allow one to calculate $\Delta G_f^o(\beta\text{-}Ga_2O_3)$ from the measured temperature and experimental cell voltage:

$$\Delta G_f^o(\beta\text{-}Ga_2O_3) = 1.5\ RT\ \ell n\ P(O_2, CO + CO_2) - 6FE. \qquad (6)$$

Here, unit activities for Ga(ℓ) and β-Ga_2O_3(c) in the mixture were assumed.

The reference oxygen partial pressure was established by the equilibrium reaction,

$$CO + \frac{1}{2}\ O_2 = CO_2 \qquad (7)$$

and is related to the Gibbs free energy change for this reaction, $\Delta G_{(7)}$, by:

$$P(O_2, CO + CO_2) = \left(\frac{P(CO_2)}{P(CO)}\right)^2 \exp\{2\Delta G^o_{(7)}/RT\} \qquad (8)$$

where $\Delta G^o_{(7)} = -68{,}270 - 0.18T \ln T - 0.34\ 10^{-3}T^2 + 0.87\ 10^5/T + 23.28T$, $cal_{th}\ mol^{-1}$ was taken from the equations given by Wicks and Block[11] for the free energies of formation of CO and CO_2. The ratio of the partial pressure of CO_2 to the partial pressure of CO in the primary standard gas was $10.322 \pm .092$.

Table 1 shows the measured open-cell potentials, partial pressures of oxygen in the reference gas mixture, the calculated equilibrium partial pressures of oxygen in the Ga, β-Ga_2O_3 mixture, and the calculated values of the Gibbs free energy of formation of β-Ga_2O_3(c) over the experimental temperature.

D. Discussion

The data obtained in this study were compared to the data reported from previous studies as shown in Fig. 4. This figure shows the experimental values of $\Delta G^o_f(\beta\text{-}Ga_2O_3)$ plotted against temperature, with the least-squares straight line drawn through the data points for each study. Also shown is the estimated Gibbs free energy of formation of Coughlin,[5] the calorimetric results of Pankratz and Kelley[8] and the emf measurements of Smith and Chatterji,[7] and of Klinedinst and Stevenson.[6]

A linear least-squares analysis of our data obtained in the present study resulted in the following expression for $\Delta G^o_f(\beta\text{-}Ga_2O_3)$:

$$\Delta G_f^o\ (\beta\text{-}Ga_2O_3(c)) = (-265,309\pm152) + (82.47\pm0.16)(T/K)cal_{th}mol^{-1}. \quad (9)$$

The uncertainties given in this expression are those computed from the standard deviations. The constant term appearing in Eq. (9) corresponds to the standard enthalpy change while the temperature coefficient represents the standard entropy change. Table 2 summarizes these values found in this study with comparisons to values obtained from previous studies.

The $\Delta G_f^o(\beta\text{-}Ga_2O_3)$ values calculated in the present study from the experimental data showed excellent internal consistency with a standard error at 1000°K of only ± .312 kcal/mole. On comparing the results with those obtained from other emf measurements, however, one finds an apparent discrepancy in both the standard enthalpy and entropy. In particular, the standard entropy found in this work was 17.5% above that of Klinedinst and Stevenson's result (see Table 2). One the other hand, the absolute values of $\Delta G_f^o(\beta\text{-}Ga_2O_3)$ show relatively good agreement but differ markedly in the temperature dependence as shown in Fig. 4.

Because of differences in the results of this study as compared to results of previous emf studies and also of the availability of good calorimetric data, a "third law" calculation was carried out. The results of this calculation are shown in Fig. 5. The values of $\Delta H_{f,298.15}^o$ for the $\beta\text{-}Ga_2O_3$ formation reaction was calculated from the following equation:

Table 2. Comparison of Reported Standard Enthalpy and Entropy of Formation of β-Ga_2O_3.

ΔH^o $\frac{kcal_{th}}{mol^{-1}}$	ΔS^o $\frac{kcal_{th}}{mol^{-1}K^{-1}}$
-252.4	.0702[a]
-252.5	.0711[b]
-259.34	.07811[c]
-265.31	.08247[d]

a. From Ref. 6, obtained by titration.

b. From Ref. 6, phase equilibrium.

c. From Ref. 7.

d. From this work.

$$\Delta H^{o}_{f,298.15} = \Delta G^{o}_{f,T} - \Delta(H^{o}_{T} - H^{o}_{298.15}) + T\left(\Delta S^{o}_{f,298.15} + \Delta(S^{o}_{T} - S^{o}_{298.15})\right) . \quad (10)$$

where $\Delta G^{o}_{f,T}$ is the experimental value of the Gibbs free energy of formation of β-Ga_2O_3. The values of $H^{o}_{T} - H^{o}_{298.15}$ and $S^{o}_{T} - S^{o}_{298.15}$ for O_2(g) were taken from Wicks and Block,[11] that for Ga(ℓ) from Hultgren,[12] and that for β-Ga_2O_3(c) from Mills.[9] A value for $\Delta S^{o}_{f,298.15}$ of -72.87 cal/mole°K was determined from the data on $S^{o}_{298.15}$ for O_2 taken from Kelley[13] and on Ga and β-Ga_2O_3 from Adams, Johnston and Kerr.[14] The calculated results for $\Delta H^{o}_{298.15}$ are compared to the data of Mah,[15] determined by direct combustion calorimetry, and to the value of Shchukarev, Semenov and Rat'kovskii[16] obtained by isothermal evaporation studies. The close agreement between the data derived from this study and the findings of the latter two different methods tend to support the experimental value for $\Delta H^{o}_{298.15}$ of -261.9 $kcal_{th}$ mol^{-1}.

Assuming all calorimetric data to be correct, the emf results would be expected to give calculated $\Delta H^{o}_{298.15}$ values which fall on a horizontal line in Fig. 5 at the value of the calorimetrically determined result. As seen in Fig. 4, the results of Klinedinst and Stevenson[6] exhibit a large temperature dependence, with the average lying somewhat above the calorimetrically determined value. In their reported results, no mention was made of correcting for the thermal emf developed by the W - Pt junction on the metal-metal

oxide electrode. Chatterji and Smith[10] measured this potential and found it sizeable (i.e., 15.6 mV at 1000°K). Adding these corrections to the data of Klinedinst and Stevenson would have the effect of flattening the calculated $\Delta H^{o}_{298.15}$ values but would also raise them (i.e., 1.515 kcal/mole at 873°K and 3.541 kcal/mole at 1273°K for the two-phase mixture).

Also shown in Fig. 4 are the emf results of Smith and Chatterji.[7] The actual data were not available for this calculation. Instead, the fitted linear equation was used. The use of this equation gave nearly temperature-independent results, but shifted to approximately 1.75 kcal above the experimental value. Smith and Chatterji reported an error range of 0.8 kcal/mole with no apparent temperature dependence from a similar third-law calculation on their data.

The calculated results of this investigation gave the value of $\Delta H^{o}_{298.15}$ reported to within the experimental error for all data points, but produced a small temperature dependence. This could be accounted for by a systematic error in our experimental data or by inaccurate specific heat data. The specific heat data for O_2 should be very accurate and the more recent calorimetric data of Mills[9] agreed to within 1% of that of Pankratz and Kelley.[8] The most likely source of error is in the specific heat of gallium, for which a constant heat capacity was assumed above 700°K.

A potential source of error in the present study was electronic conduction in the CSZ electrolyte. Shown in Fig. 2 are the conservative and liberal lower oxygen partial pressure limits to the electrolytic domain of CSZ as derived from the data of

Schmalzreid[17] and Patterson, Bogden and Rapp,[18] along with the free energies of formation of Ga_2O_3 and other oxides.[19] The conservative limit places the Ga_2O_3 - Ga - O_2 equilibrium outside the electrolytic domain. The more recent and liberal limit places the most stable equilibrium of interest well within the limits of operation. In this study the working temperature was maintained below 1100°K in order to prevent conditions allowing electronic conduction in the solid electrolyte. The fact that the emf data did not show a change in the temperature dependence at high temperatures is evidence that the electrolyte was maintained in the ionic conduction domain. The high ionic conductivity of CSZ as the solid electrolyte aids in preventing electrode-polarization errors which could more easily occur with YDT, used in the study by Klinedinst and Stevenson.[16]

Regardless of the error source, the direct measurement of $\Delta G_f^o(\beta\text{-}Ga_2O_3)$ performed in this study showed much better consistency with the calorimetric data than did the data from earlier emf studies, when compared with "third law" calculations.

REFERENCES

1. H. G. Grimmeiss and H. Scholz, Phys. Letters, 8, 233 (1964).

2. M. R. Lorenz and M. Pilkuhn, J. Appl. Phys., 37, 4094 (1966).

3. R. A. Logan, H. G. White and F. A. Trumbore, Appl. Phys. Letters, 10, 206 (1967).

4. L. M. Foster and J. Scardefield, J. Electorchem. Soc., 116, 494 (1969).

5. J. P. Coughlin, U. S. Bur. Mines Bull. 542 (1954).

6. K. A. Klinedinst and D. A. Stevenson, J. Chem. Thermodynamics, 4, 565 (1972).

7. J. V. Smith and D. Chatterji, J. Am. Cer. Soc., 56, 288 (1973).

8. L. B. Pankratz and K. K. Kelley, U. S. Bur. Mines Rep. Invest. 6198 (1963).

9. K. C. Mills, High Temp.-High Press., 4, 371 (1972).

10. D. Chatterji and D. V. Smith, J. Electrochem. Soc., 120, 889 (1973).

11. C. E. Wicks and F. E. Block, U. S. Bur. Mines Bull. 605 (1963).

12. R. Hultgren, P. D. Desai, D. T. Hawkins, M. Gleiser, K. K. Kelley and D. D. Wagman, Selected Values of the Thermodynamic Properties of the Elements, American Soc. for Metals, 1973.

13. K. K. Kelley, U. S. Bur. Mines, Bull. 477 (1950).

14. G. B. Adams, H. L. Johnston and E. C. Kerr, J. Am. Chem. Soc., 74, 4784 (1952).

15. A. D. Mah, U. S. Bur. Mines Rep. Invest. 5965, (1962).

16. S. A. Shchukarev, G. A. Semenov and I. A. Rat'kovskii, Russ. J. Inorg. Chem., 14, 1 (1969).

17. H. Schmalzreid, Z. Electrochem., 66, 572 (1962).

18. J. W. Patterson, C. C. Bogden and R. A. Rapp, J. Electrochem. Soc., 114, 752 (1967).

19. J. P. Coughlin, Contributions to the Data in Theoretical Metallurgy, XII Heats and Free Energies of Formation of Inorganic Oxides Bulletin 542, Bureau of Mines, U. S. Government Printing Office, Washington (1954).

LIST OF FIGURES

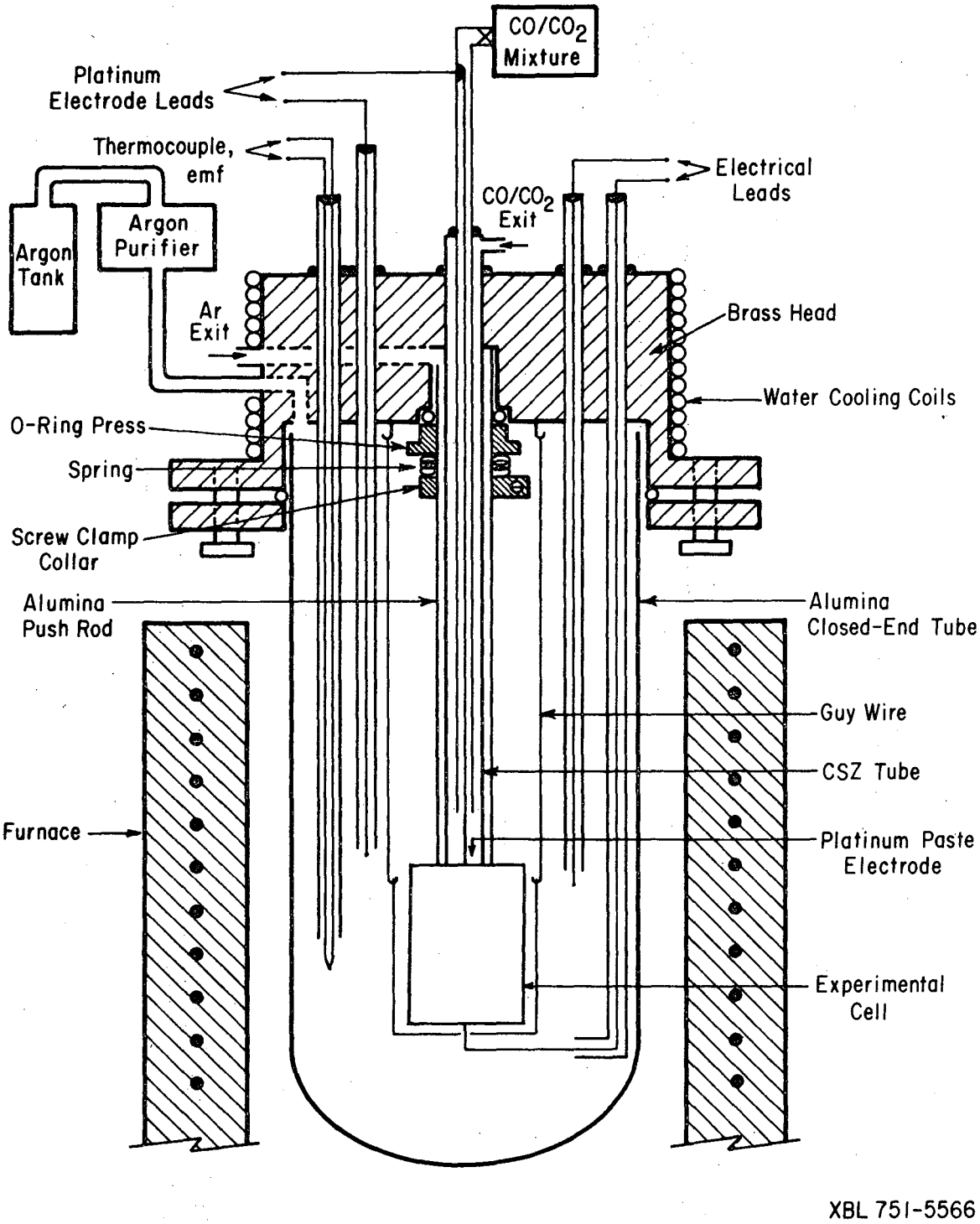
CO/CO_2 Mixture
Platinum Electrode Leads
Thermocouple, emf
Argon Tank
Argon Purifier
Ar Exit
CO/CO_2 Exit
Electrical Leads
Brass Head
Water Cooling Coils
O-Ring Press
Spring
Screw Clamp Collar
Alumina Push Rod
Alumina Closed-End Tube
Guy Wire
CSZ Tube
Furnace
Platinum Paste Electrode
Experimental Cell
XBL 751-5566

Fig. 1.

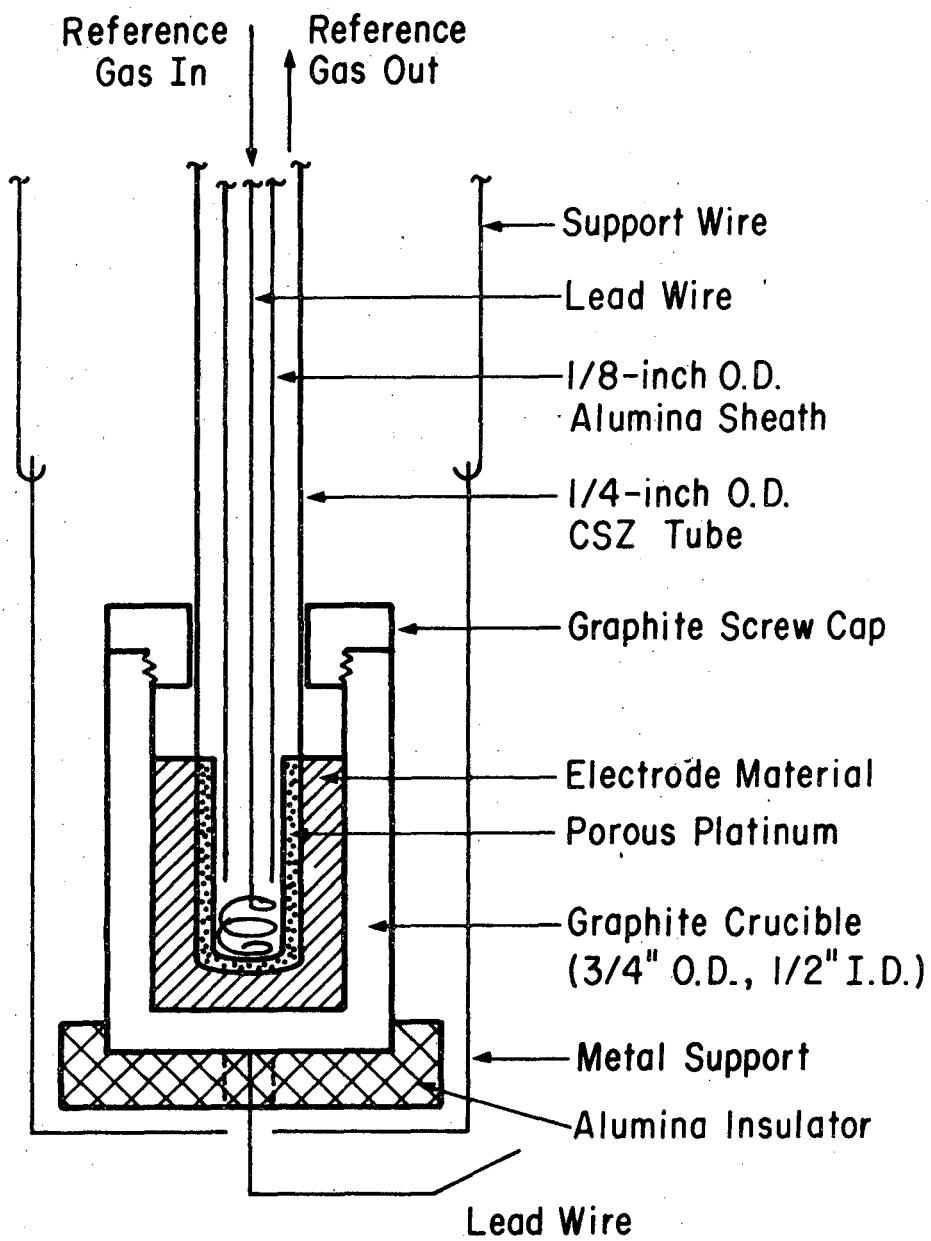

Fig. 2.

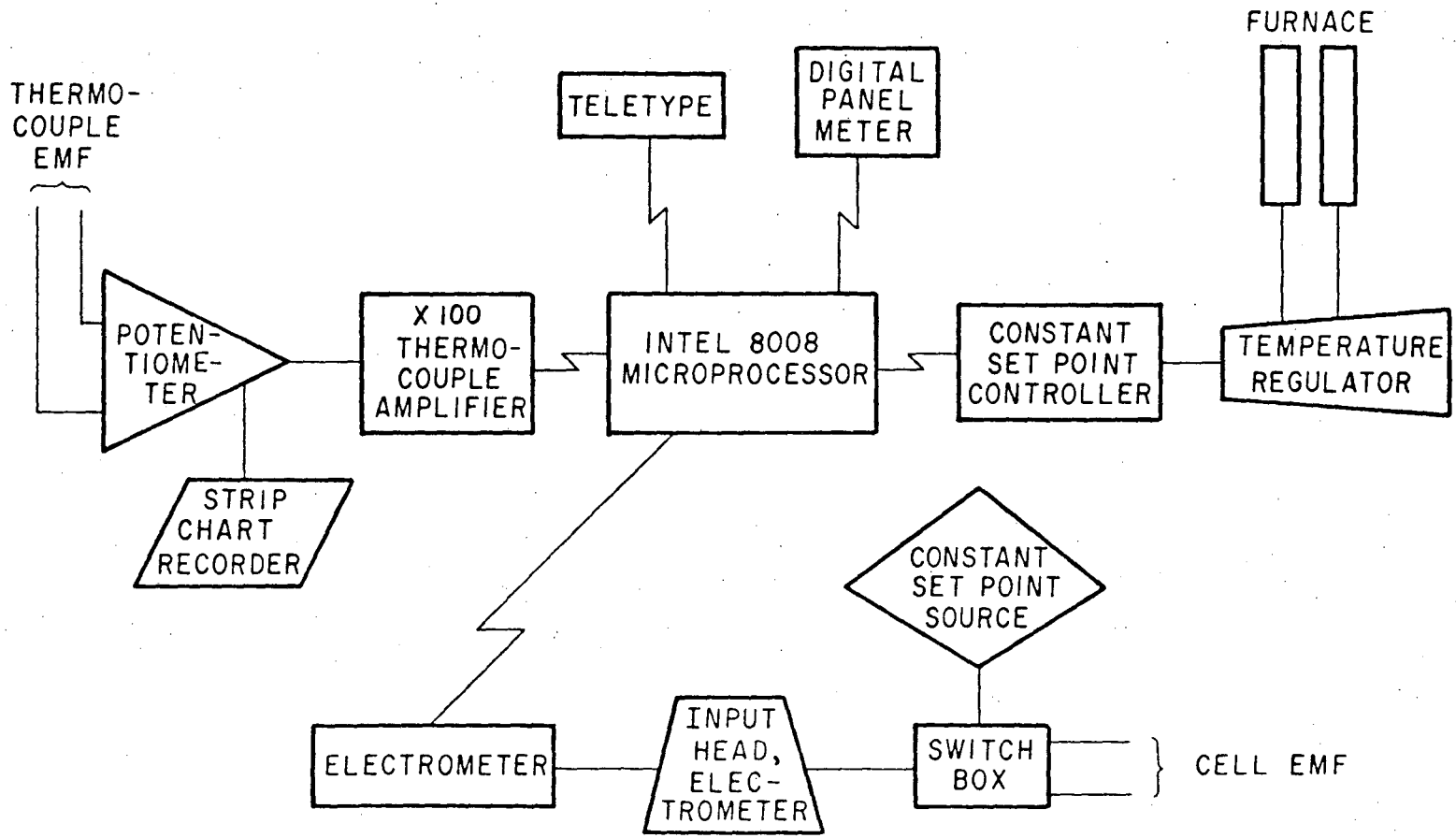

XBL 757-6781

Fig. 3.

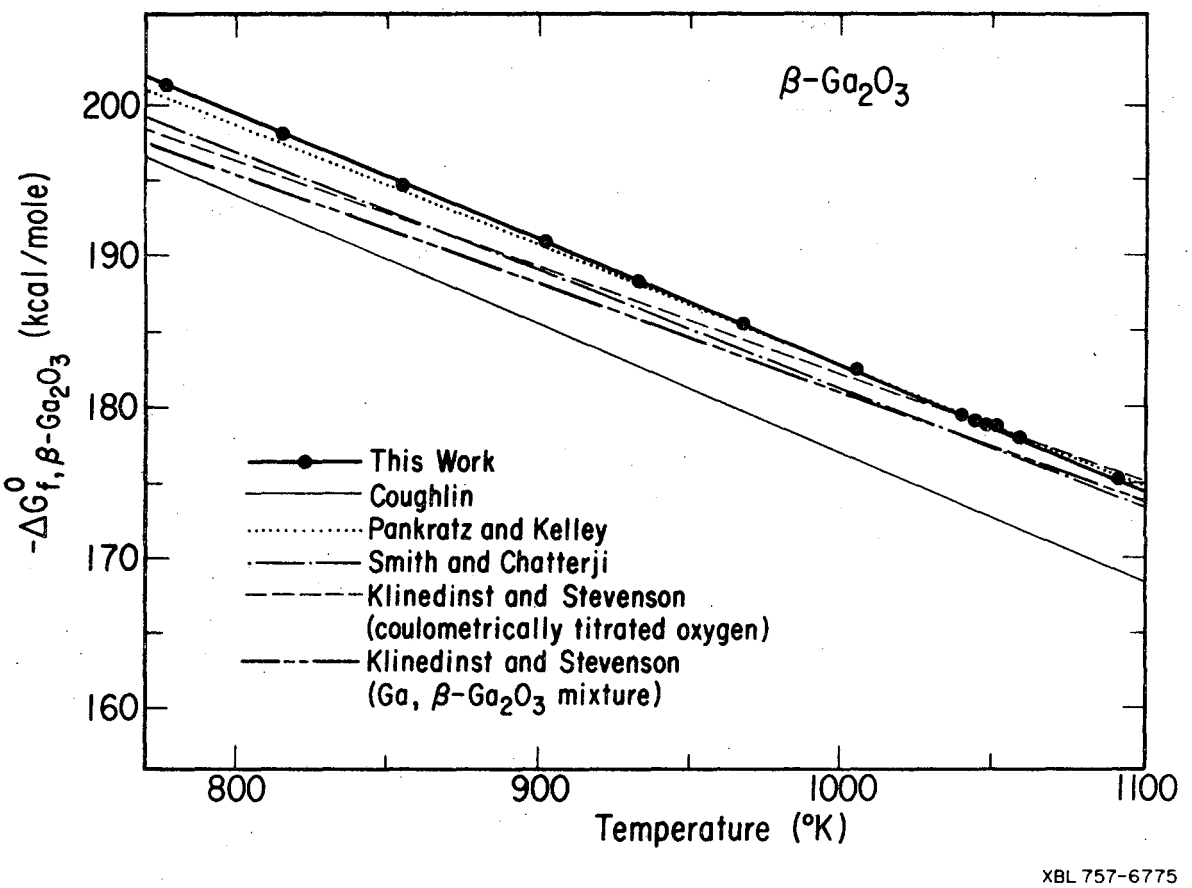

Fig. 4.

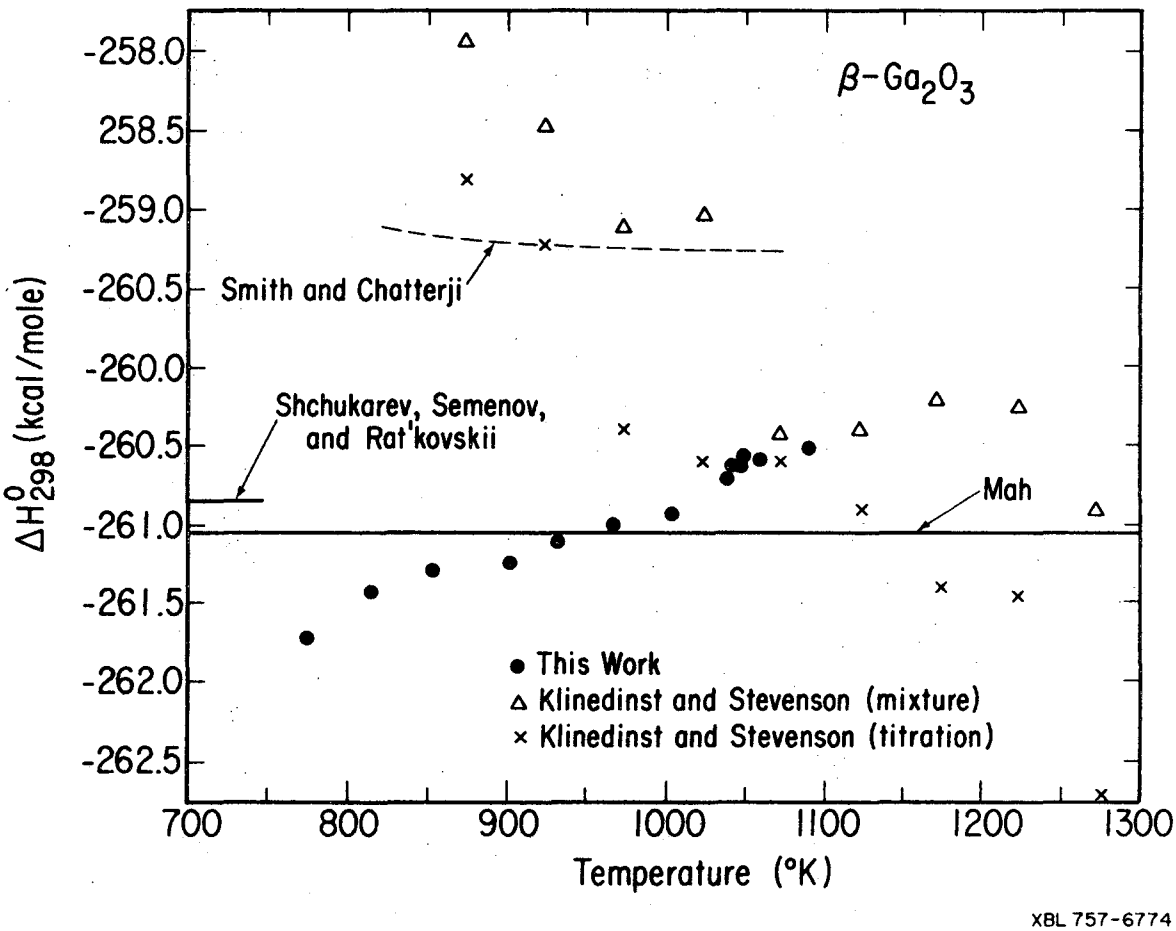
β-Ga2O3
Smith and Chatterji
Shchukarev, Semenov, and Rat'kovskii
Mah
This Work
Klinedinst and Stevenson (mixture)
Klinedinst and Stevenson (titration)
ΔH°298 (kcal/mole)
Temperature (°K)
-258.0
258.5
-259.0
-260.5
-260.0
-260.5
-261.0
-261.5
-262.0
-262.5
700
800
900
1000
1100
1200
1300
XBL 757-6774

Fig. 5.

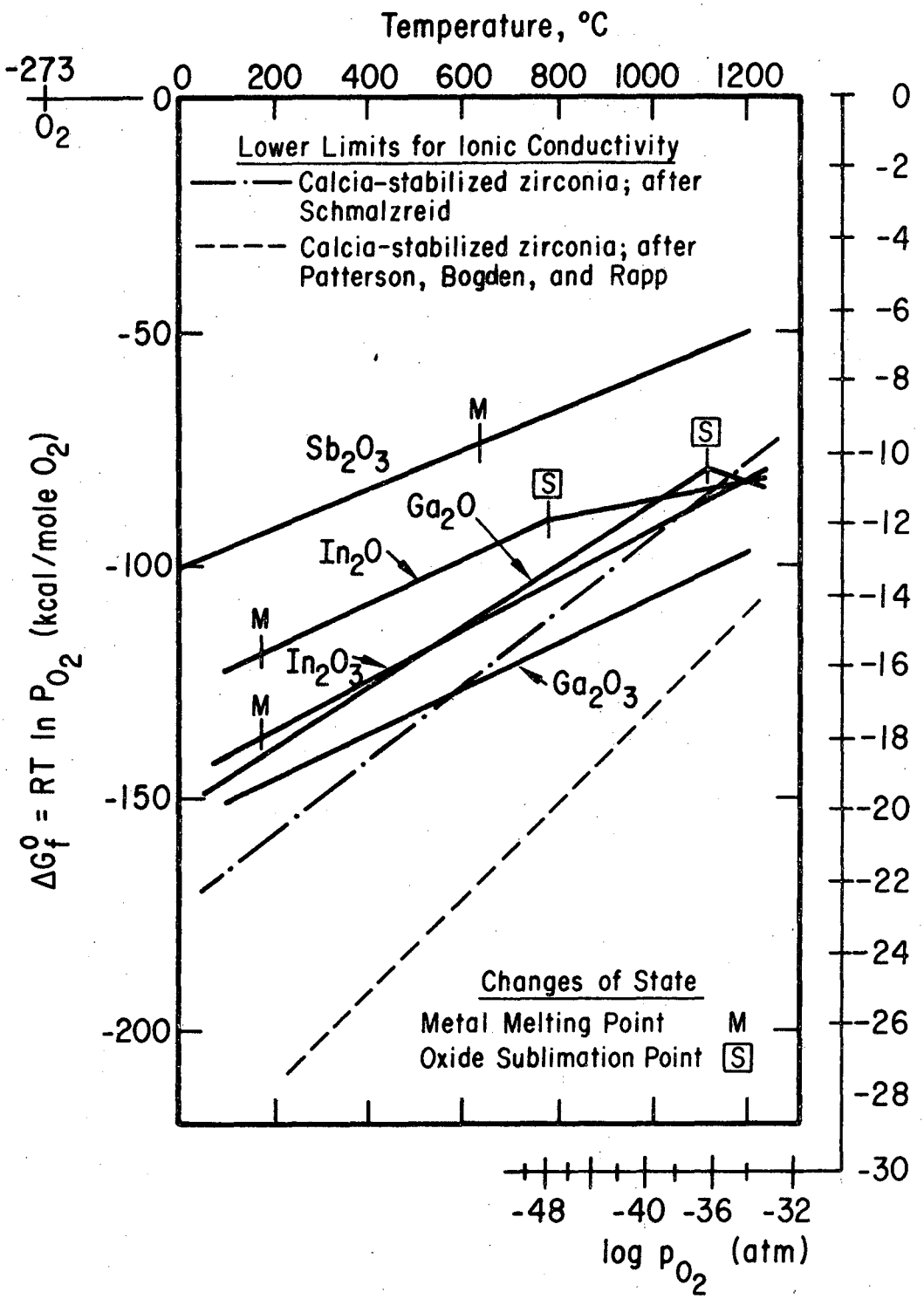

XBL 757-6780

Fig. 6.

IV. SOLID-STATE ELECTROCHEMICAL STUDY OF THE FREE ENERGY OF FORMATION OF INDIUM SESQUIOXIDE

A. Introduction

Indium sesquioxide is an n-type semiconductor which has been used as a thick film resistor. A review of its properties has been given by de Wit.[1] For the processing of In_2O_3 by chemical reactions involving oxidation, accurate information on the thermodynamic properties of In_2O_3 is important.

The standard Gibbs free energy of forming In_2O_3 by the reaction

$$2In(\ell) + \frac{3}{2} O_2(v) = In_2O_3(c) \qquad (1)$$

has been measured using electrochemical methods by a number of authors.[2-5] The Gibbs free energy of formation has also been calculated from the equilibrium partial pressures of water and hydrogen over a mixture of In and In_2O_3.[6,7] Other studies on In_2O_3 from which thermodynamic data can be derived include vaporization studies,[8,9] a thermogravimetric analysis[10] and colorimetric combustion experiments.[11-12]

In this paper, solid-state electrochemical measurements of the Gibbs free energy of the reaction given in equation (1) are reported for the temperature range from 950 to 1128 K. A solid-state galvanic cell technique is employed, utilizing calcia-stabilized zirconia as the solid electrolyte. The results of these experiments are compared with other available data from the literature by means of a third law calculation of the standard enthalpy of formation of In_2O_3. Also presented is an analysis of the equilibrium partial pressures

over a mixture of $In(\ell) + In_2O_3(c)$, based on the results of this study and on other available data. Also based on results of this study, an alternative explanation of the recent thermogravimetric data of de Wit[10] is presented.

B. Experimental

An $In+In_2O_3$ coexistence electrode and a $CO+CO_2$ gas electrode were used in the experimental cell. The coexistence electrode was prepared from 99.999% pure indium powder (Orion Chemical Co.) and 99.999% pure indium sesquioxide powder (Alfa Products). X-ray diffraction analysis showed the oxide powder to be pure In_2O_3. Measured amounts of metal and oxide powders in the weight ratio of 10:1 were thoroughly mixed and placed in a 1 in O.D. tube of graphite (spectrographic grade) closed at one end. The graphite tube was fitted with a screw cap with a central hole through which a 0.250 in O.D., closed-end calcia-stabilized zirconia (CSZ) tube containing the gas reference electrode and a platinum lead wire were inserted into the coexistence electrode. The CSZ tube (Zirconia Corporation of America) had a nominal coposition of $Ca_{0.15}Zr_{0.85}O_{1.85}$. The closed end of the tube was coated inside with unfluxed platinum paste (Englehard No. 6926) to which a spiral platinum lead wire was attached. The $CO+CO_2$ reference gas mixture (Matheson Gas Products) was prepared from high purity argon. Chemical analysis showed the gas mixture to contain (25.29 ± 0.02) percent CO_2 and (2.45 ± 0.02) percent CO. The assembled electrochemical cell showing the electrodes is shown in Fig. 1.

The electrode assembly was contained within a 2 in O.D. closed-end alumina tube sealed with a viton O-ring to a water-cooled brass cell head containing Cajon seals to alumina tubes supporting electrode leads and Pt-Pt+10% Rh thermocouples calibrated to an NBS-reference thermocouple. The coexistence electrode compartment was purged with argon purified by passing it over titanium sponge heated to 850°C. The experimental cell has been described in detail elsewhere.[13]

The cell was placed in a Marshall resistance-heated furnace and shielded from rf interference from the triac-controlled temperature regulator by a grounded platinum shield placed between the 2 in alumina tube and the furnace winding. Temperatures could be maintained to within ±0.5 K.

Cell emf was measured with a Keithley 640 electrometer which was connected to the cell leads with a triaxial cable containing a driven guard to reduce leakage currents. The electrometer output and amplified thermocouple output were monitored periodically by a microcomputer control system based on the Intel 8008 microprocessor. The control program was able to raise the cell temperature at $100\,\mathrm{Khr}^{-1}$ to the operating temperature, monitor the cell temperature and emf and print the data on a teletype, test for equilibrium, and repeat the measurements at a series of fixed temperatures within the desired temperature range.

C. Results

The free energy of formation of indium sesquioxide was determined with the cell

$$Pt|C|In,\ In_2O_3 \| CSZ \| CO,\ CO_2\ |Pt. \qquad (2)$$

The activity of oxygen in the coexistence electrode relative to that in the reference gas mixture was measured from the cell voltage, E, and the Nernst equation.

$$E = \frac{RT}{4F} \ln \{p(O_2,\ CO+CO_2)/p(O_2,\ In+In_2O_3)\} \qquad (3)$$

where R is the gas constant, T the absolute temperature, F is the Faraday constant, $p(O_2, CO+CO_2)$ the oxygen partial pressure over the $CO+CO_2$ mixture and $p(O_2,\ In+In_2O_3)$ that over the coexistence electrode.

The Gibbs free energy of forming In_2O_3 is related to the cell emf through the equilibrium constant of reaction Eq. (1). Assuming unity activities for In(ℓ) and In_2O_3(c), ΔG_f^o (In_2O_3, c, T) is given by:

$$\Delta G_f^o(In_2O_3,\ c,\ T) = 1.5\ RT(p_{CO_2}/p_{CO})^2 + 3\Delta G_{ref}^o - 6FE. \qquad (4)$$

The ratio of partial pressures of the reference gas components, (p_{CO_2}/p_{CO}), was determined by chemical analysis to be (10.322 ± 0.092). The term ΔG_{ref}^o in Eq. (4) is the Gibbs free energy of reaction for the reference gas equilibrium,

$$CO + \frac{1}{2} O_2 = CO_2 \qquad (5)$$

and was calculated from the data of Wicks and Block.[14] The measured cell potential differs from the potential generated by the In_2O_3 formation reaction by the magnitude of the Pt-C thermal emf. The potential, determined elsewhere as a function of temperature,[15] was used to correct the measured emf for this contribution.

Listed in Table 1 are the temperatures of measurement, recorded cell emf, corrected cell emf, the partial pressures of oxygen in the reference and measured electrodes, respectively, and the Gibbs energy of forming In_2O_3 as calculated from Eq. (4).

A linear least squares regression analysis of the $\Delta G_f^o(In_2O_3, c, T)$ data shown in Table 2 gave the following equation:

$$\Delta G_f^o(In_2O_3,c,T) = -(223.16\pm0.14) + (0.07947\pm0.00012)\ (T/K) \qquad (6)$$

where $\Delta G_f^o(In_2O_3,c,T)$ has the units of $kcal_{th}mol^{-1}$. The constant term represents the standard enthalpy change for the formation reaction while the temperature coefficient is that of the standard entropy change. The error limits are those of the standard deviation of the data for the least-squares line. This error was found to be 0.25 kcal at 1000 K, which corresponds roughly to a 3 K error in temperature measurement or a 1.8 mV error in cell emf measurements.

Table 1. Summary of experimental and derived data (cal_{th} = 4.184 J; atm = 101.325 k Pa)

T,K	Emf Measured, mV	Emf Corrected, mV	$\log_{10}p(O_2, CO+CO_2)$, atm	$\log_{10}p(O_2, In+In_2O_3)$,	$-\Delta G_f^o(In_2O_3, c, T)$ $kcal_{th}mol^{-1}$
950.8	128.9	131.9	-19.82	-22.61	147.58
953.6	129.0	132.0	-19.73	-22.52	147.38
986.1	128.4	131.6	-18.71	-21.40	144.83
988.2	128.2	131.4	-18.64	-21.32	144.63
1021.6	127.5	131.0	-17.67	-20.25	142.00
1026.0	127.1	130.6	-17.54	-20.11	141.60
1041.8	126.8	130.4	-17.11	-19.63	140.36
1059.0	126.6	130.3	-16.65	-19.13	139.02
1067.8	126.0	129.8	-16.42	-18.87	138.27
1094.9	125.8	129.8	-15.73	-18.12	136.18
1128.3	124.7	128.9	-14.93	-17.24	133.49

D. Discussion

The calculated values of $\Delta G_f^o(In_2O_3,c,T)$ from this study are plotted as a function of temperature in Fig. 2 and compared to data from the emf studies of Klinedinst and Stevenson[5] (using a similar cell design), of Schaefer[2] (using a $Cu-Cu_2O$ reference electrode), of Newns and Pelmore[4] (using a Ni-NiO reference electrode), and of Chatterji and Vest[3] (also using a Ni-NiO reference electrode). Also plotted in Fig. 1 are the values measured by Hochgeshwender and Ingraham employing a flowing gas equilibrating technique.[6]

Presented in Table 2 is a comparison of the standard enthalpy and entropy changes obtained from this study and from other studies. Large discrepancies are apparent in both of these terms derived from the measured Gibbs free energy of formation.

In order to better ascertain the reliability of the available data a third law calculation was performed. The results of this calculation are shown in Fig. 3. The values of $\Delta H_f^o(In_2O_3,c,298.15)$ were calculated from the equation,

$$\Delta H_f^o(In_2O_3,c,298.15) = \Delta G_f^o(In_2O_3,c,T) - \Delta_f(H_T^o - H_{298.15}^o) + T\left[\Delta S_f^o,\ 298.15 - \Delta_f(S_T^o - S_{298.15}^o)\right] \quad . \tag{7}$$

Table 2. Comparison of the standard enthalpy and entropy of the reaction, $2In(\ell) + 3/2\ O_2(g) = In_2O_3(c)$ from different sources.

$\frac{\Delta H^o}{kcal_{th}mol^{-1}}$	$\frac{\Delta S^o}{kcal_{th}mol^{-1}K^{-1}}$	Reference
-218.78	0.07534	Schaefer[2]
-222.7	0.0781	Newns[4]
-215.55	0.07263	Chatterji[3]
-218.7	0.0756	Klinedinst[5]
-223.16	0.07947	this work

Values of $S^o_T - S^o_{298.15}$ and $H^o_T - H^o_{298.15}$ for diatomic oxygen were taken from Wicks and Block,[14] for liquid indium from the selected values of Hultgren,[16] and for indium sesquioxide from the heat capacity measurements of Shchukarev, Semenov and Rat'kovskii.[8] The specific heat data reported in the latter study was reduced to the form,

$$c_p(In_2O_3,c,T) = 29.36 + 7.0\times10^{-3}T - 7.66\times10^{5}/T^2 \qquad (7)$$

The value of -73.5 e.u. was assigned to ΔS^o_f, 298.15 as suggested by Hart.[18] These values were combined according to the stoichiometry of reaction Eq. (1) to determine the values of $\Delta_f(S^o_T - S^o_{298.15})$ and used in conjunction with the measured $\Delta G^o_f(In_2O_3,c,T)$ data to determine the enthalpy of formation at 298.15 K. The calculated $\Delta H^o_f(In_2O_3,c,298.15)$ results are compared to the value of (-221.27±0.40) $kcal_{th}mol^{-1}$ as determined by Holley, Huber and Meierkord[12] by combustion calorimetry.

As shown in Fig. 3, the results of this study exhibit the most temperature-independent values of $\Delta H^o_f(In_2O_3,c,298.15)$ of all the emf studies, with all calculated values falling within the experimental error range of the calorimetric results. The values of $\Delta H^o_f(In_2O_3,c,298.15)$ obtained from the other five studies showed a definite temperature dependence of about equal magnitudes (where actual data points were available). This lead us to reexamine the enthaply and entropy functions chosen in the calculation.

The values of $S^{o}_{298.15}$ for In^{19} and O_2^{19} have been very well determined and stoichiometrically combine to give 101.31 entropy units. Becker and Roth[11] estimated the entropy of In_2O_3 at 298.15°K to be 27.0±2.5 e.u., while Stubbs, Schufle and Thompson[7] calculated a value of 30.1 e.u. from their equilibrium studies. Using these values as extrema lead us to select a range of -74.31 to -71.21 e.u. for $\Delta S^{o}_{f}(In_2O_3,c, 298.15)$. Another alternative calculation of $\Delta H^{o}_{f}(In_2O_3,c,298.15)$ is based on the assumption that $c_p(In_2O_3,c,T)$ is equal to $c_p(\beta\text{-}Ga_2O_3,c,T)$. Glassner[20] gives coefficients for a linear temperature-dependent expression for $c_p(In_2O_3,c,T)$ and estimated enthalpy and entropy functions for the In_2O_3 formation reaction. In order to reconcile the results of the other studies with those from this work, these alternative specific heat values were substituted in various combinations in the third law calculation. In all cases (except with the more negative values of $\Delta S^{o}_{f}(In_2O_3,c,298.15)$ and with other values as in the original calculation) the use of the new specific heat functions had the deleterious effect of raising the mean value of the calculated $\Delta H^{o}_{f}(In_2O_3,c,298.15)$ well above that reported by calorimetric studies. It can be concluded therefore, that the results of this study are most consistent with the third law test of all studies using the solid-state electrochemical cell method.

An important side reaction to consider at high temperatures is the decomposition of $In_2O_3(c)$ to form $In_2O(v)$. The existence of $In_2O(c)$ above 1085°K has been suggested by Klinedinst and Stevenson[5]

to explain a discontinuity in the temperature dependence of the measured oxygen activity of a coexistence electrode containing $In(\ell)$ and indium oxides formed by electrochemical titration. No such discontinuity was found in the present study for a coexistence electrode containing $In(\ell)$ and $In_2O_3(c)$. It is possible, therefore, that $In_2O(c)$ is produced by the titration of oxygen ions into $In(\ell)$ above 1085 K.

It is of interest to calculate the partial pressure of $In_2O(v)$ that would exist in the $In(\ell) + In_2O(c)$ electrode if equilibrium conditions prevailed. For the reaction,

$$4/3\ In(\ell) + \frac{1}{3}\ In_2O_3(c) \rightleftharpoons In_2O(c) \qquad (8)$$

the Gibbs free energy change is found by subtracting $\frac{1}{3}\ \Delta G_f^o(In_2O_3,c,T)$, obtained in this study, from that for $In_2O(c)$ suggested by Klinedinst and Stevenson.[5] The result is

$$\Delta G(8) = 20.286 - .01959\ (T/K),\ kcal_{th}\,mol^{-1}. \qquad (9)$$

The standard free energy change is zero for this reaction at 1097 K. Therefore above this temperature solid In_2O could form. The $In_2O(c)$ vaporization free energy can now be found by combining the formation energies of the two species,[5] for the reaction,

$$In_2O(c) = In_2O(v) \qquad (10)$$

The result is

$$\Delta G(10) = 31.0 - 0.177\ (T/K),\ kcal_{th}\,mol^{-1} \qquad (11)$$

Assuming ideal conditions, the pressure of $In_2O(v)$ over solid In_2O is then given by

$$\log_{10}\{p(In_2O/atm\} = -6949/T + 3.87 \qquad (12)$$

which gives a value of 2.75 mmHg at 1100 K. If on the other hand $In_2O_3(c)$ is present, the oxygen partial pressure is found from the equilibrium reaction,

$$In_2O_3(c) = 2In(\ell) + 3/2\ O_2(v) \qquad (13)$$

Also the reaction

$$2In(\ell) + \tfrac{1}{2}\ O_2 = In_2O(v) \qquad (14)$$

is a source of In_2O in the gas phase. Combining the last two reactions, one obtains

$$\log_{10}\{p(O_2)/atm\} = -32,513/T + 11.58 \qquad (15)$$

$$\log_{10}\{p(In_2O)/atm\} = -11,405/T + 7.93. \qquad (16)$$

These expressions also give a value of 2.93 mm Hg for the partial pressure of $In_2O(v)$ at 1100 K. Shchukarev, Semenov and Ratkovskii[8]

found the pressure of $In_2O(v)$ over a mixture of $In(\ell) + In_2O_3$ to be 0.631 mm Hg at 1101 K by mass spectrometry. Shown in Fig. 4 are the partial pressures of $In_2O(v)$ established by a direct formation reaction in the presence of $In_2O_3(c)$ or by vaporization of $In_2O(c)$. The mass spectrometer data is not sufficient for one to discern which mechanism is controlling, although the formation of $In_2O(c)$ after vacuum sublimation of the $In_2O_3(c) + In(\ell)$ mixture has been reported.[8]

Also of importance to the present study is the equilibrium pressure of $In_2O(v)$ over $In_2O_3(c)$ produced by the reaction

$$In_2O_3(c) = In_2O(c) + O_2(v) \qquad (17)$$

This reaction has a free energy change given by

$$\Delta G(17) = 169.16 - .017157\ (T/K),\ kcal_{th}mol^{-1}. \qquad (18)$$

Combined with the free energy of vaporization for solid In_2O one finds

$$\log_{10}\{p(In_2O)/atm\} = -43{,}918/T + 19.51 - \log_{10}\{p(O_2)/atm\}. \qquad (19)$$

This expression is somewhat different from that given by Van Dillen[21] which is

$$\log_{10}\{p(In_2O)/atm\} = 42.189/T + 17.7 - \log_{10}\{p(O_2)/atm\}. \qquad (20)$$

The formation of $In_2O(c)$ as a reaction product during $In_2O_3(c)$ decomposition is suggested by the thermogravimetric studies of de Witt[10]

who found a small (1 μg/min) linear weight loss of In_2O_3 over the temperature range from 1173 to 1473 K. De Wit attributed this result to a defect reaction involving either the formation of oxygen vacancies or indium interstials in $In_2O_3(c)$, however, rather than to an $In_2O(c)$ surface reaction product. In our study of the $In(\ell)$ + $In_2O_3(c)$ coexistence electrode, no discontinuities in cell emf with temperature were observed, in spite of some vaporization of $In(\ell)$. Therefore, we conclude that $In_2O(c)$ could be produced by a rapid dissociative decomposition reaction from $In_2O_3(c)$ above 1173 K, but that $In_2O(c)$ is not present in the $In(\ell)$ + $In_2O_3(c)$ coexistence electrode. This conclusion also is supported by x-ray diffraction analysis on the coexistence electrodes following high-temperature studies.

E. Conclusion

The Gibbs free energy of formation of In_2O_3 was readily measurable utilizing a solid-state electrochemical cell with a $CO + CO_2$ reference electrode. The microcomputer automation of the study proved exceptionally beneficial for automatic testing of thermodynamic equilibrium and of the reproducibility of the data. The results of the study gave the most temperature-independent values of $\Delta H_f^o(In_2O_3,c,298.15)$ of all the emf studies of the $In_2O_3(c)$ formation reaction, and in close agreement with calorimetric data. No evidence was found for the formation of $In_2O(c)$ over $In(\ell)$ + $In_2O_3(c)$ coexistence electrodes.

REFERENCES

1. De Wit, J. H. W., J. Solid State Chem. 8, 142 (1973).
2. Schaefer, S., U. S. Bur. Mines, Rep. Invest., No. 7549, 1971.
3. Chatterji, D. and Vest, R. W., J. Amer. Ceram. Soc., 55, 575 (1972).
4. Newns, G. R. and Pelmore, J. M., J. Chem. Soc. (A), 146 (1968).
5. Klinedinst, K. A. and Stevenson, D. A., J. Chem. Thermodynamics 5, 21 (1973).
6. Hochgeschwender, K. and Ingrahm, T. R., Can. Met. Quart., 6, 293 (1967).
7. Stubbs, M. F., Schufler, J. A. and Thompson, A. J., J. Amer. Chem. Soc. 74, 6201 (1952).
8. Shchukarev, S. A., Semenov, G. A. and Ratkovskii, I. A. Russ. J. Inorg. Chem. 14, 1 (1969).
9. Burns, R. P., DeMaria, G. Dorwart, J., and Inghram, M. G., J. Chem. Phys. 38, 1035 (1963).
10. De Wit, J. H. W., J. Solid State Chem. 13, 192 (1975).
11. Roth, W. A. and Becker, G., Z. Physik. Chem. A161, 69 (1932).
12. Holley, C. E. and Huber, E. J., Jr. and Neierkord, E. H. J. Amer. Chem. Soc. 74, 1084 (1952).
13. Anderson, T. J. and Donaghey, L. F., Tech Rept. LBL-4128, Lawrence Berkeley Laboratory, Berkeley, CA, August 1975.
14. Wicks, C. E. and Block, F. E., U. S. Bur. Mines Bull. 605, (1963).
15. Chatterji, D. and Smith, J. V., J. Electrochem. Soc. 120, 889 (1973).

16. Hultgren, R., Desai, P. D., Hawkins, D. T., Gleizer, M. and Kelley, K. K., Selected Values of the Thermodynamic Properties of the Elements, (American Soc. for Metals, Ohio, 1973).

17. Kelley, K. K., U. S. Bur. Mines Bull. 584 (1960).

18. Hart, D., J. Phys. Chem. 56, 202 (1952).

19. Kelley, K. K., U. S. Bur. Mines Bull. 477 (1950).

20. Glassner, A., Tech. Rept. ANL-5750 (1957).

21. Van Dillen, A. J., taken from Ref. 10.

LIST OF FIGURES

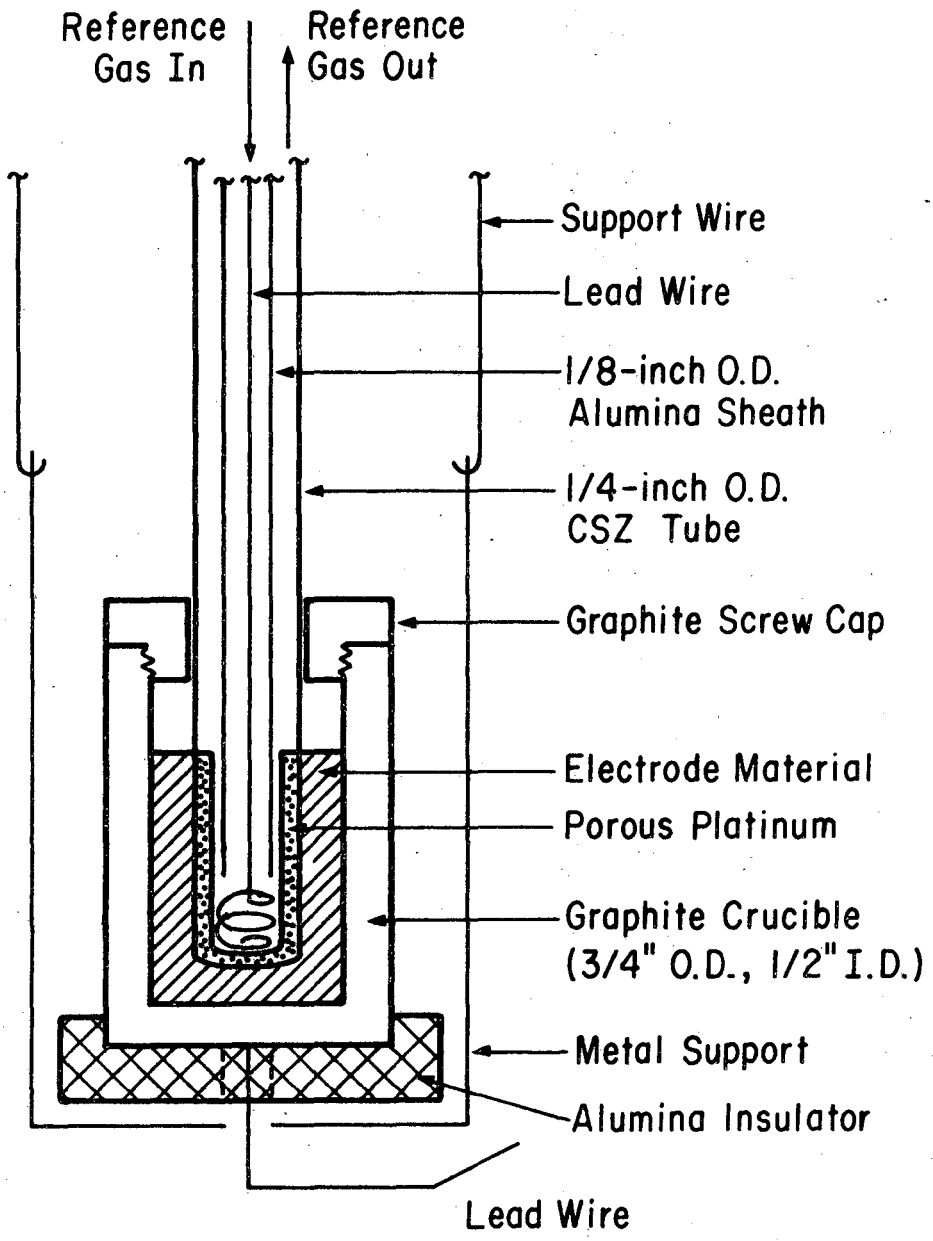

Fig. 1.

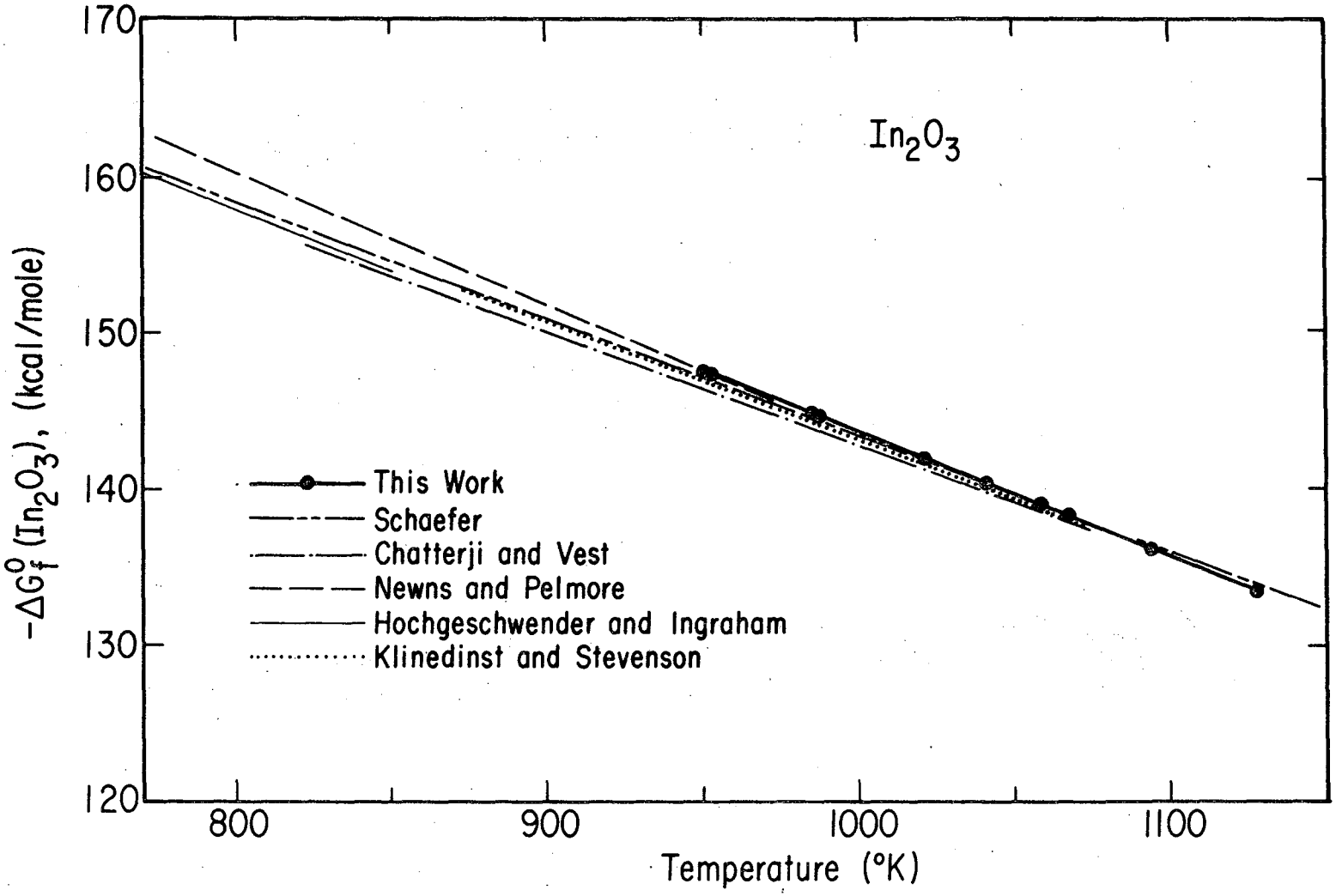

XBL 758-6786

Fig. 2.

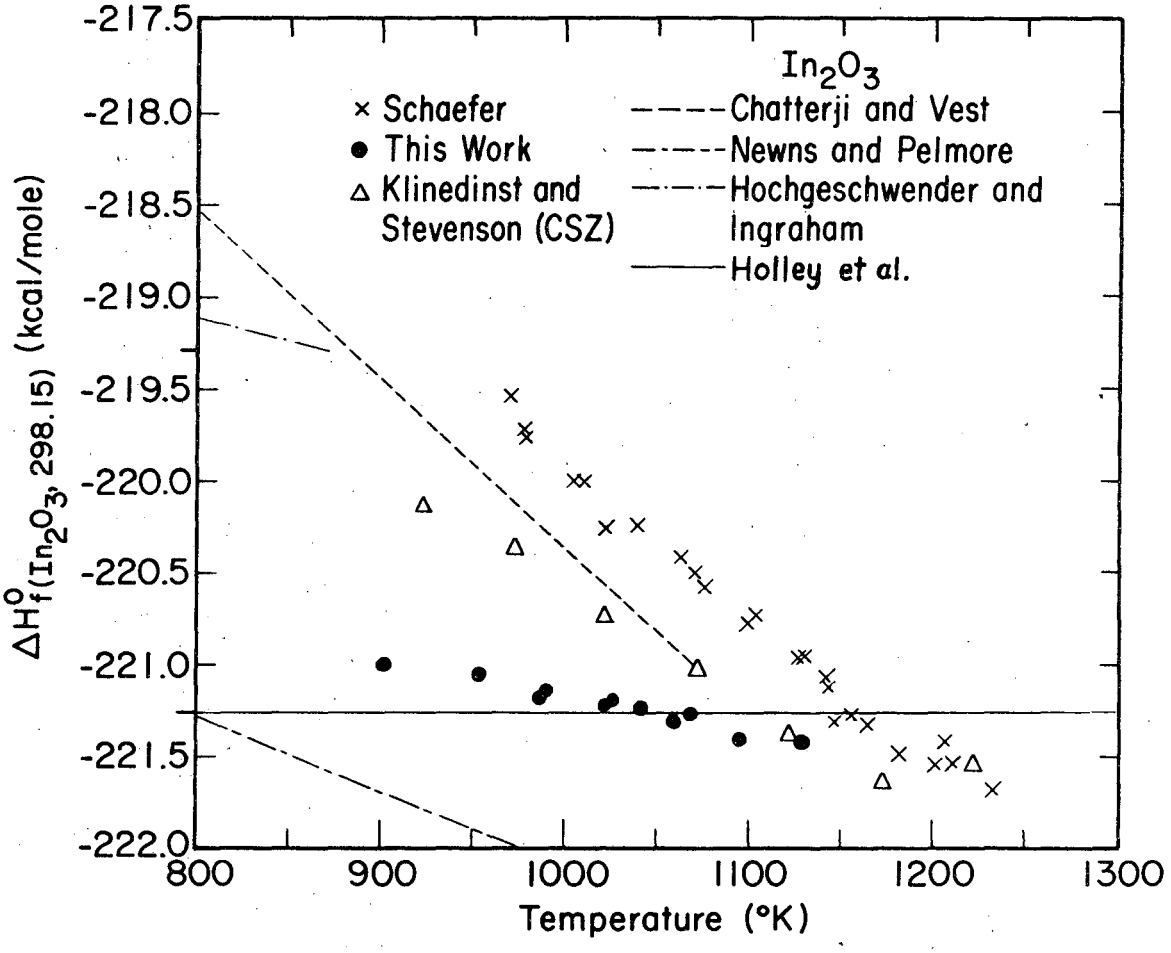

Fig. 3.

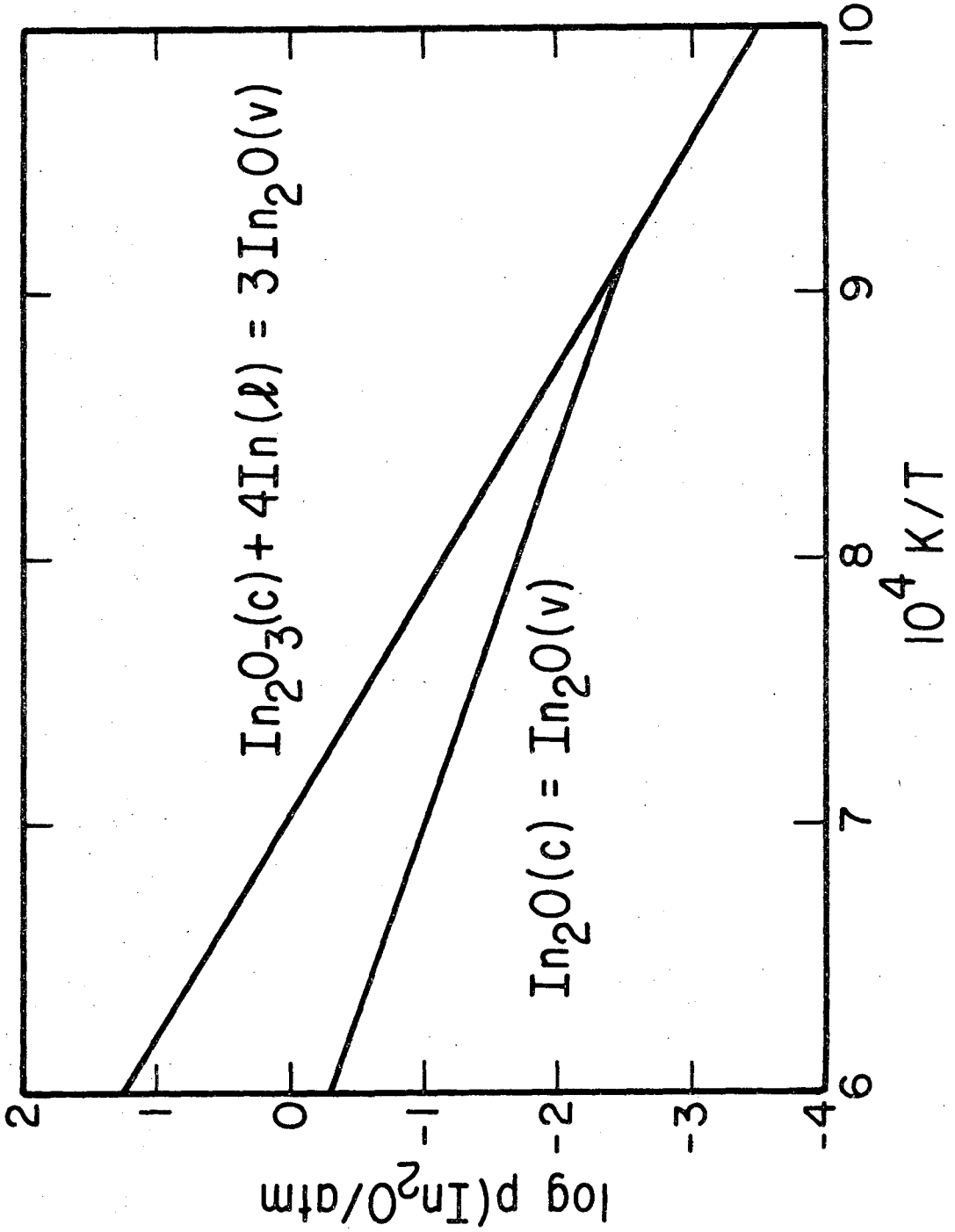

XBL 757-6791

Fig. 4.

V. SOLID-STATE ELECTROCHEMICAL STUDY OF Ga-Sb LIQUID ALLOYS

A. Introduction

Gallium and antimony combine to form a single intermetallic compound, gallium antimonide (GaSb) with the sphalerite structure. This compond is of current practical interest for its semiconducting properties, especially in application to Gunn effect diodes.[1]

The thermodynamics of the gallium - antimony system at and above the melting temperature of GaSb, has received considerable attention. Much recent consideration has been given to solution models for the prediction of thermodynamic data from liquidus temperatures. Such indirect methods, however, are sensitive to errors in available liquidus data. For example, the melting point of GaSb, T_m, as determined by different studies has been reported to be 975,[11, 12] 979,[7] 982,[14] 985,[2, 6, 13] 993,[9] and 998[10] degrees Kelvin. The melting point as measured by different investigators shows marked differences though the generally accepted value is 985 K.[15, 16] Compiled in Table 1 is a list of the experimentally determined enthalpy of fusion of GaSb, $\Delta H_f^c(GaSb)$, and entropy of fusion, $\Delta S_f^c(GaSb)$, calculated assuming the melting point is 985 K. As can be seen, the large range of 2.0 $kcal_{th}g\text{-}atom^{-1}$ exists for the reported $\Delta H_f^c(GaSb)$.

The Ga-Sb phase diagram has been determined by a number of investigators[7, 14, 18] all in generally excellent agreement, though shifted somewhat below the accepted melting point.

Enthalpy of mixing data for liquid alloys have been measured by Predel and Stein[20] and Yazawa, Kawashima and Itagaki[21] who found a maximum in this quantity of -258 and -204 $cal_{th}g\text{-}atom^{-1}$,

Table 1. Comparison of enthalpy and entropy of fusion of GaSb, as reported by different investigators. (cal_{th} = 4.184J)

$\frac{\Delta H_f^c(GaSb)}{kcal_{th}\,g\text{-}atom^{-1}}$	$\frac{\Delta S_f^c(GaSb)}{cal_{th}\,g\text{-}atom^{-1}K^{-1}}$	Reference
7.78 (± .1)	7.90 (± .11)	2
7.9	8.0	3
6.0 (± .5)	6.1	4
7.3 (± .3)	7.4	5
7.5 (± .3)	7.6	8
8.0 (± .8)	8.1	17
7.0 (± .3)	7.1	19

respectively, at an equimolar composition. Activities in the liquid phase have been measured with solid state electrochemical techniques.[22-24] All of the reported results show extremely large negative deviations from ideality. Small negative deviations were found by Yazawa, Kawashima and Itagaki when they applied a strictly regular solution model to their heat of mixing data,[21] while Predel and Stein calculated moderate positive deviations near the melting point of GaSb.[20] On the other hand, vapor pressure studies[25] have shown a moderately negative derivation from ideality. Thus, the thermodynamic properties of the Ga-Sb system at the above the melting temperature of GaSb are not well defined.

In this study, component activities in the liquid phase of the Ga-Sb system were measured with a high temperature galvanic cell employing a calcia-stabilized zirconia solid electrolyte and gaseous reference electrode.

B. Experimental

1. Materials

The alloy coexistence electrodes used in this study were prepared from high purity materials. Semiconductor-grade elemental gallium and antimony were obtained from Cominco American. Powdered Ga_2O_3 of 99.999% purity was obtained from Alfa Products. The materials were allowed to contact only high-purity alumina during the mixing process. High purity graphite was used in the preparation of the containers for the alloy coexistence electrode. Calcia-stabilized zirconia tubes having a nominal composition of $Ca_{0.15}Zr_{0.85}O_{1.85}$ were obtained from Zircoa Corporation of America. The high

temperature part of the experimental cell housing was constructed entirely of high purity recystallized alumina. The electrode assembly was contained within a split tube of 99.99 tantalum which acted as a support and as an oxygen getter.

2. Apparatus

The basic experimental cell consisted of a 2 inch-diameter closed-end alumina tube 18 inch in length secured by a Viton O-ring to the brass cell head. This envelope contained the electrodes as shown in Fig. 1. The Ga-Sb alloy and a small amount of β-Ga_2O_3 were placed within a graphite closed crucible in contact with a 0.250 inch diameter CSZ tube containing the $CO+CO_2$ reference gas and a Pt-paste contact between a Pt wire and the electrolyte. Three 1/8 inch bored-through Cajon connectors on the cell head for thermocouples were placed symetrically around a 1/4 inch central Cajon fitting containing a calcia-stabilized zirconia tube. The thermocouples used were type K (.020 inch Pt, Pt 10% Rh) which were calibrated in separate experiments within the cell against an NBS-tracable calibrated thermocouple.

In this investigation argon gas was used as the inert gas blanket. High purity, tank argon was further purified by passing it through a column of Linde 4A molecular seive at the temperature of the dry ice-acetone equilibrium to remove the majority of water vapor present, then over hot Ti sponge at 1123 K.

The cell was heated with a Marshall resistance heated furnace (20 inches in length with a 2 1/2 inch bore). Excellent temperature control was furnished by an integrating, triac-controlled regulating power supply designed and built at Lawrence Berkeley Laboratory.

Cell emfs were measured with a Keithley 640 electrometer accompanied with an adaptor input head. A guarded cable connected the cell to the electrometer input head where connection was made to a triaxial connector.

Data acquisition was automated with an Intel 8008-based microcomputer. The system had the capability of setting the cell operation temperature and monitoring cell emfs and thermocouple outputs on a predetermined time base, thus allowing continuous cell operation. The precision of recorded data was 0.01%.

C. PROCEDURE

The general experimental procedure was to assemble the desired electrode arrangement and connect it to the peripheral apparatus. The cell was then successively evacuated (approximately 10^{-5} torr) and filled with argon, and the process repeated three times. The absence of leaks was checked by sealing the cell under vacuum or under an excess pressure and monitoring the cell pressure. With the use of a ramp set-point controller, the cell temperature was then raised to the highest operating temperature at a rate of 100 K hr^{-1} in order to prevent thermal shock to the electrolyte. At this point the control was switched to the Intel 8008-based microcomputer and a control program initiated. The cell emf was monitored automatically as the microcomputer reset the temperature in increments of ~20°C over a fixed range after complete equilibrium had been reached at each temperature. At least two cycles of the temperature range of interest were completed in order to reveal any hysterisis effects in the measurement. After completion of each run the temperature was

slowly lowered at 100 K hr^{-1} and the cell disassembled. The electrode material was then examined by x-ray diffraction analysis to confirm the absence of side reaction products.

D. Results

The activity of Ga in the liquid alloys of Ga-Sb was measured electrochemically in a solid-state galvanic cell which can be represented schematically as

$$Pt|C|Ga(\ell),Sb(\ell),\ \beta\text{-}Ga_2O_3(c)||CSZ||CO,CO_2|Pt. \qquad (1)$$

At equilibrium, the electrochemical potential of oxygen is equal in both electrodes and is related to the cell emf by the Nernst equation,

$$E = (RT/4F)\ \ell n\ \{a(O_2,ref)/a(O_2,Ga\text{-}Sb)\} \qquad (2)$$

Here $a(O_2,ref)$ is the oxygen activity in the reference electrode while $a(O_2,Ga\text{-}Sb)$ is the oxygen activity in the alloy electrode, T is the thermodynamic temperature, R is the gas constant and F is the Faraday constant.

The reference oxygen activity was calculated for the equilibrium reaction

$$CO + \frac{1}{2}\ O_2 = CO_2 \qquad (3)$$

and therefore the oxygen activity is given by

$$a(O_2,\text{ref}) = \left[\left(\frac{p(CO_2)}{p(CO)}\right)\right]^2 \exp\{2\Delta G(3)/RT\} \qquad (4)$$

The free energy change for the reference gas reaction is

$$\Delta G(3) = -68{,}270 - 0.18T \ln T - 0.34\times10^{-3}T^2 + 0.87\times10^5/T + 23.28\ T,\ \text{cal}_{th}\,\text{mol}^{-1} \qquad (5)$$

from the equations of Wicks and Block.[26] The ratio $p(CO_2)/p(CO)$ was chemically analyzed and found to be (10.322 ± 0.92.)

The activity of oxygen in the measured electrode is related to the gallium activity in the same electrode through the formation of β-Ga_2O_3 by the reaction,

$$2Ga(\ell) + 3/2\ O_2(v) = \beta\text{-}Ga_2O_3(c) \qquad (6)$$

from which it follows that the oxygen activity in the alloy is

$$\ln a(O_2,\text{Ga-Sb}) = 2\Delta G(6)/3RT - (4/3)\ \ln a(Ga) \qquad (7)$$

The free energy change of reaction (6) was taken as $\Delta G(6) = (-265309\pm152)+(82.47\pm0.16)\ T,\ \text{cal}_{th}\,\text{mol}^{-1}$.[28] Combining Eq. (2), (4) and (7), one finally obtains an expression for the gallium activity in the liquid alloy,

$$RT \ln a(Ga) = 3FE - 1.5\ RT \ln\{(p(CO_2)/p(CO)\} - 1.5\ \Delta G(3) + 0.5\ \Delta G(6). \qquad (8)$$

The measured cell emf had to be corrected for the thermal emf generated by the Pt-C couple, which has been reported by Chatterji and Smith.[27] Figure 2 shows the corrected equilibrium cell potentials as a function of temperature. A linear least squares analysis was applied to the data, the results of which are listed in Table 2. Listed in Table 3 is the activity of gallium calculated from Eq. (8). The activity of Sb was found by graphical integration of the Gibbs-Duhem equation. The relative partial molar enthaply of Ga was then calculated from

$$\Delta\bar{H}_{Ga} = nF(T\,\frac{dE}{dT} - E). \tag{9}$$

Then, the relative partial molar enthalpy of Sb was obtained by graphical integration with the relation,

$$\Delta\bar{H}_{Sb} = -\int \frac{x_{Ga}}{x_{Sb}}\, d\Delta\bar{H}_{Ga}. \tag{10}$$

The relative partial molar entropy of Ga was determined by

$$\Delta\bar{S}_{Ga} = nF\,\frac{dE}{dT}, \tag{11}$$

and the relative partial molar entropy of Sb calculated from

$$\Delta\bar{S}_{Sb} = (\Delta\bar{H}_{Sb} - RT\ \ell n\ a_{Sb})/T \tag{12}$$

Table 2. Emf of the experimental cell for different Ga-Sb system.

	E = a + b(T/K), mV	
x_{Ga}	a	$-b\times10^3$
0.0390	413.41 ± 2.41	125.16 ± 2.36
0.293	432.03 ± 0.86	69.57 ± 0.83
0.500	438.82 ± 1.51	52.64 ± 1.45
0.639	439.18 ± 1.26	42.60 ± 1.22
0.833	447.44 ± 0.44	42.03 ± 0.41

Table 3. Summary of thermodynamic data for Ga-Sb alloys derived from emf measurements. (cal_{th} = 4.184J)

x_{Ga}	a_{Ga}	a_{Sb}	$\frac{\Delta\bar{H}_{Ga}}{cal_{th}mol^{-1}}$	$\frac{\Delta\bar{H}_{Sb}}{cal_{th}mol^{-1}}$	$\frac{\Delta H_{mixing}}{cal_{th}mol^{-1}}$	$\frac{\Delta\bar{S}_{Ga}}{cal_{th}mol^{-1}}$	$\frac{\Delta\bar{S}_{Sb}}{cal_{th}mol^{-1}}$	$\frac{\Delta S_{mixing}}{cal_{th}mol^{-1}}$	$\frac{\Delta G_{mixing}}{cal_{th}mol^{-1}}$
0.039	0.0126	0.959	-2192	-5	-90	6.51	0.08	0.33	-420
0.293	0.166	0.632	-902	-253	-443	2.67	0.66	1.25	-1696
0.500	0.379	0.372	-433	-571	-501	1.50	1.40	1.45	-1953
0.639	0.545	0.231	-408	-940	-442	0.80	1.97	1.38	-1829
0.833	0.739	0.0982	+164	-1874	-177	0.76	2.74	1.09	-1274

Also listed in Table 3 are the integral values of the enthalpy, entropy and Gibbs free energy of mixing. In the above calculations, a temperature of 1003 K was used.

E. Discussion

Figure 3 shows the gallium and antimony activities as a function of the gallium mole fraction, x_{Ga}, obtained from this study. For comparison, the emf results of Danilin and Yatsenko,[23] obtained at 988 K, and those of Gerasimenko et al.[24] at a temperature of 1023 K. These investigators did not report an emf temperature derivative. Also shown are the calculated activities of Yazawa et al.[21] determined by applying a regular solution model to their heat of mixing data at a temperature of 1003 K. Not depicted are recent results by Pong,[22] determined also with a solid oxygen-conducting electrolyte but with a Ga_2O_3(c) reference electrode. Pong found that the activity versus composition curve had the same general shape as that obtained in this study but shifted somewhat to more negative values. The calorimetry study at x_{Ga}=0.5 by Predel and Stein[20] gave a value of -258 cal g-atom^{-1} for ΔH_{mixing}. The calculated activities of Predel and Stein[20] show a positive deviation from ideality while the vapor pressure studies of Hsi-Hsiung et al.,[25] agree very closely with those of this study. The large negative deviations found in the other two emf studies whose results are shown in Fig. 3 might have arisen from problems in the experimental galvanic cell used. Both studies used a chloride electrolyte and assumed a value of 3 for the number of equivalents in the Nernst equation whereas

gallium has known valences of both + 3 and + 1 and therefore the value of n is indeterminent. A value for n less than 3 would raise the measured activities, but the general shape of the activity curve would still differ from that found in this study.

Figure 4 shows the Gibbs free energy, enthalpy and entropy changes for mixing the liquid elements, as determined in this study. It can be seen that gallium and antimony mix exothermically and nearly randomly (with an excess entropy of mixing of only 0.08 cal_{th} g-atom^{-1} for the stoichiometric liquid), indicating that the liquid alloys are nearly regular in nature. Also show in Fig. 3 are the entropy of mixing determined calorimetrically by Predel and Stein[20] and Yazawa, et al.[21] The latter results are more endothermic by about a factor of 2, and should be the more accurate due to their reproducibility and to the reliability of the experimental technique.

It should be noted that the temperature dependence of the activity (used to calculate ΔH_{mixing}) illustrated in Eq. (8) involves three other temperature coefficients, those in $\Delta G(3)$, $\Delta G(6)$ and the thermal emf correction. Adding the experimental errors of the above to those found from the emf fit results in sufficiently large error in the partial molar enthalpies that measured ΔH_{mixing} here agree well with that obtained from calorimetric studies. Shown also in Fig. 4 is ΔS_{mixing} obtained from the calorimetric value of ΔH_{mix} in conjunction with ΔG_{mixing} measured here. This method gives a significant positive excess entropy of mixing.

A pair potential analysis was applied to these results. This analysis indicated a preference for Ga-Sb pairing which is consistent with the negative total enthalpy for the alloy. The pairing, though not extensive because of the small values of ΔH_{mixing}, would produce a negative contribution to the excess entropy. This contribution is probably offset by a positive excess volume (as has been found for the related In-Sb[29] system and in other metallic solutions) and by possible changes in excitation of internal degrees of freedom resulting from the pairing, which contribute to the positive excess entropy observed.

In order to quantify these observations a short-range order parameter, α, was calculated based on a lattice theory discussed by Averbach.[30] This parameter is defined as

$$\alpha = 1 - P_{Ga-Sb}/\{ZN_o x_{Ga} x_{Sb}\} \tag{13}$$

where P_{Ga-Sb} is the number of Ga-Sb pairs in the liquid solution, Z is the number of nearest neighbors, N_o is the number of lattice sites and x is the mole fraction of gallium or antimony. Through statistical methods Averbach shows that the excess entropy can be approximated by

$$\Delta S^E_{mixing} \cong |\alpha| kN_o [x_{Ga} \ell n x_{Ga} + x_{Sb} \ell n x_{Sb}] - \frac{\partial}{\partial T} [Z N_o x_{Ga} x_{Sb} (1-\alpha) g(T)] \tag{14}$$

and the enthalpy of mixing by

$$\Delta H_{mixing} = Z\, N_o x_{Ga} x_{Sb} (1-\alpha)\, [\mu + j(x)] \qquad (15)$$

where k is the Boltzman constant. The quantities $\mu + j(x)$ and $g(T)$ are defined in terms of the quasichemical interchange energy, Ω, and

$$\Omega = Z\, N_o [\, \mu + j(x) + g(T)] \qquad (16)$$

thus allowing the interchange energy to have a composition and temperature dependence. The authors are aware that the quasichemical solution theory is not directly applicable here because a positive excess entropy cannot be predicted, but the theory gives some insight into the relative amount of ordering in this system. Finally, α can be expanded in terms of the mole fraction and the interchange energy, and truncated after the first terms to give

$$\alpha \cong \frac{2x_{Ga}x_{Sb}[\, \mu + j(x) + g(T)]}{kT} . \qquad (17)$$

If the excess entropy and enthalpy are known, then Eqs. (14, 15 and 17) can be solved simultaneously for α. The temperature dependence of $g(T)$ was assumed to be linear and given by

$$g(T) = \bar{g}T . \qquad (18)$$

Figure 5 shows the calculated short-range order parameter, α, as a function of the antimony mole fraction. Listed in Table 4 is the calculated value of α, the terms $N_o[\mu + j(x)]$ and $N_o\bar{g}$ and the reduced interaction energy, Ω/ZRT, for the five compositions studied. In these calculations the heat of mixing of Predel and Stein[20] was used with the excess entropy obtained using our free energy data. A value of 6 was used for Z which is substantiated by x-ray measurements on In-Sb[30] which showed that the number of nearest neighbors was 5.7. The temperature of calculation was 1003 K.

The values of α listed can be used to predict values of ΔH_{mixing}, ΔS^E_{mixing} when used in Eqs (14) and (15). It is observed that the effect of the temperature dependent term, g(T), is nearly twice that of the term $\mu + j(x)$, therefore the degree of Ga-Sb pairing is much greater than would be predicted by using the heat of mixing data alone.

The experimental data for the liquidus temperature of the Ga-Sb system as well as direct determinations from other sources can be checked for consistency with the following two expressions for the liquidus temperature derived elsewhere[31]

$$T_\ell = \frac{2\Delta H^c_f(GaSb)+\Delta\bar{H}_{Ga}(x)+\Delta\bar{H}_{Sb}(x)}{2\Delta S^c_f(GaSb)+R\ \ell n\{a^s_{Ga}(T_m)a^s_{Sb}(T_m)\}+\Delta\bar{S}_{Ga}(x)+\Delta\bar{S}_{Sb}(x)} \qquad (19)$$

and

Table 4. Short-range order parameter and quasichemical interchange energies. (cal_{th} = 4.184J).

x_{Ga}	α	$\frac{N_o[\mu+j(x)]}{cal_{th}\cdot mol^{-1}}$	$\frac{N_o[\bar{g}]}{cal_{th}\cdot mol^{-1}K^{-1}}$	Ω/ZRT
0.039	-0.0162	-140.4	-.291	-0.216
0.293	-0.0920	-146.6	-.295	-0.222
0.500	-0.1088	-153.9	-.279	-0.218
0.639	-0.0996	-152.4	-.277	-0.215
0.833	-0.0683	-98.7	-.389	-0.245

$$T_\ell = \frac{2\Delta H_f^o(GaSb) - \Delta\bar{H}_{Ga}(x) - \Delta\bar{H}_{Sb}(x)}{2\Delta S_f^o(GaSb) - \Delta\bar{S}_{Ga}(x) - \Delta\bar{S}_{Sb}(x)} \qquad (20)$$

where $\Delta H_f^o(GaSb)$ and $\Delta S_f^o(GaSb)$ are the standard enthalpy and entropy of forming solid GaSb from the pure liquid elements, T_ℓ is the liquidus temperature and $a_{Ga}^s(T_m)$ and $a_{Sb}^s(T_m)$ are the activities of gallium and antimony in solid GaSb at the melting point. All quantities in Eqs (19) and (20) are expressed on a g-atom basis. In these equations GaSb(c) is considered an equimolar line compound, and the temperature dependence of the partial molar quantities and formation enthalpy and entropy is neglected. The liquidus temperature for the Sb-rich region then becomes

$$T = \frac{\Delta H_f^c(Sb) + \Delta\bar{H}_{Sb}}{\Delta S_f^c(Sb) + \Delta\bar{S}_{Sb}} \; . \qquad (21)$$

Tables 5 and 6 show the liquidus temperature calculated from either Eqs. (18), (19) or (20) for the five alloy compositions studied here. In these calculations the partial molar enthalpies of Predel and Stein[20] were used while partial molar entropies were obtained from our experimental results. The fusion data listed in Table 1 was used in Eq. (18).

The free energy of formation of GaSb has been previously measured with emf methods by two other investigators.[32, 33]

In order to use their results in Eq. (19), the enthalpy and entropy change for the melting of Sb had to be introduced. An

Table 5. Comparison of liquidus temperatures, (T/K) in the Ga-Sb system.

Method	x_{Ga} = 0.293	x_{Ga} = 0.500	x_{Ga} = 0.639	x_{Ga} = 0.833	Reference Source of Data for H_f^c(GaSb)/ H_f^o(GaSb)
Equation (18)	949.3	986.0	971.4	906.2	2
"	952.5	988.8	974.4	909.8	3
"	937.6	985.1	966.1	882.9	4
"	948.6	987.8	972.2	902.7	5
"	950.0	988.2	973.0	905.2	8
"	953.1	988.9	974.7	910.9	17
"	946.4	987.3	971.0	898.8	19
Equation (19)	982.9	1019.2	1004.9	940.3	32
"	974.0	1011.5	996.6	930.0	33
Experimental	952.8	985.0	970.7	895.2	14

Table 6. Comparison of liquidus temperatures (T/K) of an antimony-rich Ga-Sb alloy.

x_{Ga}	T_ℓ, Equation (20)	T_ℓ, Ideal	T_ℓ, Experimental
0.039	889.8	897.2	890.7

enthalpy of fusion value of 4750 $cal_{th} mol^{-1}$ and a melting temperature of 904 K was selected from Hultgren et al.[15]

Listed also in Table 5 for comparison is the liquidus temperature as determined by Maglione and Potier,[14] which required a small linear correction to bring their data into agreement with the accepted melting point of GaSb.

Based on the results shown in Table 5, several conclusions can be made. The accepted liquidus temperature in the Ga-Sb system is very well predicted by our activity data and the enthalpy data of Predel and Stein,[20] along with accepted data for the heat of fusion. The results obtained here show that value of $\Delta H_f^c(GaSb)$ obtained by Schottky and Bever[4] is probably too low. The results of this study are consistent with other literature data, although the measured activity for the alloy $x_{Ga} = 0.833$ appears to be a few percent low. When the calculations of T_ℓ is performed with the literature data for the GaSb formation reaction the liquidus temperatures predicted are much to high, however. Owing to the good consistency found with Eq. (18), the probable cause of this error is in the values assigned in previous studies to the enthalpy and entropy of the GaSb formation reaction. Table 6 shows the liquidus temperature calculated for an antimony-rich Ga-Sb liquid alloy. The accepted temperature is in excellent agreement with that derived from our experimental value, whereas an ideal solution model gives a large difference between the accepted and calculated liquidus temperature. This result also supports the consistency and accuracy of the present results.

F. Conclusion

Previous studies on the Ga-Sb system have concluded that the liquid alloys are either ideal[4, 14] or regular[20, 21] solutions, while direct free energy determinations have indicated that the solutions are highly non-ideal, showing strong negative deviations from ideality. The results of this study have shown the Ga-Sb system to deviate negatively, but moderately so, from Raoults' law with a significantly positive excess entropy of mixing. Other thermodynamic data for the Ga-Sb system were examined and found to give good consistency with the experimental results obtained in this study, with the exception that the reported values for the enthalpy and entropy of the GaSb(c) formation reaction did not conform with the other data.

REFERENCES

1. McGroddy, J. C., "Negative Differential Conductivity in Semiconductors," in Proceedings of the Tenth International Conference on the Physics of Semiconductors, U. S. Atomic Energy Commission, 1970.

2. Lichter, L.D., and Sommelet, P., Trans. TMS-AIME, 245, 1021 (1969).

3. Hultgren, R., Desai, P. D., Hawkins, D. T., Gleiser, M., and Kelly, K. K., Selected Values of the Thermodynamic Properties of Binary Alloys, Amer. Soc. Met. (1973).

4. Schottky, W. F. and Bever, M. B., Acta Met. 6, 320 (1958).

5. Blachnik, R., and Schneider, A,. Z. Anorg. Allgem. Chem., 372, 314 (1970).

6. Bednar, J., and Smirous, K., Czech. J. Physics, 5, 546 (1955).

7. Greenfield, I. G., and Smith, R. L., J. Metals, 7, 351 (1955).

8. Mechkovskii, L. A. Savitskii, A. A., Skums, V. F.. and Vecher, A. A., Russ. J. Phys. Chem. 45, 1143 (1971).

9. Welker, H., Physica, 20, 893 (1954).

10. Cunnell, F. A., Edmond, J. T., and Richards, J. L., Proc. Phys. Soc. (London), B67 848 (1954).

11. Blunt, R. F., Hosler, W. R., and Frederikse, H. P. R., Phys. Rev., 96, 576 (1954).

12. Welker, H., Z. Naturforsch., 8a, 248 (1953).

13. Glazov, V. M., Petrov, D. A., Izv. Akad. Nauk SSSR, Otd. Tekhn. Nauk, No. 4, 125 (1958).

14. Maglione, M. H., Potier, A., J. Chim. Phys., 65, 1595 (1968).

15. Hultgren, R., Desai, P. D., Hawkins, D. T., Gleiser, M., Kelly, K. K., and Wagman, D.D., Selected Values of the Thermodynamic Properties of the Elements, Amer. Soc. Met. (1973).

16. Hall, R. N., J. Electrochem. Soc., 110, 385 (1963).

17. Cox, R. H., and Pool, M. J., J. Chem. Eng. Data, 12 247 (1967).

18. Koster, W., and Thoma, B., Z. Metallk., 46, 291 (1955).

19. Blachnik, R., Ph. D. Dissertation, Technischen Hochschule, Clausthal (1967).

20. Predel, B., and Stein, D. W., J. Less-Common Metals, 24, 391 (1971).

21. Yazawa, A., Kawashima, T., and Itagaki, K., J. Japan Inst. Metals, 32, 1788 (1968).

22. Pong, R., M.S. thesis, "Thermodynamic Studies of Ga-In, Ga-Sb and Ga-In-Sb Liquid Alloys by Solid State Electrochemistry with Oxide Electrolytes," April (1975).

23. Danilin, V. N., and Yatsenko, S.P., Tr. Inst. Khim., Akad. Nauk SSSR, Ural. Finial No. 20, 142 (1970).

24. Gerasimenko, L. N., Kirichenko, I. V., Lozhkin, L. N., and Morachevskii, A. G., Zashchitn. Met. i Oksidyne Pokrytiya, Korroziya Metal.i Issled. v Obl. Electrokhim,. Akad. Nauk SSSR, Otd. Obshch. i Tekhn. Khim., Sb. Statei (1965) p. 236.

25. Hsi-Hsiung, C., Peng-Nien, C., and Chin-Chi, Mo., Acta. Met. Sinica, 9, 113 (1966).

26. Wicks, C. E., Block, F. E., U. S. Bur. Mines Bull. 605 (1963).

27. Chatterji, D., and Smith, D. V., J. Electrochem. Soc., 120, 889 (1973).

28. Anderson, T. J., and Donaghey, L. F., to be published.

29. Hoshino, H., Nakamura, Y., Shimoji, M., and Niwa, K., Ber. Bensenges, 69, 114 (1965).

30. Buschert, R., Gelb, I. G., and Lark-Horovitz, K., Bull. Am. Phys. Soc. Ser. 11, 1, 111 (1965).

31. Brebrick, R. F., Met. Trans., 2, 1657 (1971).

32. Siorta, N. N., Yushkevich, N. N., Khim. Svyas Poluprov. Tverd. Telakh, Akad. Nauk Belorussk. SSSR, p. 122 (1965).

33. Abbasov, A. S., Nikolskaya, A. W., Gerasimov, Ya. I., and Vasilev, V. P., Dokl. Akad. Nauk SSSR, 156, 118 (1964).

LIST OF FIGURES

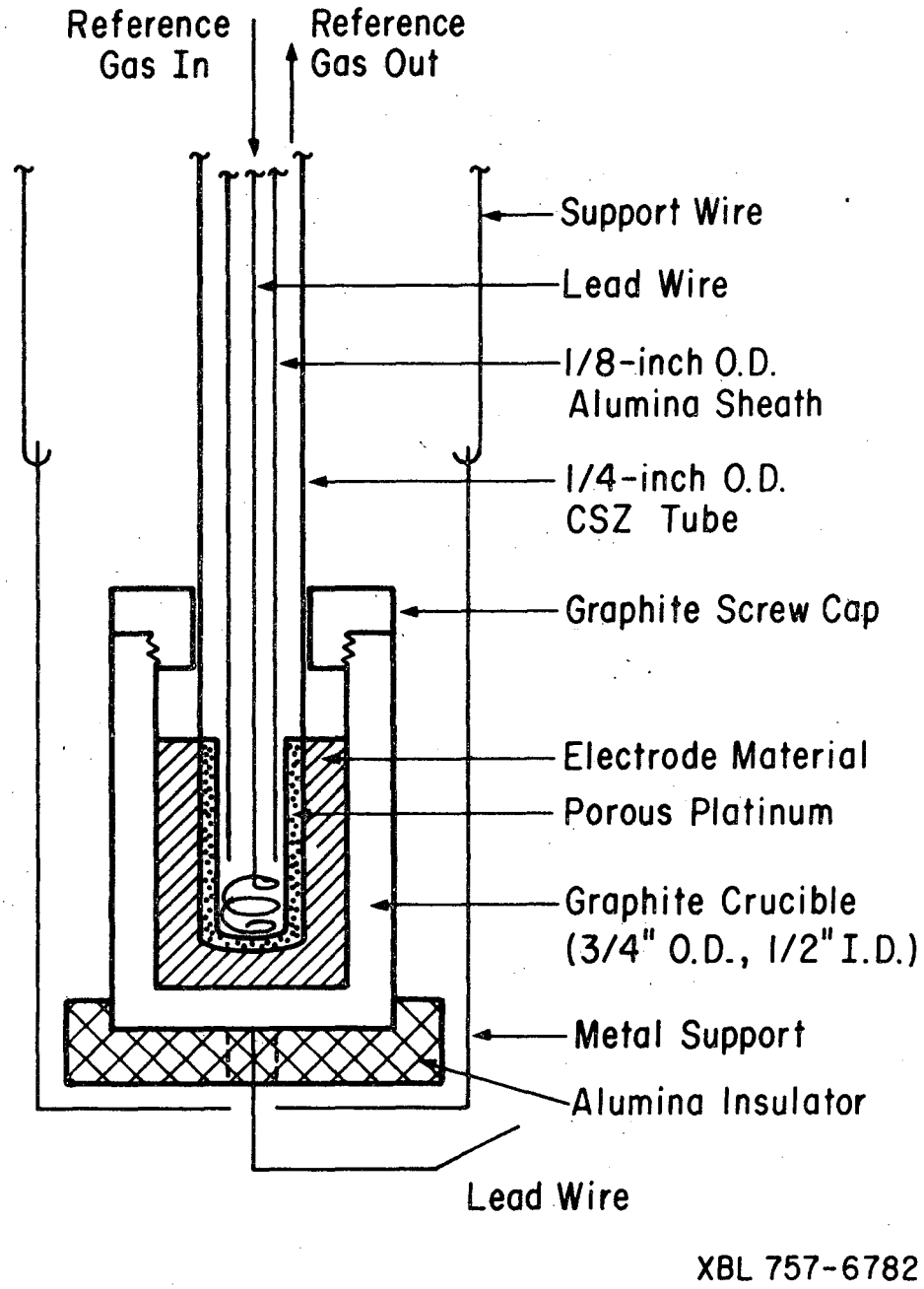
Reference Gas In
Reference Gas Out
Support Wire
Lead Wire
1/8-inch O.D. Alumina Sheath
1/4-inch O.D. CSZ Tube
Graphite Screw Cap
Electrode Material
Porous Platinum
Graphite Crucible (3/4" O.D., 1/2" I.D.)
Metal Support
Alumina Insulator
Lead Wire
XBL 757-6782

Fig. 1.

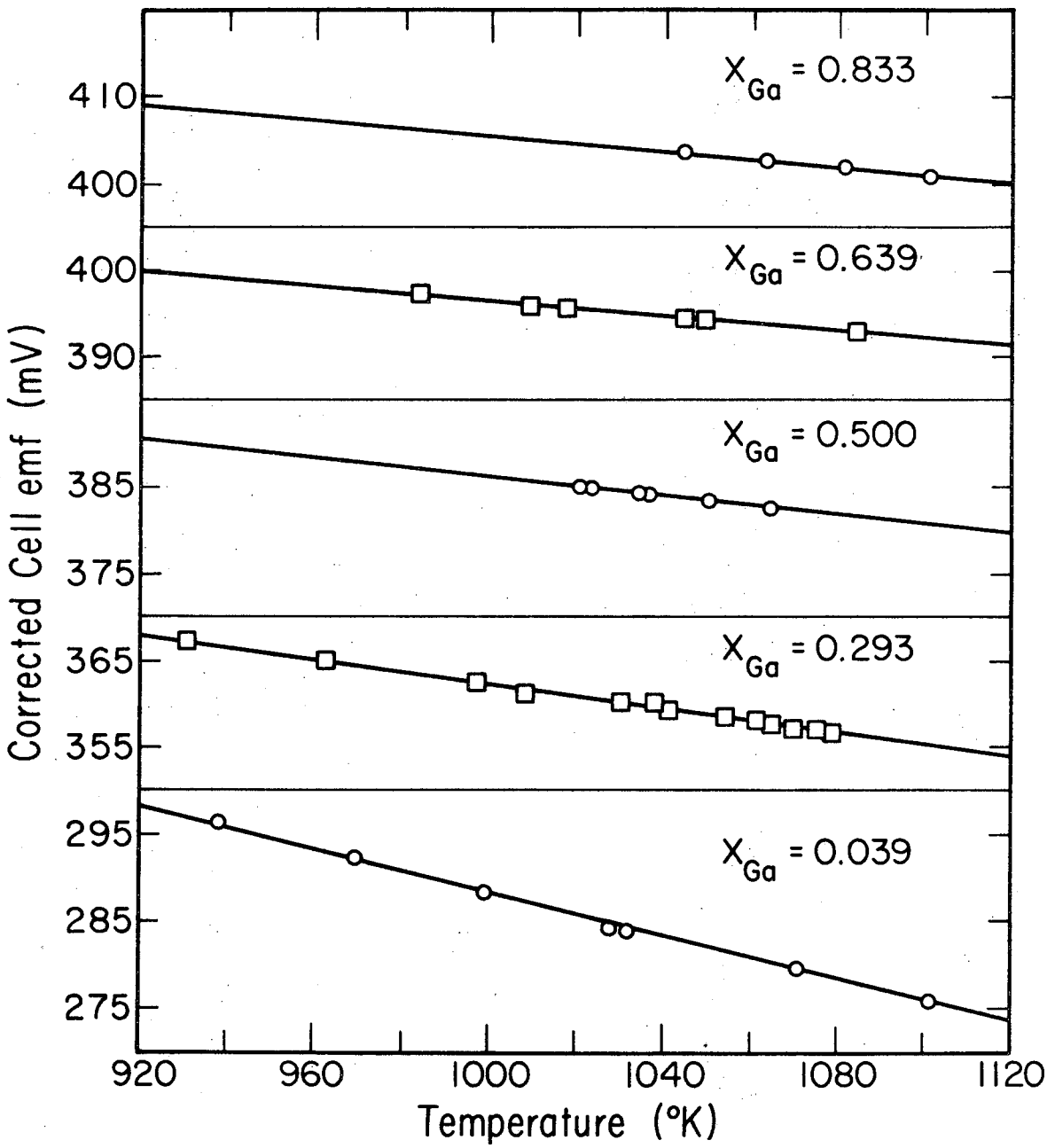

XBL 757-6794

Fig. 2.

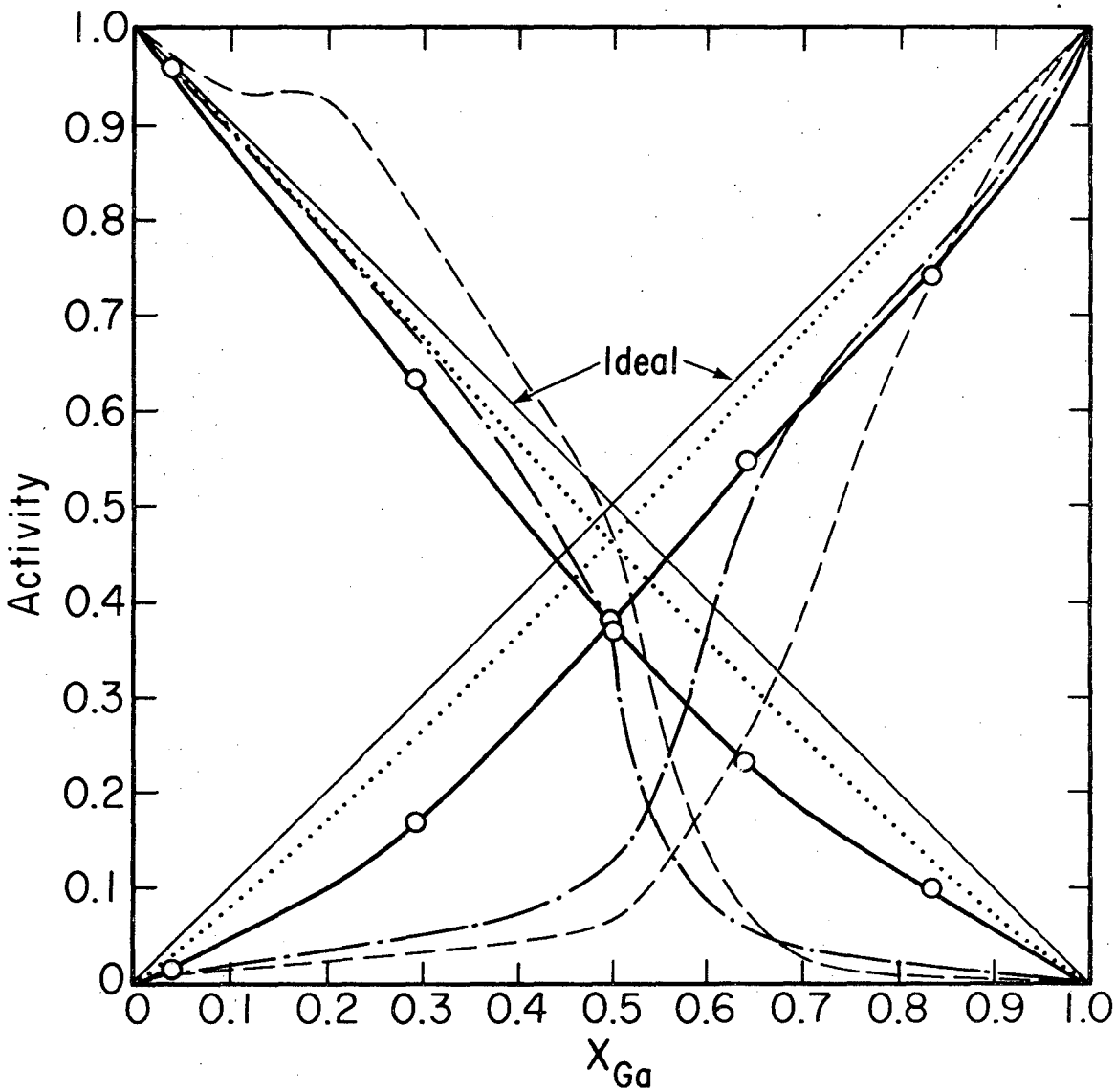

XBL 757-6788

Fig. 3.

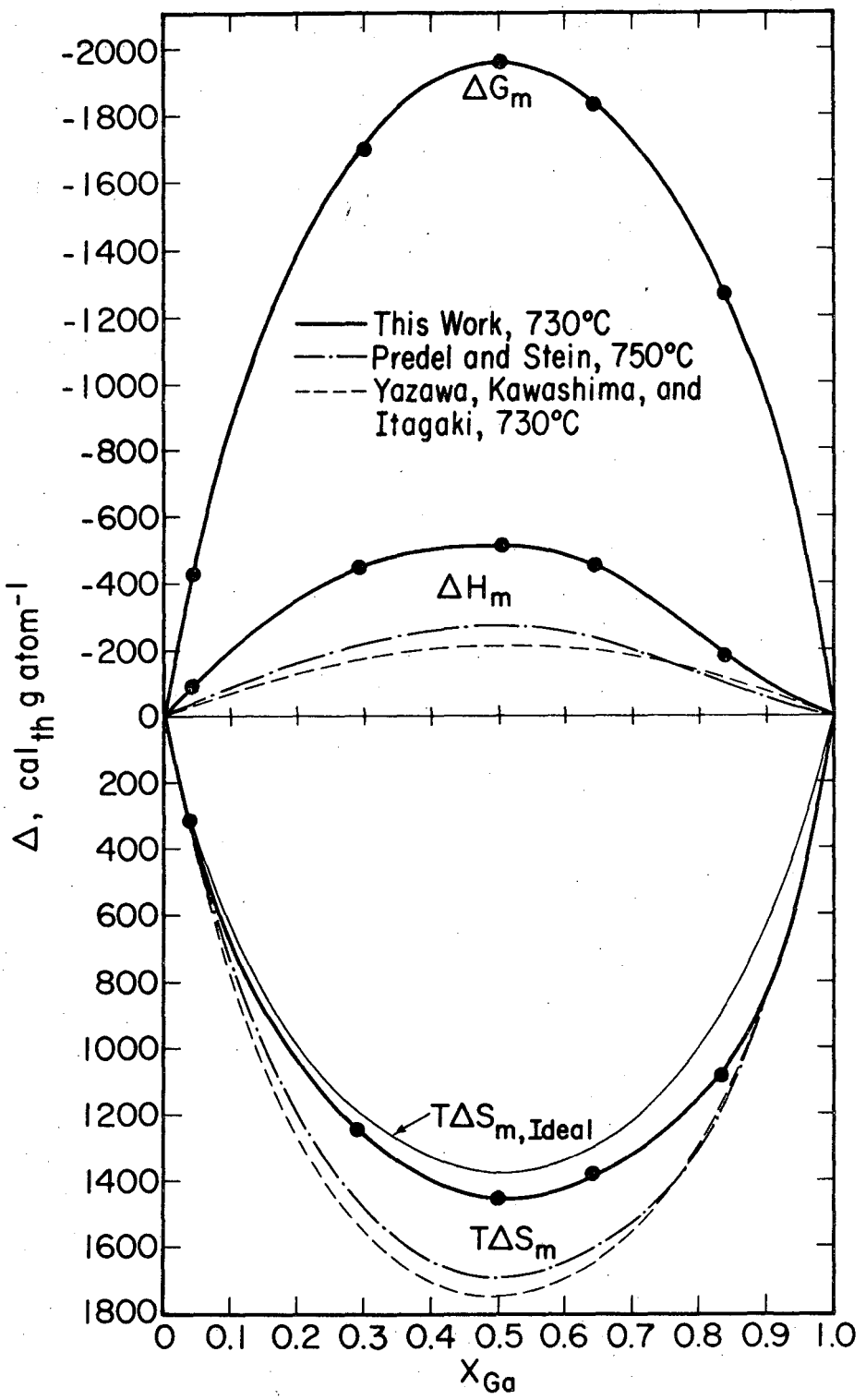

Fig. 4.

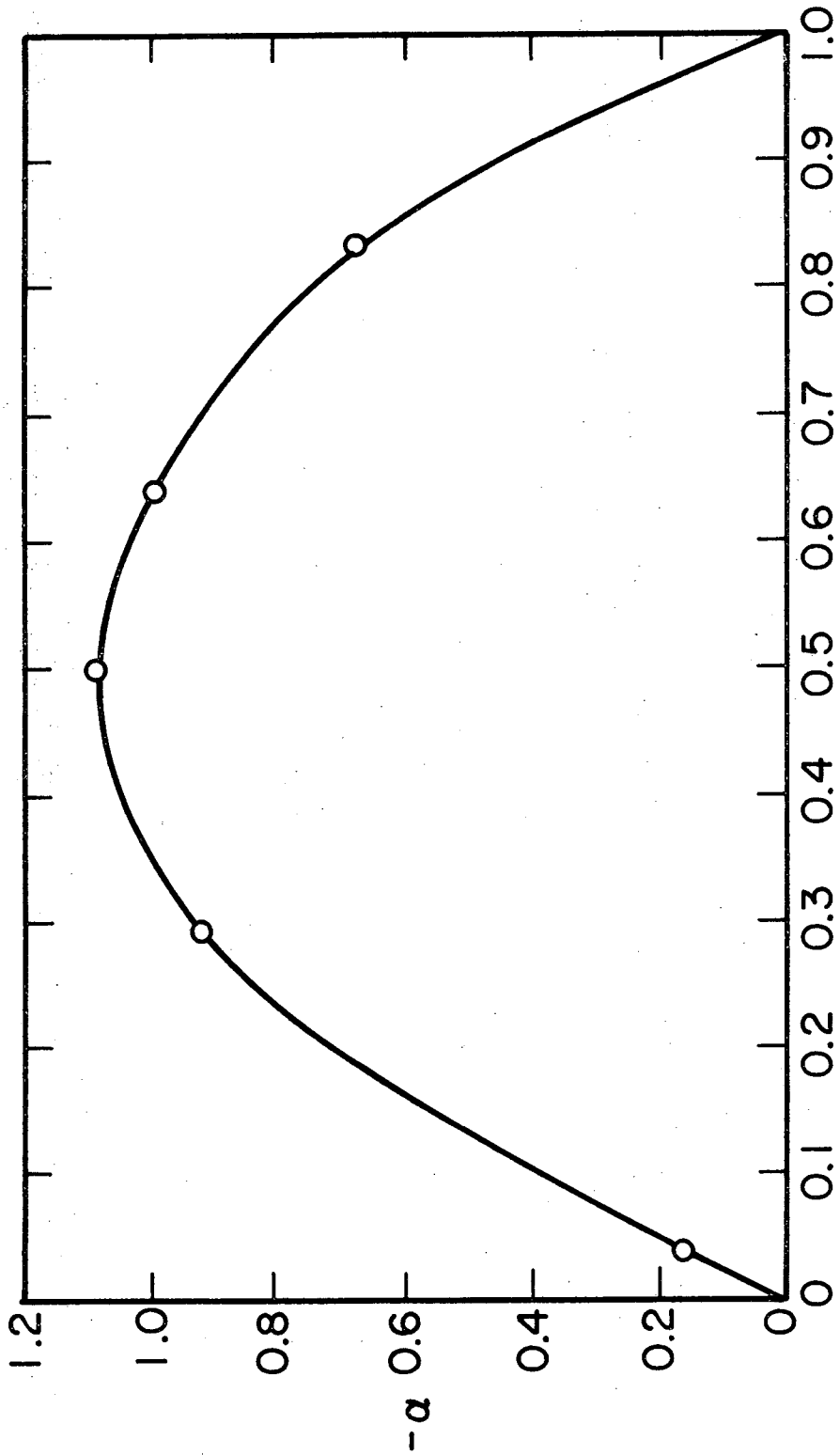

XBL 757-6792

Fig. 5.

VI. THE SOLUBILITY AND DIFFUSIVITY OF OXYGEN IN LIQUID INDIUM

A. Introduction

As a continued study of the properties of the Group III elements, the compounds formed with Group V materials, and their relationship with oxygen, the solubility and diffusivity of oxygen in liquid indium was determined. The Group III element Al has received considerable attention with respect to its relation with oxygen as a result of the important ceramic applications. Foster and Scardefield[1] have measured the solubility of oxygen in liquid gallium over the temperature range from 900 to 1200 C by a gravimetric method while the diffusivity of atomic oxygen in gallium has been determined by Klinedinst and Stevenson[4] with galvanostatic methods. To our knowledge no measurement of the solubility of oxygen in liquid indium has been performed while the only diffusivity determination is that of Klinedinst and Stevenson.[4]

A solid state coulometric titration technique was first introduced by C. Wagner[5] to study the dependence of the silver activity on the Ag/S ratio in silver sulfide. Several other investigators have employed solid oxide electrolytes to determine oxygen solubilities and diffusivities in liquid metals.[6-11] An oxygen ion conducting solid electrolyte has been used in this study to measure the oxygen diffusivity and solubility in liquid indium at a temperature of 908 K. The solubility was determined by coulometrically changing the dissolved oxygen content and measuring the resulting activity of atomic oxygen. By observing the cell potential response in a galvanostatic experiment, a diffusivity of oxygen could be determined.

B. Experimental

A schematic of the electrode arrangement used in this study is shown in Fig. 1. The electrolyte consisted of a flat closed one-end cylinder of calcia stabilized zirconia with an outside diameter of 0.95 cm. A pool of liquid indium was placed inside the electrolyte crucible which was dipped into the reference electrode mixture of indium and indium sesquioxide. The reference electrode material was contained inside an alumina crucible and electrical contact was made with tungsten wire. Once the cell was assembled it was placed in the peripheral apparatus discussed in Appendix I. Accurate data acquisition and precise timing were accomplished with the aid of a microcomputer. All other experimental equipment, procedures and materials were as summarized in Appendices I and II.

C. Theory

The electrochemical cell utilized in this study is the concentration cell,

$$W\,|In_{(\ell)}\,\|\,\underset{\text{electrolyte}}{\text{oxide}}\,\|\,In_{(\ell)}, In_2O_3\,|\,W, \qquad (1)$$

where calcia-stabilized zirconia was the solid electrolyte. If the oxygen concentration in the liquid indium electrode is less than the saturation concentration, then oxygen will diffuse through the solid oxide electrolyte - as doubly negative ions - to the indium electrode from the $In(\ell) + In_2O_3$ buffered electrode, whose oxygen activity is fixed by the two-phase equilibrium. The indium electrode thus becomes

progressively more negative as electronic charge accumulates until the diffusion of oxygen ions ceases. At equilibrium, the cell voltage is given by the Nernst equation,

$$\varepsilon = \frac{RT}{4F} \ln \frac{P_{O_2}}{P^{eq}_{O_2}} , \tag{2}$$

where P_{O_2} and $P^{eq}_{O_2}$ are the oxygen partial pressures in the In(ℓ) and In(ℓ)+In_2O_3 electrodes, respectively. Since the dependence of the equilibrium oxygen partial pressure is known, the measurement of the cell voltage is sufficient to determine the oxygen partial pressure in the liquid indium. The resulting partial pressure is

$$P_{O_2} = P^{eq}_{O_2} \exp\left(\frac{4F\varepsilon}{RT}\right) . \tag{3}$$

When the indium is undersaturated in oxygen, then ε is a negative quantity. On the other hand, when the liquid indium becomes saturated in oxygen, then the cell voltage becomes zero.

The partial pressure of diatomic oxygen in liquid indium can be established by considering the reaction for the dissolution of oxygen in liquid indium which is,

$$O_2 \rightarrow 2[O]_{In} . \tag{4}$$

For this reaction, the equilibrium constant at one atmosphere total pressure and the temperature of interest is

$$K = \frac{a^2_{[O]_{In}}}{P_{O_2}} \tag{5}$$

where $a_{[O]_{In}}$ is the activity of dissolved oxygen in liquid indium. Combining Eqs. (3) and (5) results in the following expression for the dissolved oxygen activity,

$$a_{[O]_{In}} = \sqrt{K\ P^{eq}_{O_2}}\ \exp\left(\frac{2F\epsilon}{RT}\right) \tag{6}$$

Finally, the activity of oxygen can be expressed in terms of an activity coefficient, γ_o, and the oxygen mole fraction, x_o, to give

$$x_o = \frac{\sqrt{K}}{\gamma_o}\sqrt{P^{eq}_{O_2}}\ \exp\left(\frac{2F\epsilon}{RT}\right) \tag{7}$$

Provided the term $\sqrt{K}\ /\gamma_o$ is known, the cell voltage is sufficient for determining the oxygen mole fraction in the indium electrode.

The term, $\sqrt{K}/\gamma_o$, can be determined as a function of oxygen content as follows. By applying a constant current for a known amount of time the composition of the indium electrode can be changed by an amount

$$\Delta n_o = \frac{Q}{2F} \tag{8}$$

where Q is the total charge passed. Assuming the number of moles titrated is small in comparison to the initial number moles of $[O]_{In}$ and In, Eqs. (7) and (8) combine to give

$$\frac{\sqrt{K}}{\gamma_o} = \frac{Q}{2Fn_{In}\sqrt{P_{O_2}^{eq}}} \left[\frac{1}{\exp \frac{2F\varepsilon_1}{RT} - \exp(\frac{2F\varepsilon_2}{RT})} \right] \tag{9}$$

Here, ε_1 and ε_2 represents the equilibrium cell voltage before and after the titration is performed and n_{In} is the number of moles of indium liquid present in the electrode. Thus, the term $\sqrt{k}/\gamma_o$ can be determined as a function of concentration in cell (1) and this value can be used to calculate the solubility of oxygen in liquid In.

Alternatively the solubility can be determined as follows. The change in oxygen atom fraction produced by titration is given by

$$x_{0,1} - x_{0,2} \cong \frac{n_{0,1} - n_{0,2}}{n_{In}} = \frac{Q}{2Fn_{In}} \tag{10}$$

From Eq. (7) we find

$$x_{0,1}/x_{0,2} = \frac{\gamma_{0,2}}{\gamma_{0,1}} \exp \left[\frac{2F}{RT}(\varepsilon_1 - \varepsilon_2)\right] \tag{11}$$

Combining Eqs. (10) and (11) we obtain

$$1 - \frac{\gamma_{0,1}}{\gamma_{0,2}} \exp\left[\frac{2F}{RT} (\varepsilon_2 - \varepsilon_1)\right] = \frac{Q}{2Fn_{In}x_{0,1}} \tag{12}$$

Assuming Henry's law is valid and letting state 1 represent the saturation condition Eq. (12) reduces to

$$1 - \exp\left[\frac{2F}{RT}\,\varepsilon_2\right] = \frac{Q}{2Fn_{In}x^{sat}} \tag{13}$$

Therefore a plot of $\exp(\frac{2F}{RT}\,\varepsilon_2)$ versus Q (or It) should yield a straight line of slope $-1/(2Fn_{In}x^{sat})$ thus allowing the calculation of a saturation solubility.

D. Results

Electrochemical titrations were performed on the electrochemical cell (1). Listed in Table 1 are the equilibrium cell potentials measured before and after the titration of this cell operating at a temperature of 908 K. In each titration a constant current of 50 μA was put across the cell for a period of 30 min. Also given in Table 1 is the term $\sqrt{K}/\gamma_o$, which was caluclated from Eq. (9). The value of $P_{O_2}^{eq}$ was calculated from the Gibbs free energy of the reaction

$$2In(\ell) + \frac{3}{2}\,O_2(v) = In_2O_3(c) \tag{14}$$

The reference oxygen partial pressure is thus given by

$$P_{O_2}^{eq} = \exp\left(\frac{\Delta G^o(14)}{1.5\ RT}\right) \tag{15}$$

where $\Delta G^o(14)$ was taken from Chapter IV as

Table 1. Titration of oxygen into liquid indium results.

Equilibrum emf (mV) before titration	Charge transferred into indium Electrode (Coulombs)	Equilibrium emf (mV) after titration	$\frac{\sqrt{K}}{\gamma_o}$ $\times 10^{-9}$
- 0.99	+0.045	- 0.17	1.60
- 0.32	-0.045	- 1.04	1.82
-52.64	-0.09	-55.94	3.13
-55.94	-0.09	-60.44	2.53
-60.44	-0.09	-62.55	5.88
-62.55	-0.09	-64.80	5.83
-64.80	-0.09	-67.92	4.51
-67.92	-0.09	-72.12	3.67
-72.12	-0.09	-75.42	5.15
-75.42	-0.09	-79.23	4.88
-79.23	-0.09	-81.64	8.36
-81.64	-0.09	-85.30	5.95
-85.30	-0.09	-89.50	5.73

$$\Delta G^{o}(14) = 223.16 + 7.947\times10^{-2}T \text{ , } kcal_{th}\,mol^{-1} \text{ .} \qquad (16)$$

Shown in Fig. 2 is a typical response of the cell voltage to the applied current both during the actual titration and the following approach to the new equilibrium value.

E. Discussion

Upon examination of Table 1 it is observed that the term $\sqrt{K}/\gamma_o$ is nearly constant with respect to the dissolved oxygen content. Each titration resulted in oxygen mole fraction changes of $x_{[O]_{In}} = 5\times10^{-5}$. The fact that this term is constant implies that the oxygen activity varies linearly with the oxygen mole fraction or that Henry's law is applicable as is usual in most dilute metal solutions. This is especially apparent when the oxygen content is far from the saturation value. Using a mean value of 5×10^{9} for $\sqrt{K}/\gamma_o$ allows the solubility of oxygen in liquid indium at 908 K to be calculated from

$$x_{[O]_{In}} = \frac{\sqrt{K\,P_{O_2}}}{\gamma_o} = 5\times10^{9}\sqrt{P_{O_2}} \text{ .} \qquad (17)$$

The solubility of oxygen in indium at saturation was found to be $x_{[O]_{In}} = 1.2\times10^{-3}$, which was calculated using a value of $\sqrt{K}/\gamma_o = 1.6\times10^{9}$ since this was found when the cell voltage was nearest to zero or saturation. Unfortunately these measurements were performed at only one temperature thus not permitting the temperature dependence of $\sqrt{K}/\gamma_o$ to be found. It is possible to estimate the standard Gibbs free energy of reaction Eq. (4) with the data as found here. Expressing the equilibrium constant, K, in terms of its standard Gibbs free energy change and combining this with Eq. (7) gives

$$\Delta G^{o}(4) = 4FE - RT \ln \left[\frac{[\%O]}{P^{eq}_{O_2}}\right]^2 - 2RT \ln f_o \cdot \qquad (18)$$

Here, the oxygen standard state is taken as 1 atm and the oxygen activity is given by the product of an activity coefficient, f_o, and the weight percent of dissolved oxygen, [% O]. In the limit that the oxygen weight percent goes to zero the oxygen activity coefficient goes to unity thus eliminating the last term in Eq. (18):

$$\Delta G^{o}(4) = \lim_{[\%\,O]\to 0} \{4FE - RT \ln [\frac{[\%\,O]^2}{P^{eq}_{O_2}}]\} \cdot \qquad (19)$$

Thus by plotting the bracketed term in the above equation versus the oxygen content, [% O], $\Delta G^{o}(4)$ can be found by extrapolation. The oxygen weight percent can be measured from the total titration current provided the titration was started at the onset of saturation (approach to zero cell voltage) and the saturation solubility is known. On the other hand, if Henry's law is assumed to hold at very small mole fraction the resulting plot will be horizontal at the value of $\Delta G^{o}(4)$ given by

$$\Delta G^{o}(4) = 2RT \ln \left[\frac{\sqrt{K}}{\gamma_o} \frac{M.W.(O)}{M.W(In)}\right] \qquad (20)$$

where M.W.(O) and M.W(In) are the molecular weights of atomic oxygen and indium, respectively. The small mass of the dissolved oxygen relative to the indium was neglected.

Using an average value of $\sqrt{K}/\gamma_o = 5.056\times10^9$ (obtained by averaging all data except the first two listings of Table 1) results in $\Delta G^o(4) = (73.5\pm2.4)$ $kcal_{th}mol^{-1}$. For more concentrated solutions the oxygen activity coeffecient will deviate from unity and can be calculated by using Eq. (18). When the value of K determined is combined with the average $\sqrt{K}/\gamma_o$, γ_o is found to be 0.138.

Shown in Fig. 3 is a plot of $\exp(\frac{2F\epsilon}{RT})$ vs the differential charge titrated. If Henry's law is applicable the plot should be linear with a slope inversely proportional to the saturation solubility and have an intercept of unity. Good linearity was found in the less concentrated solutions with non-linearity at higher oxygen content. Thus either the Henry's law constant varies with [% O], or the first three titrations were in error. Assuming the latter to be true yields a saturation solubility of $x_o^{sat} = 3.3\times10^{-3}$. The x-axis in Fig. 3 is arbitrary because titration was not started at saturation. Thus the intercept is not useful to determine the accuracy of the early data. But an examination of the extrapolated intercept and the results of the titrations performed near saturation suggests that the data of the early titrations are in error. The value of x_o^{sat} found agrees well with that found by extrapolating with the response curve.

By monitoring the cell potential during a titration experiment it is possible to extract kinetic data. In this galvanostatic experiment charge-carrying oxygen ions are transferred across the solid electrolyte with oxidation occuring at the positive cell electrode and reduction at the negative electrode. Several mechanisms for oxygen transfer between the electrodes are operative while

usually one step is rate limiting. If the redox reaction rate is controlled by the adsorption or desorption of neutral oxygen atoms then the electrical potential is nearly independent of time[2] and in contradiction with our results. An assessment of other mechanisms indicates that the rate-limiting step is the diffusion of oxygen in liquid indium.[3,4] Thus the diffusion coefficient of atomic oxygen in liquid indium can be ascertained from the data presented in Fig. 2.

During the passing of the constant current, I, the measured potential, ε is given by

$$\varepsilon - \varepsilon_o + IR_o = \frac{RT}{4F} \ln \{P_{O_2}/P^{eq}_{O_2}\} \tag{21}$$

where ε_o is the equilibrium cell voltage before the titration and R_o is the ionic electrolyte resistance.

The solution of the diffusion equation for one dimensional oxygen diffusion out of a semi-infinite indium specimen with the initial condition

$$x_o = x_o(t_o) \quad z \geq 0, \; t = 0$$

and the boundary conditions

$$x_o = x_o(t_o) \text{ for } z = \infty, \qquad t > 0$$

$$\left(\frac{\partial x_o(z,t)}{\partial z}\right)_{z=0} = \frac{I\, V_{In}}{2FAD_o} \quad \text{for} \quad t > 0$$

and evaluated at the electrode - electrolyte interface, z = 0, is given by

$$x_o(t) = x_o(t_o) - \frac{V_{In} I t^{1/2}}{FA\pi^{1/2} D_o^{1/2}} \quad . \tag{22}$$

Here, V_{In} is the indium molar volume, A the interfacial surface area and D_o the oxygen diffusivity. Eqs. (21), (22), and (5) can be combined to give

$$\varepsilon(t) + IR_o - \varepsilon_o = RT/2F \ \ell n \left\{ \frac{\gamma_o}{\sqrt{K P_{O_2}^{eq}}} \left(x_o(t_o) - \frac{V_{In} I t^{1/2}}{FA\pi^{1/2} D_o^{1/2}} \right) \right\} . \tag{23}$$

Therefore a plot of $\frac{\sqrt{K P_{O_2}^{eq}}}{\gamma_o} \exp\left[\frac{2F}{RT} (\varepsilon(t) + IR_o - \varepsilon_o)\right]$ versus $-It^{1/2}$ should yield a straight line of slope $V_{In}/FA\pi^{1/2} D_o^{1/2}$ and intercept $x_o(t_o)$.

Figure 4 shows such a plot from which an oxygen diffusivity of 2.2×10^{-6} cm^2 sec^{-1} was determined. This value is in good agreement with the value of Klinedinst and Stevenson[4] of $(7.6 \pm 4.7)\ 10^{-7}$ who used the potentiostatic method with cylindrical geometry. The extrapolated value of $x_o(t_o)$ was 1.05×10^{-3}. The errors involved in these results include those associated with the measured emf, the determined $\sqrt{K}/\gamma_o$, and R_o, the fact that the electrode was not a semi-infinite medium, and the possibility of radial diffusion.

F. Conclusion

The results presented show that oxygen follows Henry's law when

dissolved in liquid indium at low concentrations. At concentrations more near to saturation it could not be shown that the solution is Henrian in nature. Further work on this system should involve both galvanostatic and potentiostatic measurements at several temperatures. The preferred geometry should be cyclindrical because of ease of electrode separation and because an independent measurement of the diffusion coefficient can then be made which does not require solubility data.

REFERENCES

1. L. M. Foster and J. Scardefield, J. Electrochem. Soc., 116 304 (1973).

2. K. Goto and W. Pluschkell, Physics of Electrolytes, Vol. 2, J. Hladik, ed., Academic Press, 1972.

3. L. F. Donaghey and R. Pong, to be published.

4. K. A. Klinedinst and D. A. Stevenson, J. Electrochem. Soc., 120, 304 (1973).

5. C. Wagner, J. Chem. Phys., 21, 1819 (1953).

6. C. B. Alcock and T. N. Belford, Trans. Taraday Soc., 60, 822 (1964).

7. T. N. Belford and C. B. Alcock, Trans. Faraday Soc. 61, 443 (1965).

8. J. Gerlach, J. Osterwald and W. Stichel, Z. Metallk., 59, 576 (1968).

9. J. Osterwald and G. Schwarzlose, Z. Physik. Chem., 62, 119 (1968).

10. H. Richert and A. Elmiligy, Z. Metallk., 59, 635 (1968).

11. R. L. Pastorek and R. A. Rapp, Trans. Met. Soc. AIME, 245, 1711 (1969).

LIST OF FIGURES

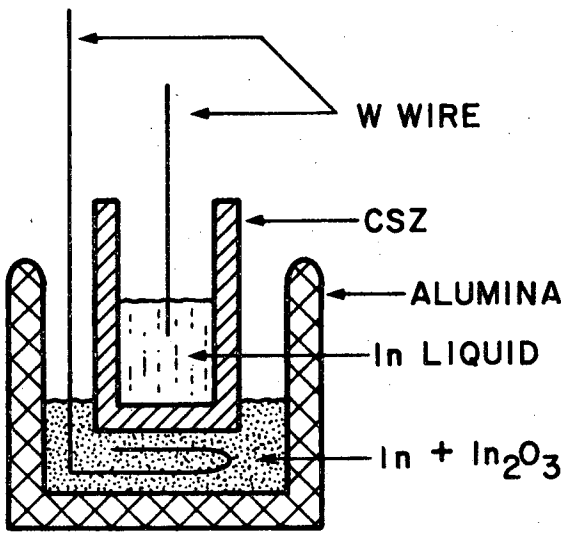

XBL 757-6796

Fig. 1.

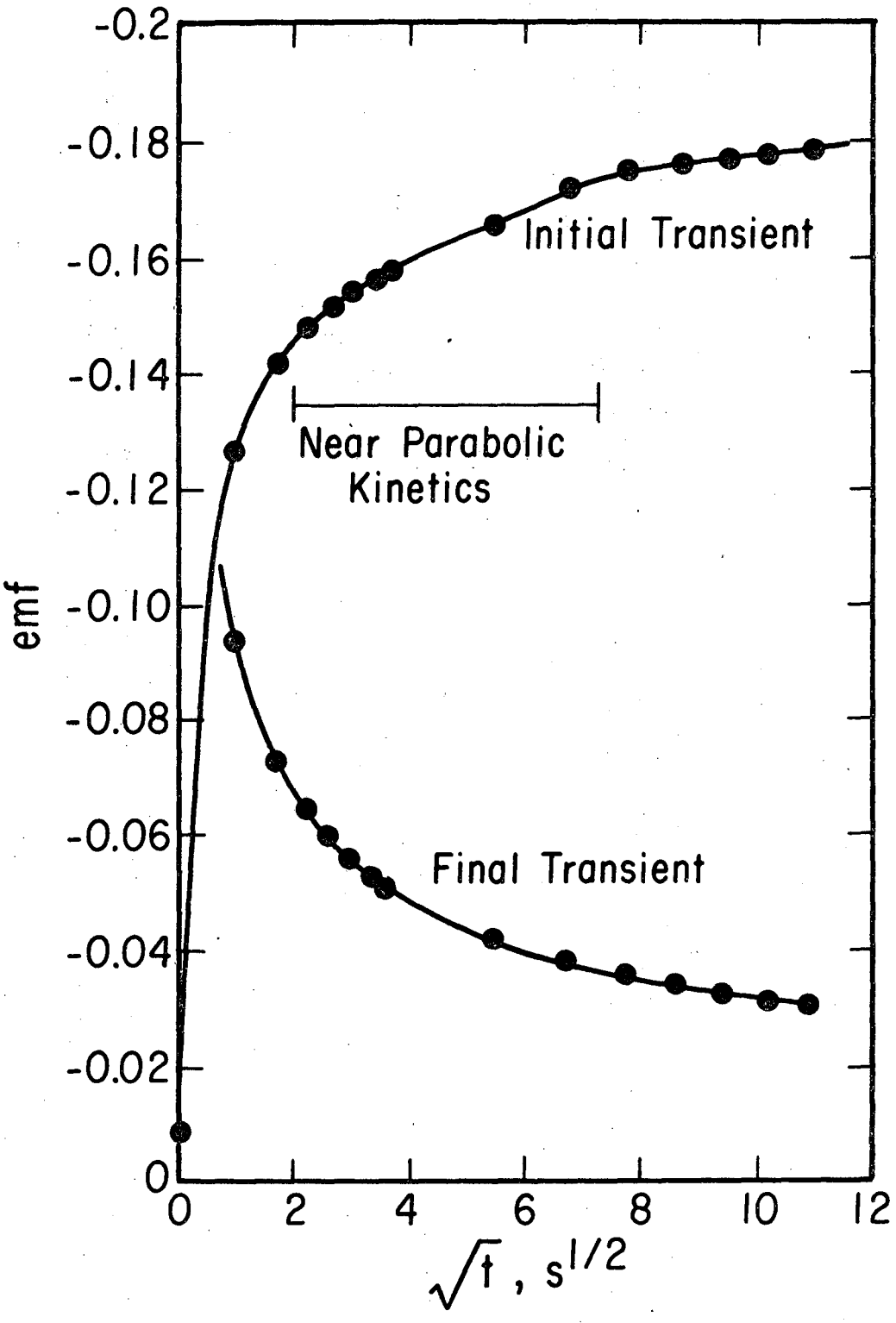

XBL 757-6795

Fig. 2.

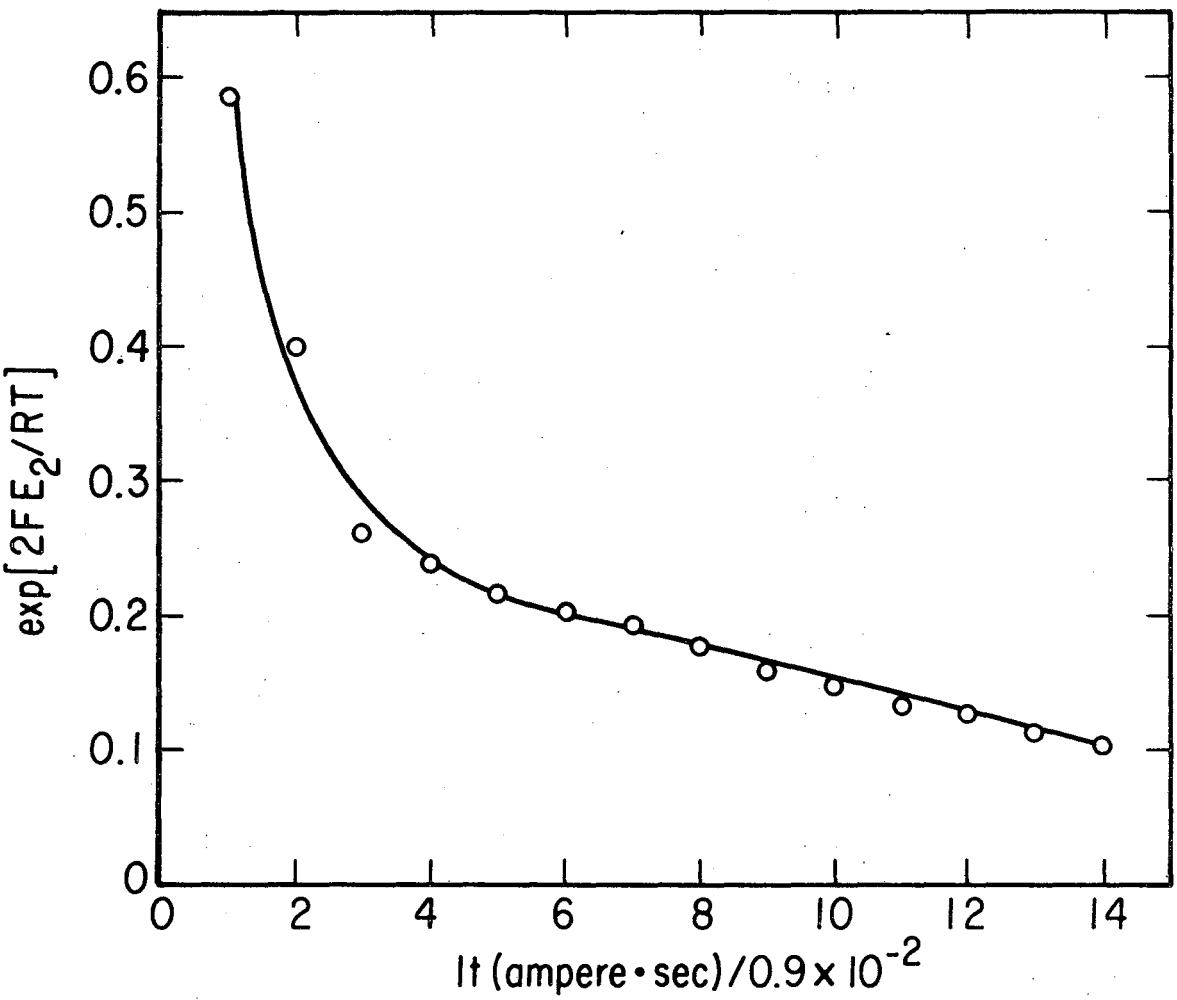
0.6
0.5
0.4
0.3
0.2
0.1
0
exp[2FE2/RT]
0
2
4
6
8
10
12
14
It (ampere • sec)/0.9 x 10-2
XBL 657-6798

Fig. 3.

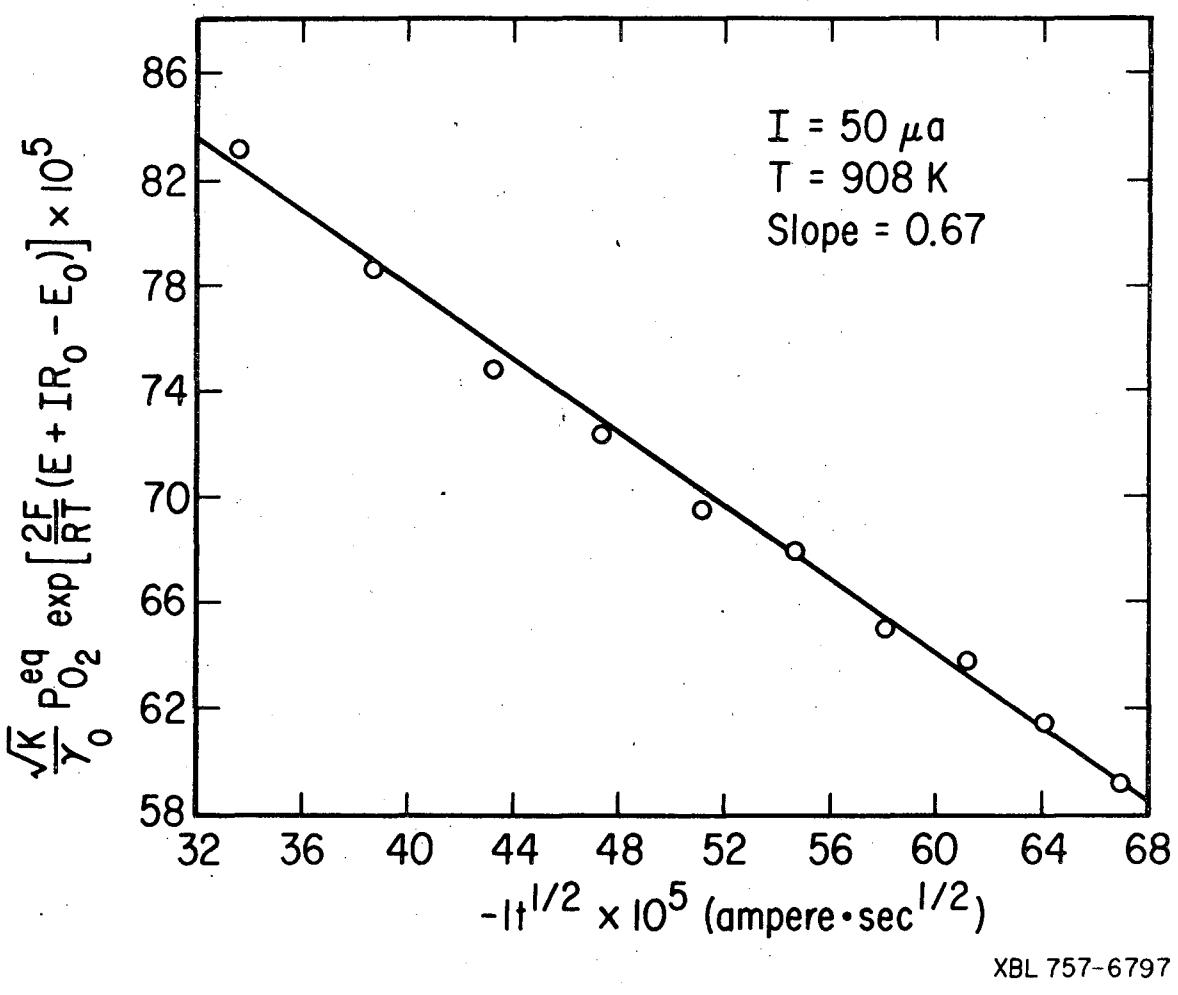

XBL 757-6797

Fig. 4.

VII. SOLID-STATE GALVANIC CELLS CONDUCTIVE TO FLUORINE

A. Introduction

Thermodynamic and kinetic measurements with the use of a CaF_2 solid electrolyte greatly enhance the range of applicability of galvanic cell measurements to Group III and V semiconducting compounds. Only two thermodynamic studies of III-V compounds employing CaF_2 as the solid electrolyte are known. Samokhaval' and Vetcher[22] measured the free energy of formation of solid AlSb from 718 to 896°K in the following galvanic cell,

$$Mo|graphite|Al,CaAlF_5,CaF_2||CaF_2||AlSb,Sb,CaAlF_5,CaF_2|graphite|Mo. \quad (1)$$

The equilibrium mixture of Al, $CaAlF_5$, CaF_2 was used to prevent the reaction,

$$2Al + AlF_3 \rightleftharpoons 3AlF. \quad (2)$$

The free energy of formation determined was found to be in good agreement with data taken on a molten salt galvanic cell. In 1969, Samokhval studied solid solutions of AlSb - GaSb in the cell,

$$AlSb,Sb,CaAlF_5,CaF_2|CaF_2||Al,Ga|Sb,Sb,CaAlF_5,CaF_2 \quad (3)$$

at 850K. The overall cell reaction was

$$AlSb \rightleftharpoons AlSb(\text{in solid solution}). \qquad (4)$$

Strong negative deviations from ideality were found in the AlSb activity in the solid solution.

A discussion of the possible applications of CaF_2 is given in Chapter VIII. Presented here are results of studies on cells designed to determine the Gibbs free energy of formation for the fluorides of Al, In and Ga along with that of solid GaSb. As a test for the experimental apparatus a well known galvanic cell was first studied.

B. The Gibbs Free Energy of the Reaction $Mg + NiF_2 \rightarrow MgF_2 + Ni$

1. Introduction

In order to test the reliability of the CaF_2 solid electrolyte galvanic cell a well defined cell arrangement was first investigated. The cell employed consisted of two coexistence electrodes and had the following configuration:

$$Ta|Mg,MgF_2||CaF_2||Ni,NiF_2|Ni\ , \qquad (5)$$

with the cell reacting as follows:

$$Mg + 2F^- \rightarrow MgF_2 + 2e^- \quad \text{(left)} \qquad (6)$$

$$NiF_2 + 2e^- \rightarrow Ni + 2F^- \quad \text{(right)} \qquad (7)$$

$$Mg + NiF_2 \rightarrow MgF_2 + Ni \quad \text{(overall)} \qquad (8)$$

The Gibbs free energy of the above overall reaction is given by

$$\Delta G_4^o = -nFE. \qquad (9)$$

where E is the measured cell potential, F the Faraday constant and n the number of equivalents.

This electrode arrangement is particularly suited as a test cell for several reasons. The displacement reaction has a well known Gibbs free energy change, with experimental data from both calorimetric[8,9, 13-17] and galvanic methods.[1, 3, 5, 18] The use of the Mg and MgF_2 coexistence electrode is a good test of the performance of the CaF_2 single crystal due to the very reducing nature of this element. Furthermore, since Mg is a relatively volatile metal (vapor pressure of 10^{-3} atm at 857 K), electrode containment devices are thoroughly verified.

2. Experimental

A general description of the experimental apparatus, procedures and materials can be found in Appendices I and II. Three different cell arrangements were tested and, are depicted in Fig. 1. The first half electrode was prepared by mixing powdered Mg and MgF_2 in a 2:1 volume ratio. CaF_2, still in the powdered form, was then placed on the top of the metal-metal fluoride in a Ta crucible and pressed at 20 tons/in^2 forming a CaF_2 cap that extended a few millimeters above the Ta surface. The second half cell was prepared

by first pressing a pellet of the metal-metal fluoride of approximately 3/8" diameter followed by pressing CaF_2 on all sides (with the bottom excepted) thus forming a more complete seal. The third arrangement consisted of placing the powdered electrode material into a spiked top Ta crucible with gravity forming the electrolyte-electrode interface. A photograph of this cell is shown in Fig. 2. The Ta crucible edge was sealed to the single crystal by the force of the spring loaded pushrod. As a further step quartz wool was placed around the outside perimeter of the crucible. The CaF_2 single crystal used here had a larger diameter (1 in x 2 mm versus 1/2 in. x 2 mm). The Ni-NiF_2 electrode was prepared in the same manner as the Mg-MgF_2 electrode for run 1. In all cases the electrodes were electrically insulated by Al_2O_3 cups and the lead wires were made of the same material as the crucible. The six half cells were each annealed in vacuum at 600°C for a period of 24 hours to promote a fast approach to equilibrium. All other experimental techniques were as discussed in the general experimental procedure [Appendix I].

3. Results

The first electrode design failed as a result of a vapor leak in the Mg electrode. During operation of the cell, Mg had coated the entire cell area. Electrical shorts were found across the ceramic insulators and around the single crystal. In conjunction with the electrical shorting the cell could have also failed as a result of fluorine transport around the cell. The second cell also shorted through a thin film resistor formed from a vapor deposit. The cell voltage

peaked at 1.6 volt after a period of 12 hours with a subsequent steady decay in voltage. Potentiostatic titrations were attempted but did not result in an equilibrium cell potential. The electrode design of the third cell proved to operate the most effectively. Fig. 3 shows the initial cell voltages as a function of time at 820 K. Though this temperature is on the lower end of the CaF_2 electrolyte operating temperature, the lower setting depressed vapor leakage rates and thus enhanced the cell lifetime. Equilibrium was induced by titrating the cell with a constant potential, and observing the emf decay. Such experiments were carried out at various voltages for several different time periods with the results being reproducable. This technique is useful to insure equilibrium by titrating in both directions and also has been used when an inherent emf decay is taking place.[19] A typical decay curve is depicted in Fig. 4. The initial fall in voltage can be attributed to the IR drop across the cell followed by the exponential portion due to a diffusion overpotential. The equilibrium portion of the curves had a small decay slope due to either electrical or fluorine short circuiting. In one experiment the cell emf remained for a period of 1 hour at a value of 2.341 volts. After 1 week of operation, the cell was completely shorted. After each run the electrode material was analysed by X-ray diffraction, and no side reaction products were detected.

4. Discussion

Table 1 summarizes the literature values of the emfs obtained for this galvanic cell. This data is shown graphically in Fig. 5 along with the cell emf found in this experiment. It is seen that the value obtained agrees very well with the literature values.

Electrode containment proved to be a major problem in the use of CaF_2 as a solid electrolyte. A closed type of arrangement would be preferable to the open cell used but tubes made from single crystal CaF_2 are unavailable. Two different cell designs for those electrode compositions were reported in the literature. Both types were attempted in this work (runs 1 and 3) but a stable operating cell was not found.

C. Other Fluoride Galvanic Cells

1. Introduction

The solid electrolyte CaF_2 was used to measure the free energy of formation of the Group III metal fluorides, $M_{III}F_3$, in the following cell,

$$Ni|Ni,NiF_2||CaF_2||M_{III},\ M_{III}F_3|C|Pt \qquad (6)$$

here the overall cell reaction is

$$M_{III} + NiF_2 = M_{III}F_3 + Ni. \qquad (7)$$

The free energy of forming the metal fluoride can be found from

Table 1. Literature emf values for check cell.

Cell Voltage (mV)	Temp. Range, °K	Voltage At 873°K	Ref.
Calvanic Cell Method			
1. $E = 2315(\pm 11.9)+0.002(\pm 0.014)\cdot T$	751-919	2316	1
2. $E = 2290(\pm 10)$	873.16	2290	3
3. $E = 2343$	873.16	2343	5
4. $E = 2407.8-0.0765\cdot(T)$	725-913	2341	18
Calorimetric Methods			
5. $E = 2432.9-0.5214\cdot T-2.60\times 10^{-5}\times T^2+2.664\times 10^2/T^2+0.06576\cdot T \ln T$	630-919	2346.6	8,9* 13-17
Estimated			
6. $E = 2314-0.247\cdot(T)$	298-923	2098	4
7. $E = 2360.4-0.1724\cdot(T)$	298-923	2210	2
8. $E = 2311-0.188\cdot(T)$	298-923	2147	7
9. $E = 2305-0.102\cdot(T)$	500-923	2216	6

* S^o_{298} for Ni, F_2, and Mg from Ref. 15. S^o_{298} for NiF_2 from Ref. 16. S^o_{298} for MgF_2 from Ref. 17. C_p for Ni, F_2, MgF_2 from Ref. 13. C_p for NiF_2 from Ref. 14. $\Delta H^{formation}_{298}$ for NiF_2 from Ref. 9. $\Delta H^{formation}_{298}$ for MgF_2 from Ref. 8.

$$\Delta G^{o}_{\text{formation, } M_{III}F_3} = 3/2\ \Delta G^{o}_{\text{formation, } NiF_2} - 3FE \qquad (8)$$

the free energy of forming 3/2 NiF_2 was taken as $-234{,}750 + 49.5T$ cal_{th} mol^{-1}.[20] The Group III metal fluorides were gallium, indium and aluminum. Five different electrode designs were tried with both gallium and aluminum and two with indium.

A cell designed to measure the free energy of formation for solid GaSb was also constructed and can be schematically represented as

$$Pt|C|Ga,GaF_3||CaF_2||Sb,\ GaSb,\ GaF_3|C|Pt \qquad (9)$$

The overall cell reaction is the formation reaction and the cell emf is directly related to its Gibbs free energy,

$$\Delta G^{o}_{\text{formation, GaSb}} = -3FE. \qquad (10)$$

Two cell arrangements were attempted.

In all the cells operated a stable and reproducable cell potential could not be obtained, though the emf's observed showed the correct sign and were close to those expected.

2. Experimental

A description of the general experimental apparatus and procedure can be found in Appendix I while the materials used are listed in Appendix II. The possibility of the intermetallic, $M_{III}CaF_2$,

forming at the electrode interface was investigated by heating an intimate mixture of the metal fluoride and CaF_2 to a temperature above the highest operating one. The material was then analyzed by x-ray diffraction and no intermetallic phases were found for either gallium or indium but one was found for aluminum. Crucible materials were selected so as not to dissolve the electrode material.[10-12]

3. Discussion

Though successful CaF_2 cells have already been reported in the literature, (see 21), no concrete results were found when using the open cell arrangement outlined. It is believed that the main reason for the unstable results of these cells was a vapor deposit short circuiting the cell around the electrolyte and vapor flourine transport between the two electrodes. Attempts were made to titrate to an equilibrium value in emf but no reproducible results could be reached.

Several variations of the basic cell design were explored in these measurements. Sealing of the electrodes compartments were tried with the application of a zirconia paste and also by wrapping with quartz wool. A fluorine getter of tantalum was placed near the electrodes. In another cell an alumina tube was placed around the top electrode and placed on the CaF_2 electrolyte thus forcing the inert gas stream to pass through the upper cooler region before contacting the lower electrode. Lava insulators were placed in series with the guy wire to prevent shorting to the cell head. Both pelleted and powdered forms of the electrode materials were used.

It can be concluded that the open cell configuration employed in these studies is very difficult to operate due in part to the high vapor pressures of the materials involved (especially of the metal fluorides). In future studies it is recommended that a closed type of cell be used. Here, the two electrodes should be separated completely with separate inert gas purges to each electrode.

REFERENCES

1. W. H. Skelton and J. W. Patterson, J. Less-Common Metals, 31, 47-60 (1973).
2. E. Steinmetz and H. Roth, J. Less-Common Metals, 16, 295 (1968).
3. R. J. Huess and J. J. Egan, Z. Phys. Chem., 49, 38 (1966).
4. W. J. Hammer, M. S. Malmberg and B. Rubin, J. Electrochem. Soc., 112, 750 (1965).
5. T. L. Markin, R. J. Bones and V. J. Wheller, Proc. Brit. Cer. Soc. 8,51 (1967)
6. L. Brewer, L. A. Bromeley, P. W. Gilles and N. L. Lofgren, in The Chemistry and Metallurgy of Miscellaneous Materials, (McGraw-Hill, New York, 1950) p. 76.
7. C. E. Wicks and F. E. Block, U. S. Bur. Mines Bull. 605 (1965).
8. E. Rudzitis, H. M. Feder and W. N. Hubbard, J. Phys. Chem. 68, 2978 (1964).
9. E. Rudzitis, E. H. Van Deven and W. N. Hubbard 12, 133 (1967).
10. M. Hansen and K. Aderko, Constitution of Binary Alloys, 2nd edition, (McGraw-Hill, New York, 1958).
11. R. P. Elliott, Constitution of Binary Alloys, first supplement, (McGraw-Hill, New York, 1965).
12. F. A. Skunk, Constitution of Binary Alloys, second supplement, (McGraw-Hill, New York, 1969).
13. O. Kubaschewski and E. L. Evans, Metallurgical Thermochemistry, (Permagon, Oxford, 4th ed. 1967).

14. J. S. Binford and T. H. Herbert, J. Chem. Thermo. 2, 407 (1970).

15. R. Hultgren, P. D. Desai, D. T. Hawkins, M. Gleiser, K. K. Kelley and D. P. Wagman, Selected Values of Thermodynamic Properties of the Elements, 1973.

16. E. Catalano and J. W. Stout, J. Chem. Phys., 23, 1284 (1955).

17. K. K. Kelley and E. G. King, U. S. Bur. Mines Bull. 592 (1961).

18. N. L. Lofgren and E. J. McIver, U.K.A.E.A. Report AERE-R5169.

19. C. M. Diaz and F. D. Richardson, in Electromotive Force Measurements in High-Temperature Systems, C. B. Alcock, ed., The Institution of Mining and Metallurgy, 1968.

20. K. K. Kelley, U. S. Bur. Mines Bull. 584, 1960.

21. Y. D. Tretyakov and A. R. Kaul, in Physics of Electrolytes, J. Hladik, ed., (Academic Press), Vol. II, 1972.

22. V. V. Samokhval and A. A. Vetcher, Zh. Fiz. Khim., 42, 644 (1968).

LIST OF FIGURES

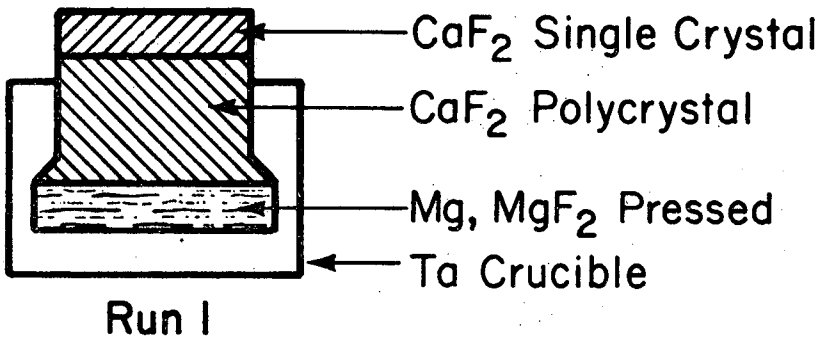

Run 1

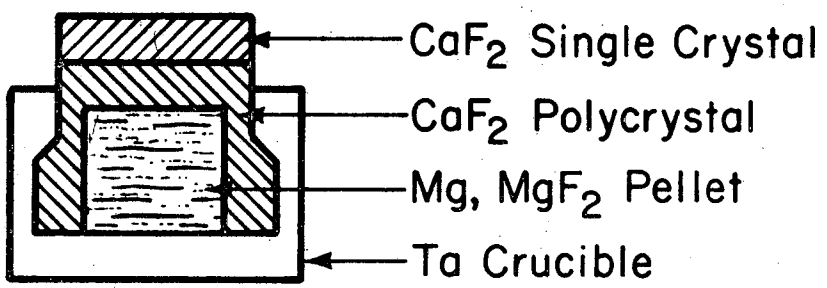

Run 2

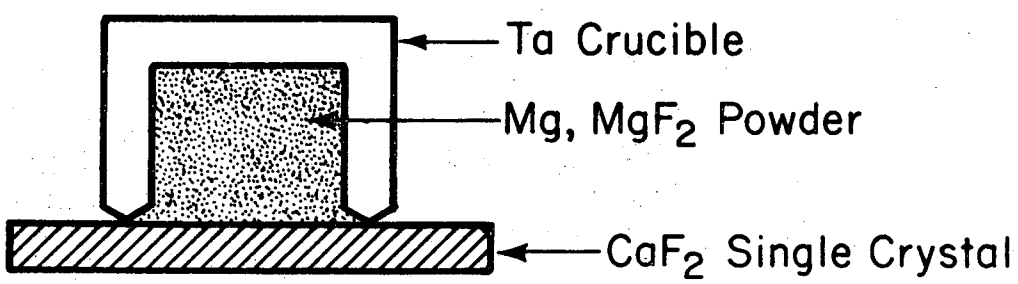

Run 3

XBL 757-6790

Fig. 1.

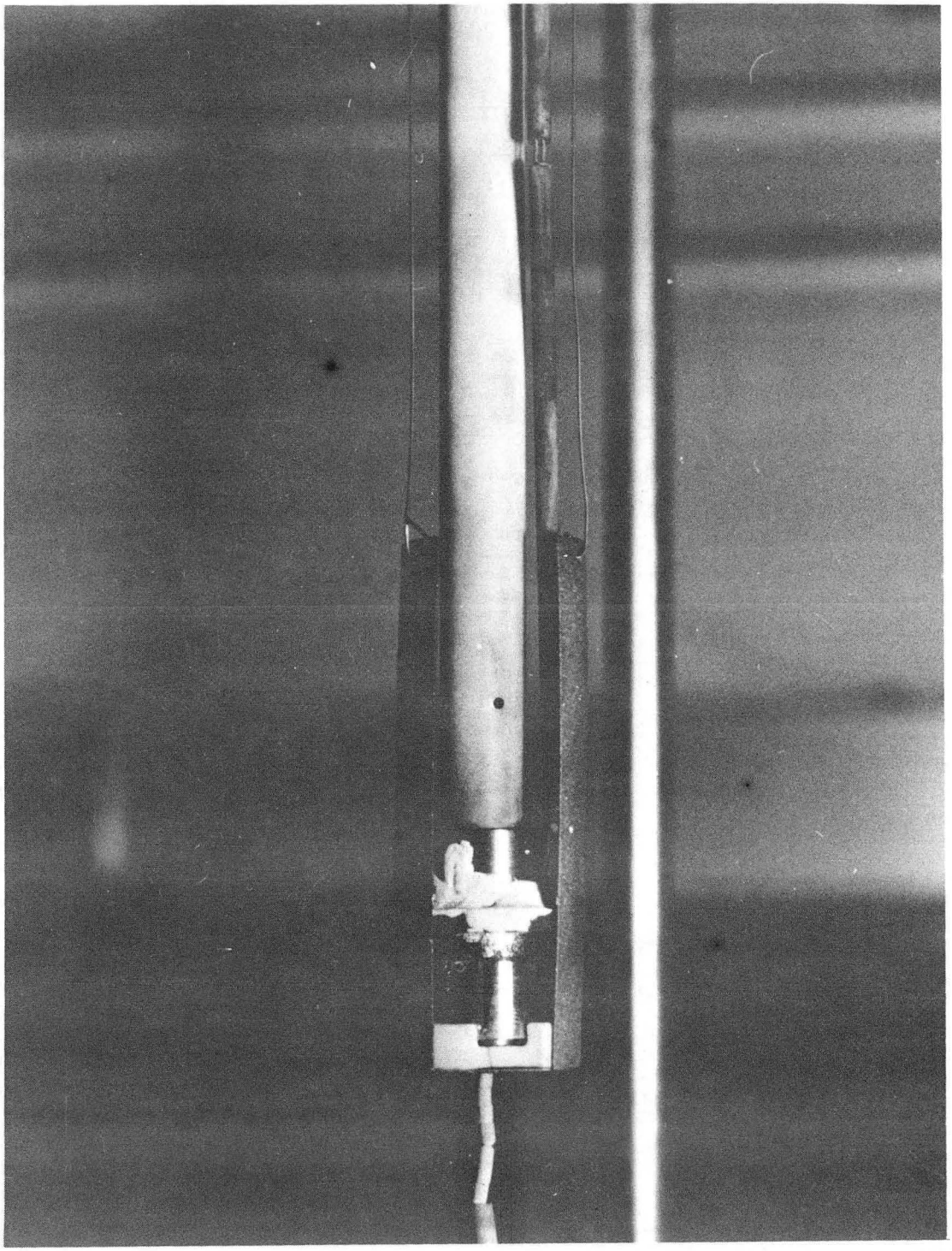

XBB 757-5246

Fig. 2.

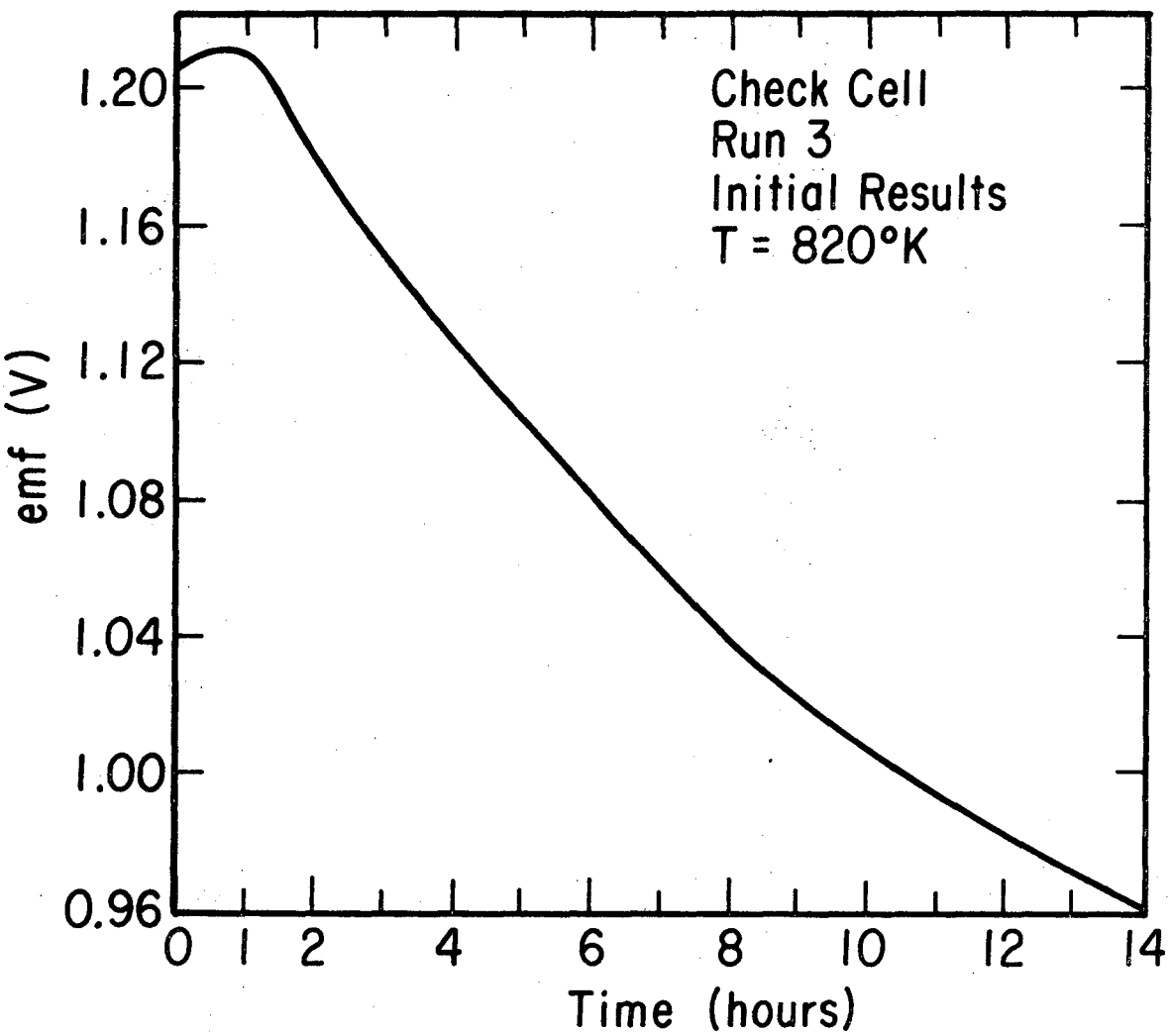

Fig. 3.

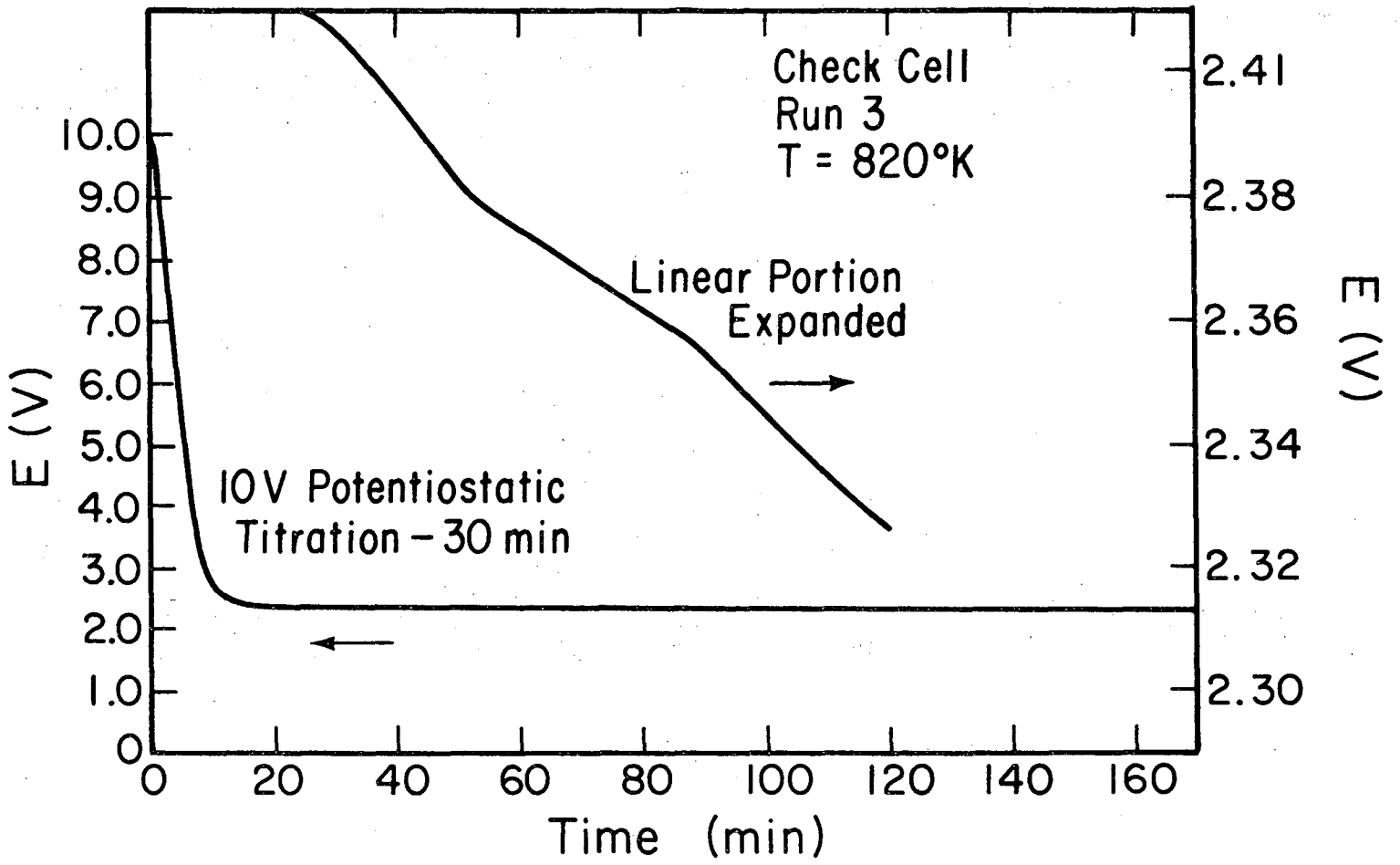

XBL 757-6793

Fig. 4.

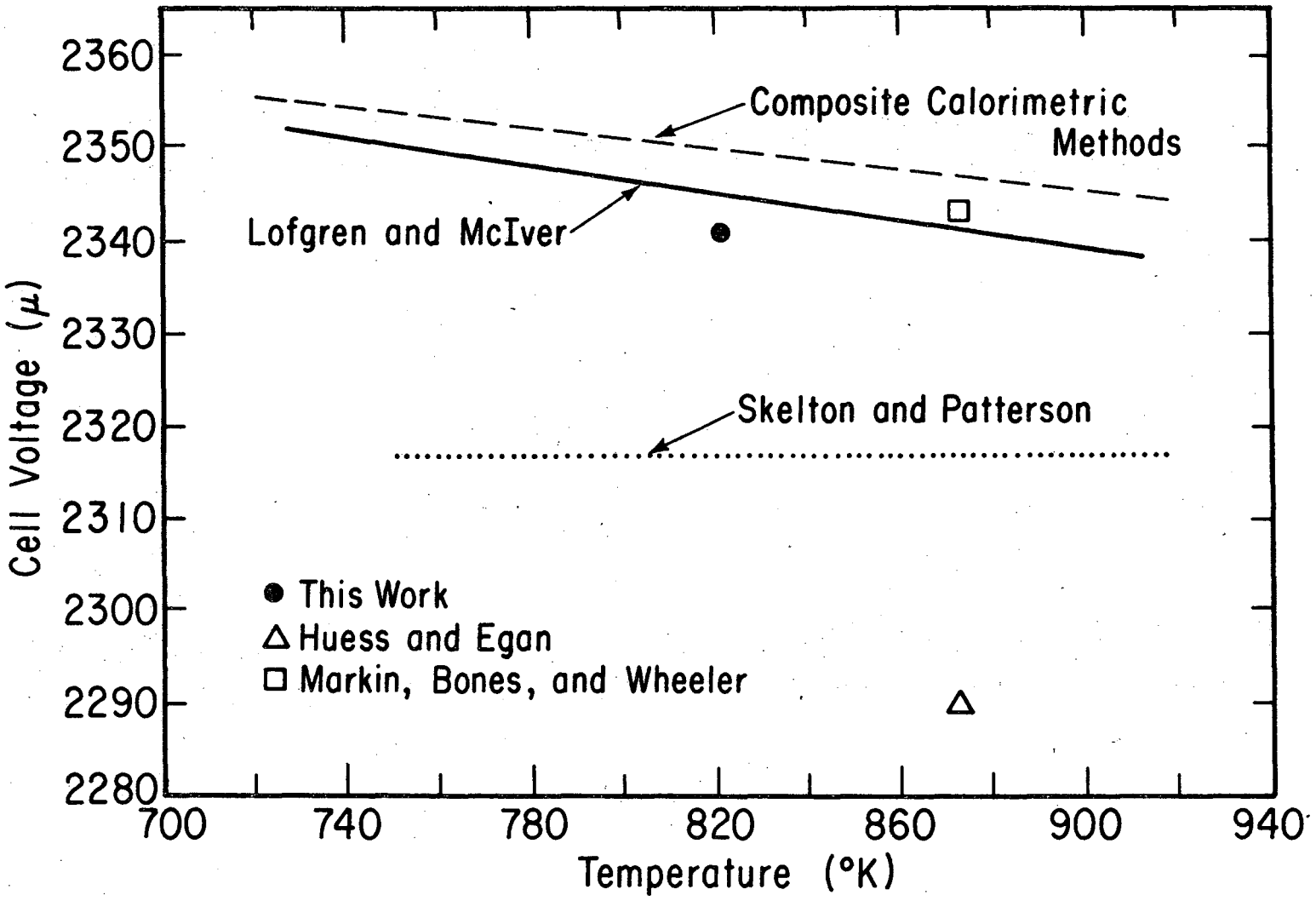

Fig. 5.

VIII. GENERAL CONCLUSIONS

Solid electrolytes have been used in this study to investigate some thermodynamic and kinetic properties related to Group III and V elements. Specifically, Gibbs free energies of forming the stable oxides of the Group III elements of Ga and In have been measured. The results show good agreement with other literature values and are particularly consistent when viewed from a 'third law' point of view. The thermodynamics of the Ga-Sb system at and above the liquidus line has been examined and component activities in the melt measured. The solubility and diffusion of oxygen in liquid In has also been studied electrochemically. The solid electrolyte CaF_2 was explored for applications with respect to Group III and V elements and compounts. Finally a critical assesment of the experimental apparatus and techniques has been put forth.

With the age of solid state electronics having relatively recently been born, future product development will depend in part on a accurate description of the properties of the materials involved. In light of this thought I would like to conclude with a preface to future areas of study on the properties of Group III-V semiconducting compounds in view of the ground work just presented.

Concerning oxide electrolytes, of the Group III elements Al, Ga and In and the Group V elements P, As and Sb the only oxides able to produce a measurable oxygen partial pressure are those of Ga and In. The oxygen partial pressure of Al_2O_3 is out of the conduction range of the common oxide electrolytes while the large vapor pressures

of P and As limit their applicability. This leaves the alloys obtained from the elements Ga, In and Sb. The Ga-In melt has received attention with a solid oxide electrolyte[1,2] with good consistency found in the measured gallium activity. The thermodynamics of In-Sb has received the most attention in the literature,[3] though all emf measurements have been taken with a liquid electrolyte and only one measurement with the liquid alloys. There exist an approximately 25 $kcal_{th}mol$ difference between the Gibbs free energy of formation of the two oxides thus making an oxide investigation feasible. The third system, Ga-Sb, has been reported on previously in the manuscript. It is thus concluded that possible areas for future study with oxygen electrolytes would include indium activities in the In-Sb liquid alloy and gallium activities in the increasingly important ternary system In-Ga-Sb.

The second solid electrolyte considered was CaF_2. The use of CaF_2 has three distinct advantages: 1). AlF_3 is now included in the range of applicability 2) Much lower temperature can be employed 3) Good response enables data to be taken also on the solid compounds and solutions. Thus measurements of the free energy of formation of the solid compounds $M_{III}Sb$, where M_{III} represents a Group III element, can be measured by the following cell,

$$M_{III}Sb(c),\ M_{III}F_3,\ Sb\|CaF_2\|M_{III},\ M_{III}F_3 \qquad (1)$$

Here the overall cell reaction is the formation reaction. This cell can be carried above the liquidus line and M_{III} activities measured.

By determining the point at which the emf changes slope the liquidus temperature can also be defined for regions in the Sb rich portion of the phase diagram. Since the emf of cell (1) is a measure of the M_{III} activity, this arrangement can also be used to measure the homogenity gap for the line compound $M_{III}Sb$. If a known weight of $M_{III}Sb$ (Sb absent) makes up the left electrode, the gallium concentration can be altered by coulometrically titrating flourine to or from this electrode with a constant current supply. On either side of the gap the gallium activity is constant (though at much different values). The amount of current passed is a measure of the width of the homogenity gap,

$$n_{titrated} = \frac{It}{nF} \tag{2}$$

where I is the constant current passed, t is the time required to go between the constant values of emf, n is the number of equivalents, F the Faraday constant and $n_{titrated}$ is the number of moles of gallium titrated. The gap, in mole fraction of gallium, is

$$\Delta x_{gap} = x_{Ga}^{initial} - x_{Ga}^{final} = \frac{n_{Ga}^{o}}{n_{Sb}+n_{Ga}^{o}} - \frac{n_{Ga}^{o} + n_{titrated}}{n_{Ga}^{o}+n_{titrated} + n_{Sb}} \tag{3}$$

Assuming $n_{titrated} << n_{Ga}^{o}+n_{Sb}$ equations 2 and 3 give

$$\Delta x_{gap} = \frac{It}{NF(n_{Ga}^{o}+n_{Sb})} \tag{4}$$

where I, t and $(n^{o}_{Ga}+n_{Sb})$ are all measurable quantities. The only way to fix the location of the gap is by titrating from the pure Sb phase with a large excess of GaF_3 present (at least equal molar with respect to Sb). This approach is prohibited by the time involved. As an example, if 0.05 moles of GaSb are initially present and a constant current of 0.1 ma is passed for 100 sec a gap of 1.04×10^{-6} in mole fraction would be detected.

It is possible to measure the free energy of formation of the metal fluorides with the following cell.

$$M_{III}, M_{III}F_3 \,|\, CaF_2 \,\|\, \text{reference electrode} \qquad (5)$$

The reference electrode should be thermodynamically defined and could be either solid (Ni, NiF_2) or gas (as used in the studies with oxygen).

Similar studies might be performed on the ternary solid solutions and liquid melts. A typical cell might be

$$M_{III}{}^{A}F_3, M^{A}_{III}Sb, Sb \,|\, CaF_2 \,|\, Sb,\ M^{A}_{III}\text{-}M^{B}_{III}Sb, M^{A}_{III}F_3 \qquad (6)$$

where $M^{A}_{III}F_3$ is the most stable fluoride. In particular the ternary III-V solid solutions are receivng attention in heterojunction laser diode applications and as Gunn-effect device material.[4-6]

Finally the diffusion of fluorine in M_{III} metals can be studied. Consider the following cell arrangement:

$$Ni,NiF_2||CaF_2||Ga[+F\ \text{dissolved}]| \qquad (7)$$

$$|\rightarrow X \qquad\qquad |\leftarrow X=L$$

If a constant potential is applied with the negative pole on the Ga side a current will begin to flow. The electrons introduced on the Ga side will react with dissolved fluorine and form fluorine ions. These ions will ionically conduct through the CaF_2 electrolyte and upon reaching the Ni electrode will react to form NiF_2, thus liberating electrons.

$$2\ F_{\text{dissolved}} + 2e^- \rightarrow 2F^- \quad \text{(right)} \qquad (8)$$

$$2\ F^- + 2Ni \rightarrow NiF_2 + 2e^- \quad \text{(left)} \qquad (9)$$

Initially, an equilibrium of fluorine ions is established such that:

$$\mu(F_{\text{dissolved}}) = \mu(F_{\text{reference electrode}}) + nFE \qquad (10)$$

if the emf is taken from the Ga side to the Ni electrode. The chemical potential is related to the activity by, $\mu_i = RT\ \ell n\ a_i$, thus

$$a_{F_{\text{dissolved}}} = \exp[\frac{EF}{RT}] + a_{F_{Ni}} \qquad (11)$$

The activity of fluorine in the nickel electrode can be determined from the well known free energy of forming NiF_2, $a_F = \exp[\frac{\Delta G^*}{2RT}]$ (12)

where ΔG^* is determined from the following reactions:

$$Ni+F_2 \rightarrow NiF_2 \quad \Delta G_1 \tag{13}$$

$$2F^- \rightarrow F_2 \quad \Delta G_2 \tag{14}$$

$$Ni+2F^- \rightarrow NiF_2 \quad \Delta G^* \tag{15}$$

At the time the constant potential is applied, the fluorine concentration at the electrolyte -Ga electrode interface drops essentially to zero (3 orders of magnitude differential in concentration is sufficient). The applicable equation is Ficks second law ($\frac{\partial C}{\partial T} = D \frac{\partial^2 C}{\partial X^2}$) with a solution, for the linear geometry of our current cell design, given by

$$C_{F^-} = (C_o,_{F^-}) \operatorname{erf}[\frac{x}{2\sqrt{(D_{F^-})\,t}}] \tag{16}$$

where $C_o,_{F^-}$ is the initial concentration, D_{F^-} is the diffusion coefficient of F^- in the metal, t is the time and x is distance from the interface. The flux, j, is given by Ficks first law and results in

$$j = \frac{(D_{F^-})(Co_{F^-})}{\sqrt{\pi (D_{F^-})\,t}} \tag{17}$$

The above solution assumes the initial uniformly concentrated Ga electrode is of infinite length. Due to the finite thickness of the electrode the above solution is an approximation. This problem can be circumvented by two methods. First of all the cell data at large times can be neglected. A second possibility would be to form a cell of the following design,

$$Ni,NiF_2||CaF_2||Ga(\text{Fluorine dissolved})||CaF_2||Ni,NF_2 \qquad (18)$$

$$| \rightarrow x \qquad\qquad |\leftarrow x=L$$

With the use of this cell a constant fluorine solubility (the equilibrium one) would be maintained at the x=L interface. Also the emf of this cell would indicate any deviations from equilibrium by measuring the potential across the right cell.

The current density is related to the flux of fluorine ions by,

$$i = |nFj| = \frac{F(D_{F^-})(C_{o,F^-})}{\sqrt{\pi (D_{F^-})t}} = \frac{\sqrt{(D_{F^-})}}{\sqrt{t}} \frac{F(C_{o,F^-})}{\sqrt{it}} \qquad (19)$$

Therefore if we plot $|i|$ vs. $\frac{1}{\sqrt{t}}$ we should obtain a straight line of slope $\frac{F(C_{o,F^-})}{\sqrt{it}}\sqrt{(D_{F^-})}$.

The current density is found by measuring the current across the cell and dividing by the surface area available to the diffusing fluorine ions. The current can be measured by putting a known resistance (higher than the cell impedence to prevent cell drainage) in series with the cell and measuring its voltage drop. The

initial concentration of fluorine can be calculated from observing the initial cell emf.

By employing cell type (18) and applying a constant voltage for an extended period of time different than that of the equilibrium one, a resulting C_{o,F^-} different than that of the equilibrium value can be obtained, thus allowing one to study the affects of concentration on the diffusion coefficient. At time t = 0, the potential across the left cell is changed such that fluorine is titrated out of the Ga electrode while the right cell is maintained at constant potential to ensure the infinite source of fluorine.

By using the dual cell arrangement we could apply a different potential to each cell and develop a steady state profile. Measuring the steady state current and assuming the current is limited by the diffusion of fluorine through the Ga(ℓ) we could study the affect of concentration on the diffusion coefficient

In conclusion the solid CaF_2 electrolyte is a much better candidate than an oxide for future studies in view of the larger number of systems it can be used with, though greater experimental difficulties are encountered.

REFERENCES

1. K. A. Klinedinst, M. V. Rao, D. A. Stevenson, J. Electrochem. Soc. 119, 1261 (1972).

2. R. Pong, Thermodynamic Studies of Ga-In, Ga-Sb and Ga-In-Sb Liquid Alloys by Solid State Electrochemistry With Oxide Electrolytes (M.S. thesis), April 1975.

3. R. Hultgren, P. D. Desai, D. T. Hawkins, M. Gleiser, K. K. Kelley and D. D. Wagman, Selected Values of the Thermodynamic Properties of Binary Alloys, American Society for Metals, Ohio, 1973.

4. J. C. McGroddy, Negative Differential Conductivity in Semi-doncutors in Proceedings of the Tenth International Conference on the Physics of Semiconductiors, U. S. Atmoic Energy Commission 1970, p. 31.

5. C. Hilsum, H. D. Rees, A Detailed Analysis of Three-level Electron Transfer in Proceedings of the Tenth International Conference on the Physics of Semiconductors, U. S. Atomic Energy Commission, 1970, p. 45.

6. A. Joullie, J. Allegre and G. Bougnot, Mat. Res. Bull. 7, 1101 (1972).

ACKNOWLEDGMENTS

I am obliged to the U. S. Energy Research and Development Administration for their financial support of my research. Recognition is deserving to the employees of Lawrence Berkeley Laboratory, Paul Stagnaro, George Gordon, Brian Pope and Phil Eggers, to mention only a few. Special appreciation is given to Carl, Slim and Andy who helped make ideas a reality. Much gratitude is given to Mike and Earl for delivering in time of need. I am beholden to the Department of Chemical Engineering faculty and fellow students for their support and guidance. Thanks to Professors C. Tobias and A. Searcy for their critical review of this manuscript. And to the director of this research, Dr. L. F. Donaghey, whose counsel and assistance made this work possible, I give thanks. I would like to thank Lorine, Shirley and Jean for their patience in the preparation of this manuscript. To my parents, brother and sisters--thank you. And finally to the person who made this all possible, my wife, Sandy--I dedicate this to you.

APPENDIX I

EXPERIMENTAL APPARATUS AND PROCEDURES

A. Introduction

In this study of some thermochemical properties of Group III and V elements and compounds two different electrolytes were employed. The first type was almost entirely solid state, using a disc of CaF_2 single crystal as the solid electrolyte, while the second arrangement had a tube of calcia stabilized zirconia (CSZ) and used a gas reference electrode. Though differing in some respects the operation and apparatus of the two cell types had many common points. Thus the communal pertinent aspects of the cell designs and operation will be developed before degressing into a discussion of each cell's individual characteristics. In addition, several excellent reviews of high temperature operation of solid electrolyte galvanic cells can be found in the literature.[1-5]

B. General Apparatus

1. Peripheral Apparatus

Solid state galvanic cells are usually operated either under a vacuum or in an inert gas purge. In this investigation argon gas was used as the inert gas blanket. High purity, tank argon was further purified by passing it through a column of Linde 4A molecular seive at dry ice-acetone temperature to remove the majority of water vapor present and then further purified by flowing over hot Ti sponge (850°C). A further discussion of the purifying apparatus and its effectiveness can be found in Appendix III.

The basic cell design is depicted in Fig. 1. It consisted of a 2 inch diameter closed end alumina tube (18 inches in length) secured by a Viton O-ring to the brass cell head. Three 1/8 inch Cajon fitted through-bores on the cell head were placed symetrically around a 1/4 inch Cajon fitted center bore. The 1/8 inch bores were used to pass the thermocouples and lead wires to the atmosphere via ceramic sheaths. The larger center opening was used to house the oxygen sensor. The thermocouples used were Type K (0.02 inch Pt - Pt 10% Rh) and were calibrated in the cell under vacuum against a NBS standardized thermocouple. The calibration was performed with the standard thermocouple occupying the position normally that of the electrode, while the unknown thermocouples were placed in their normal positions thus accounting for any temperature differences between the thermocouple and the actual electrode. A Leeds-Northrup Type K-3 potentiometric facility was used to measure the thermocouple emfs. Included in the brass head were bores for gas entrance and exit. The exit placement was such that the gas had to flow across the cell and through the alumina pushrod. Three hooks provided support for the guy wires. Water flowed through copper tubing wrapped around the head to cool it and insure proper O-ring operation. The cell was heated with a Marshall resistance heated furnace (20 inches in length with a 2 1/2 inch bore). Excellent temperature control was furnished by an integrating, temperature regulating power supply designed and built at Lawrence Berkeley Laboratory. Temperature uniformity and stability was required to prevent the generation of thermal emfs across the electrodes

and to allow an equilibrium to be reached.

Cell emfs were measured with a Keithley 640 electrometer accompanied with an adaptor input head. Coaxial cable was ran from the cell to the input head where connection was made from a BNC coaxial connector (on cable) to a BNC triaxial connector (on input head). The triaxial input had a copper pushrod mounted to connect it to the input head's spring loaded contact. The inner wire of the coaxial cable was connected to the positive lead wire of the cell. The outer wire was driven by the unity gain feedback of the electrometer, thus acting as a driven guard. Leakage sources at the input head were very unlikely since the line was guarded up to the sapphire insulated electrometer contact. Extraneous ground loop currents were eliminated by grounding in a tree configuration.

Data acquisition was automated with the connection of an Intel 8008 microprocessor. The facility is schematically shown in Fig. 2. The system had the capability of setting the cell operation temperature and monitoring cell emfs and thermocouple outputs on a predetermined time base, thus allowing continuous cell operation. The digital panel meter used was a 4 1/2 digit 1 volt instrument from Newport. The temperature regulator set point controller was ten speed, linear ramp motor drive. The current source was a Electronic Measurements Model C638 constant current power supply. All other equipment depicted in Fig. 2 was either as described earlier or designed and built at Lawrence Berkeley Laboratory or the electronic shop.

For purposes of out-gassing and leak-detection a vacuum system was connected to the cell. This system consisted of a mechanical pump in series with a diffusion pump and could be evacuated to about 1×10^{-5} torr. All electrical leads were sealed, after the application of a layer of glyptol insulating paint, by melting black wax into a tapered glass tube, through which the wires extended, and sealing to the alumina sheaths with Cajon ultra-torr union fittings. All valving was accomplished with Nupro shutoff bellow valves except where fine control was needed in which case Nupro, double pattern, very fine metering valves were used. The exiting argon gas purge was passed consecutively through: dry ice-acetone cold trap purge tube, silicon oil bubbler, and a soap film flowmeter.

C. Procedure

The general experimental procedure was to assemble the desired electrode arrangement and connect it to the peripheral apparatus. The cell was then evacuated (approximately 10^{-5} torr) and back purged with argon three times. Leaks were checked during the evacuation and also by placing the cell under an excess argon pressure. With the use of the ramp set-point controller the temperature was raised, at a rate of 100°C/hour, in order to prevent thermal shock to the electrolytes, to the highest operating temperature and held there until an equilibrum cell potential was observed. At this point the control was switched to the digital microprocesser. At least two cycles over the temperature range of interest were completed in order that possible hysteresis effects might be illuminated. In the basic mode of control, the temperature regulator set point

would be ramped to a new valve (usually a change of 20°C) and held there until an equilibrium voltage was recorded. Temperature and cell voltage were recorded at 5 minute intervals. After completion of each run the temperature was slowly lowered and the cell disassembled. The electrode material was analyzed by x-ray diffraction to confirm the absence of side reaction products.

1. Experimental Precautions

When using a galvanic cell there are many potential sources of error which must be designed out of the system. The formost pitfall is the previously mentioned (Chapter 2) electronic conduction within the electrolyte. A second problem is that a flowing inert gas atmosphere can affect the cell potential by carrying the gaseous conducting ion around the open type of electrode and thus short-circuiting the cell. Non-inert components in the gas blanket can also affect the measured cell voltage. Specifically, oxygen can react with CaF_2 and promote hole conduction, though the literature data is in conflict on this possibility.[6-10] In the oxide electrolyte systems the oxygen pressure should be on the order of that over the most stable oxide. The effect of gas flow can be demonstrated by changing the flow rate at a given equilibrium. In the limit of a high flow rate cooling affects would be noticed while at very low flows, leaks or gaseous short circuting would cause a voltage shift. Between these limits a flow rate should be available at which these affects can be neglected. The cells studied showed such a region and were ran in the range of 10 to 15 cc/min of argon gas.

Finally, some other practices that should be followed include: a given equilibrium state should be approached from both a higher and lower temperature - both giving reproducable results (accomplished with the cycling). The reversibility of reactions can be checked by passing a small amount of current (thus offsetting the equilibrium) and observing if the cell emf returns to the original potential. The furnace should be properly shielded to prevent production of induced currents (a platinum foil cylinder grounded to the electrometer was used). Also the temperature gradient across the cell should be kept to a minimal for obvious reasons -- a 6 inch zone in which the cell was placed was calibrated to within 1°C throughout with external resistors. Good electrode-electrolyte contacts are essential to prevent possible polarization effects--solid state surfaces were lapped and polished and gas electrodes had a high surface area accomplished with the porous platinum paste. Finally a check cell should be run to test the reproducibility of the final cell design.

D. Electrode Designs

1. CaF_2 Galvanic Cells

Several different electrode designs were used but the basic arrangement was prepared as follows. Each cell consisted of a single crystal CaF_2 disc (12 x 3 mm, 25 x 3 mm, or 25 x 6 mm) sandwiched between two half cells and was constructed by placing a pressed pellet of electrode material into a metal crucible and then capping with polycrystalline CaF_2. The CaF_2 cap served two main functions. First

of all, composition changes with time due to vaporization were decreased. Also, vapor phase transport of fluorine, causing a short circuiting would be depressed. This cap would not impair cell operation since the fluorine ion mobility is greater in the polycrystalline material due to grain boundaries, etc. The crucible material selection was governed by the solubility of the electrode materials in the various crucible candidates.[11-13] The inside edge of the crucible was rounded to prevent cleavage of the CaF_2 cap and thus allow the cap to extend above the crucible level. Before filling the crucible, it was baked out in a vacuum at a temperature above the subsequent operating one. After preparation of the electrode the CaF_2 cap was hand lapped on a quartz plate to enhance contact. Finally the half cell was annealed in a vacuum of 10^{-5} mm Hg at a temperature above the highest measurement for a predetermined length of time.

Once the half cells were prepared, they were assembled as shown in Fig. 3. The alumina insulator caps served to prevent any short circuit via the metal support (0.005" Tantalum sheet). Both the insulator and the support had the sides cutaway in three sections to allow good contact between the cell and inert gas. The support was held in place by guy wires connecting the three arms of the support to hooks on the cell head. The opposing force was provided by a spring loaded alumina tube. The lead wires were made of the same material as the crucible to prevent the development of thermal emfs. Contact between the crucible and lead wire was made

by spot welding the wire end to a 3/8 inch disc of the same material.

The pressing apparatus is that shown in Fig. 4. The general procedure was as follows: powdered electrode material in predetermined proportions was loaded in the dry box into body 1 and plate 1 attached. With the plunger in place, the powder was hand pressed while still in the dry box. The powder was then pressed at 10 to 20 tons/inch^2. The 1/2 inch diameter pellet was pressed out of the die using plate 2 and placed in the crucible. The CaF_2 cap was made by employing die 1 and body 2. Die 1 was a split collar device mounted with an aluminum handle to separate it from the press. With this arrangement, ultrapure CaF_2 was pressed at 10-20 tons/inch^2 such that the surface extended about 2 mm over the crucible level.

2. CSZ Galvanic Cells

Depicted in Fig. 5 is a schematic of the cell arrangement used. The reference oxygen partial pressure was provided by the CO_2-CO equilibrium and its construction is discussed in Chapter 3. In all cases the measured electrode consisted of a pool of the liquid metals being investigated and a small amount of powder of the most stable oxide. The electrode materials were contained by a 2 inch, closed one end, graphite tube afixed with a screw cap to allow additional material to be added. The center bore of the cap was machined to slip over the CSZ tube. When in place, powdered graphite was placed around the diameter to further seal the electrode. Platinum lead wires were used and the cell was supported and insulated as discussed in conjunction with the CaF_2 cells.

REFERENCES

1. T. A. Ramanarayanan and W. L. Worrell, private communication.

2. D. O. Raleigh, Progress in Solid State Chemistry, Vol. III, H. Reiss, ed., (Permagon Press, New York, N. Y., 1967), Chapter 3.

3. C. B. Alcock, Ed., Electromotive Force Measurements in High Temperature Systems, (American Elsevier Publishing Co., New York, N. Y., 1968).

4. R. A. Rapp and D. A. Shores, Physicochemical Measurements in Metals Research, Part 2, R. A. Papp, ed., (Wiley-Interscience, New York, N. Y., 1970).

5. J. Hladik, ed. Physics of Electrolytes, Vol. 2, (Academic Press Inc.,(London) Ltd.) 1972).

6. R. W. Ure, J. Chem. Phys., 26, 1363 (1957).

7. R. Benz and C. Wagner, J. Phys. Chem. 65, 1308 (1961).

8. R. W. Taylor and H. Schmalzried, J. Phys. Chem. 68, 2444 (1964).

9. T. N. Rezukhina and Y. Baginska, Elektrokhimiya, 3, 1146 (1967).

10. D. V. Vetcher, Dissertation, Moscow State Univ., Moscow (1970).

11. R. P. Elliott, Constitution of Binary Alloys, First Supplement, McGraw-Hill, New York, N. Y. (1965).

12. F. A. Skunk, Constitution of Binary Alloys, Second Supplement, McGraw-Hill, New York, N. Y. (1969).

13. M. Hansen and K. Aderko, Constitution of Binary Alloys, 2nd edition, McGraw-Hill, New York, N. Y. (1958).

LIST OF FIGURES

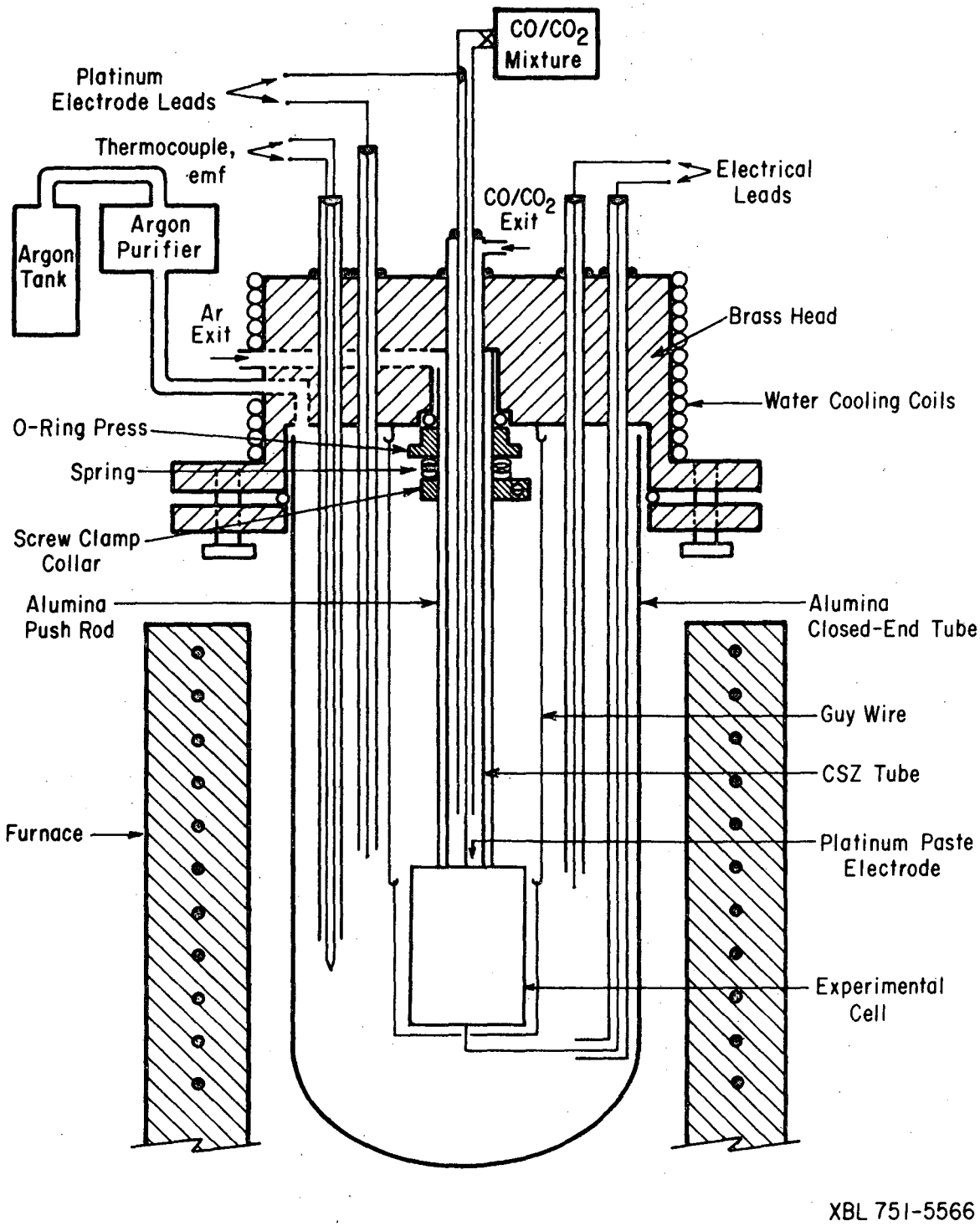
CO/CO_2 Mixture
Platinum Electrode Leads
Thermocouple, emf
Argon Tank
Argon Purifier
Ar Exit
CO/CO_2 Exit
Electrical Leads
Brass Head
Water Cooling Coils
O-Ring Press
Spring
Screw Clamp Collar
Alumina Push Rod
Alumina Closed-End Tube
Guy Wire
CSZ Tube
Furnace
Platinum Paste Electrode
Experimental Cell
XBL 751-5566

Fig. 1.

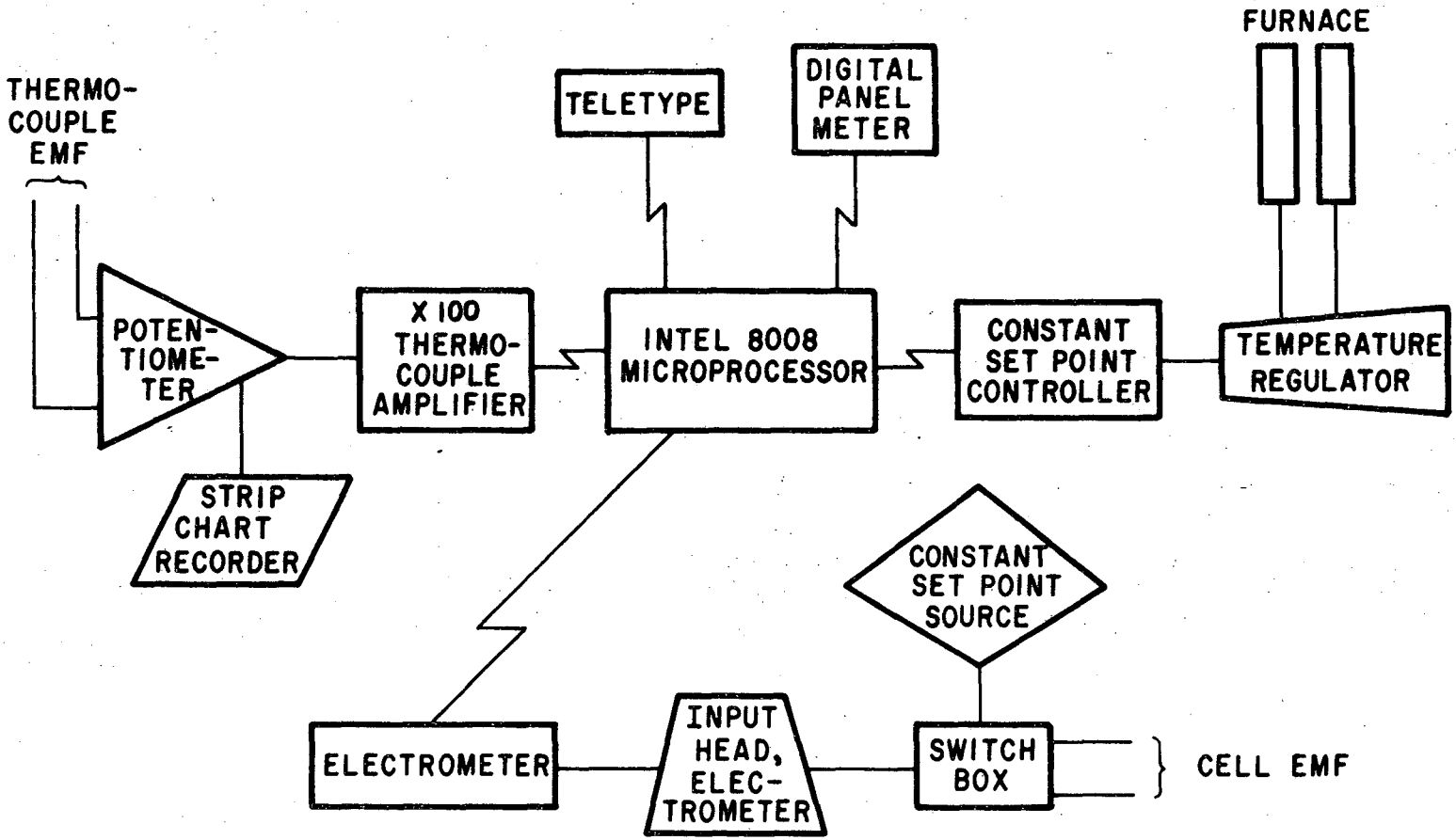

Fig. 2.

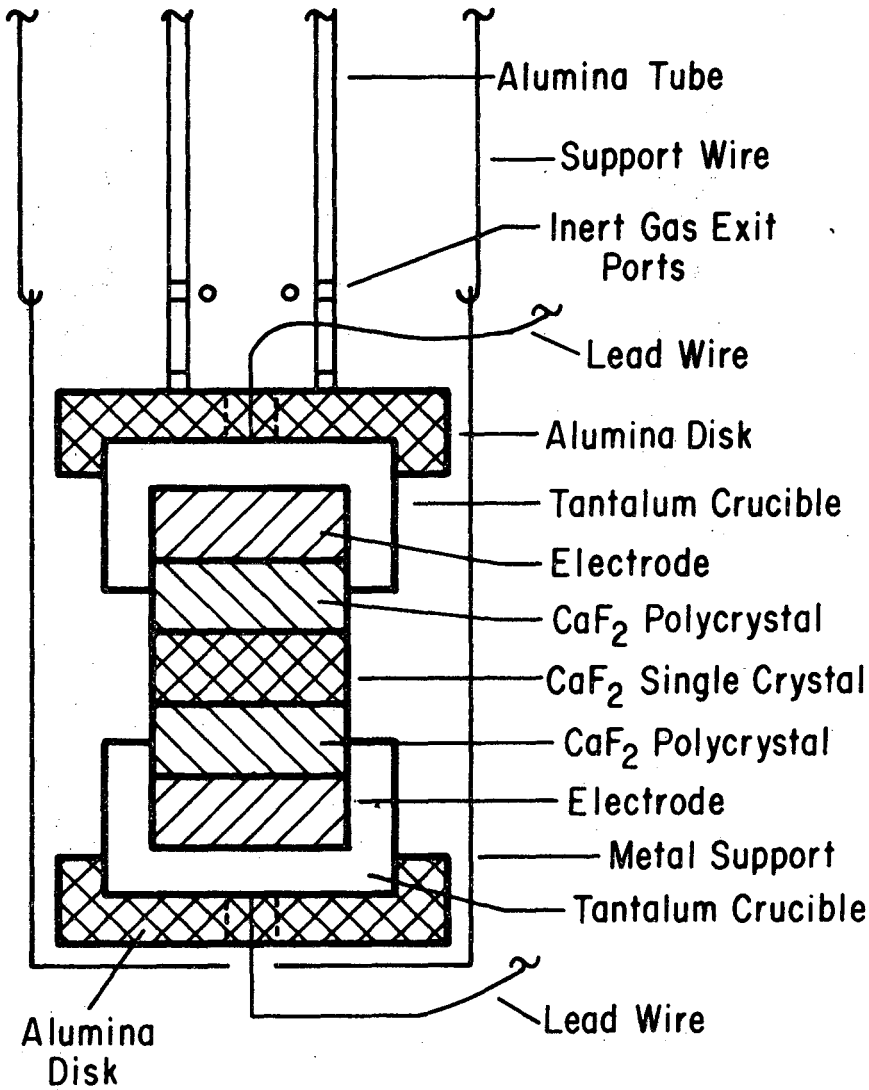

Experimental Cell

XBL 751-5567

Fig. 3.

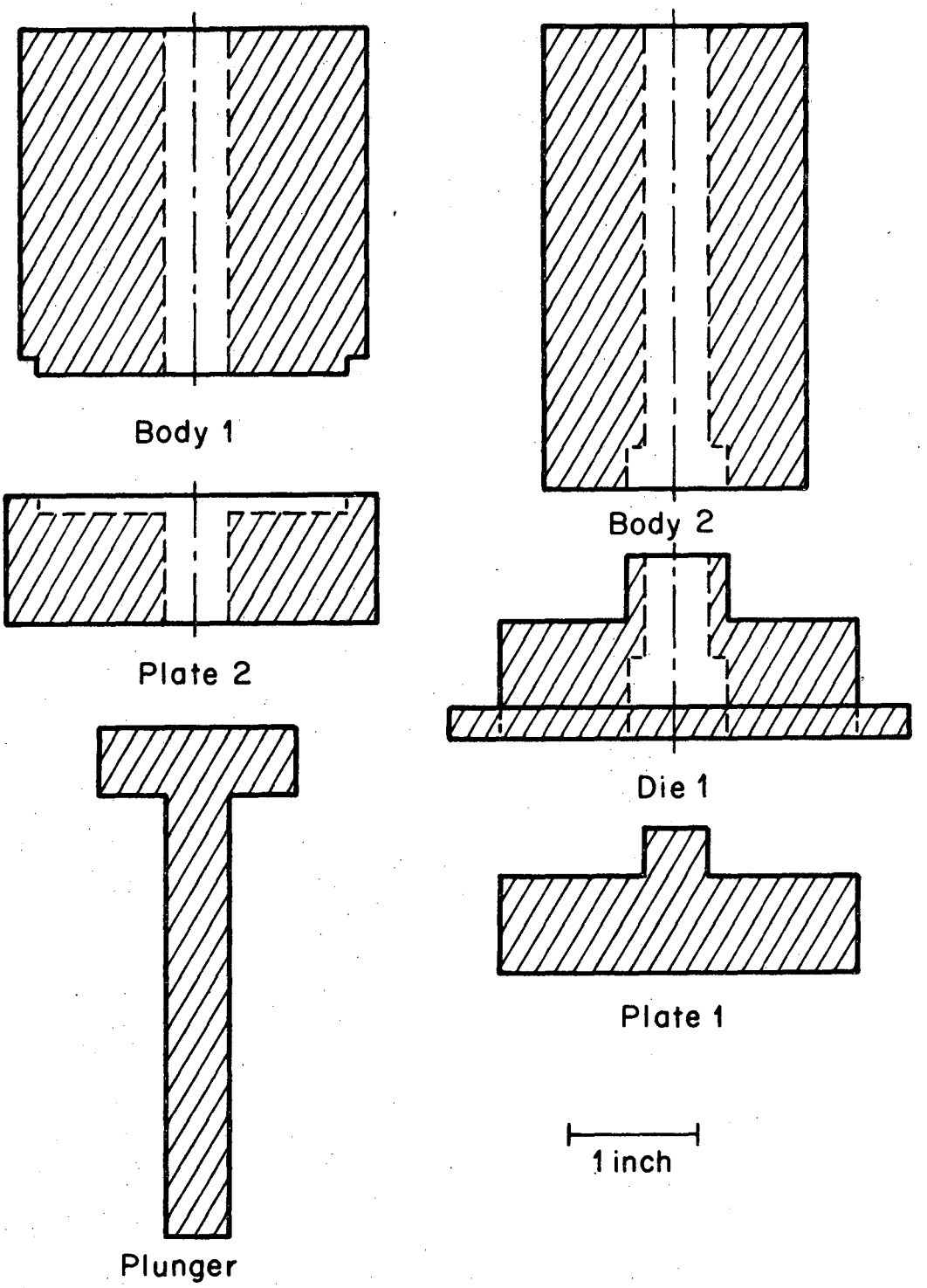

XBL 751-5568

Fig. 4.

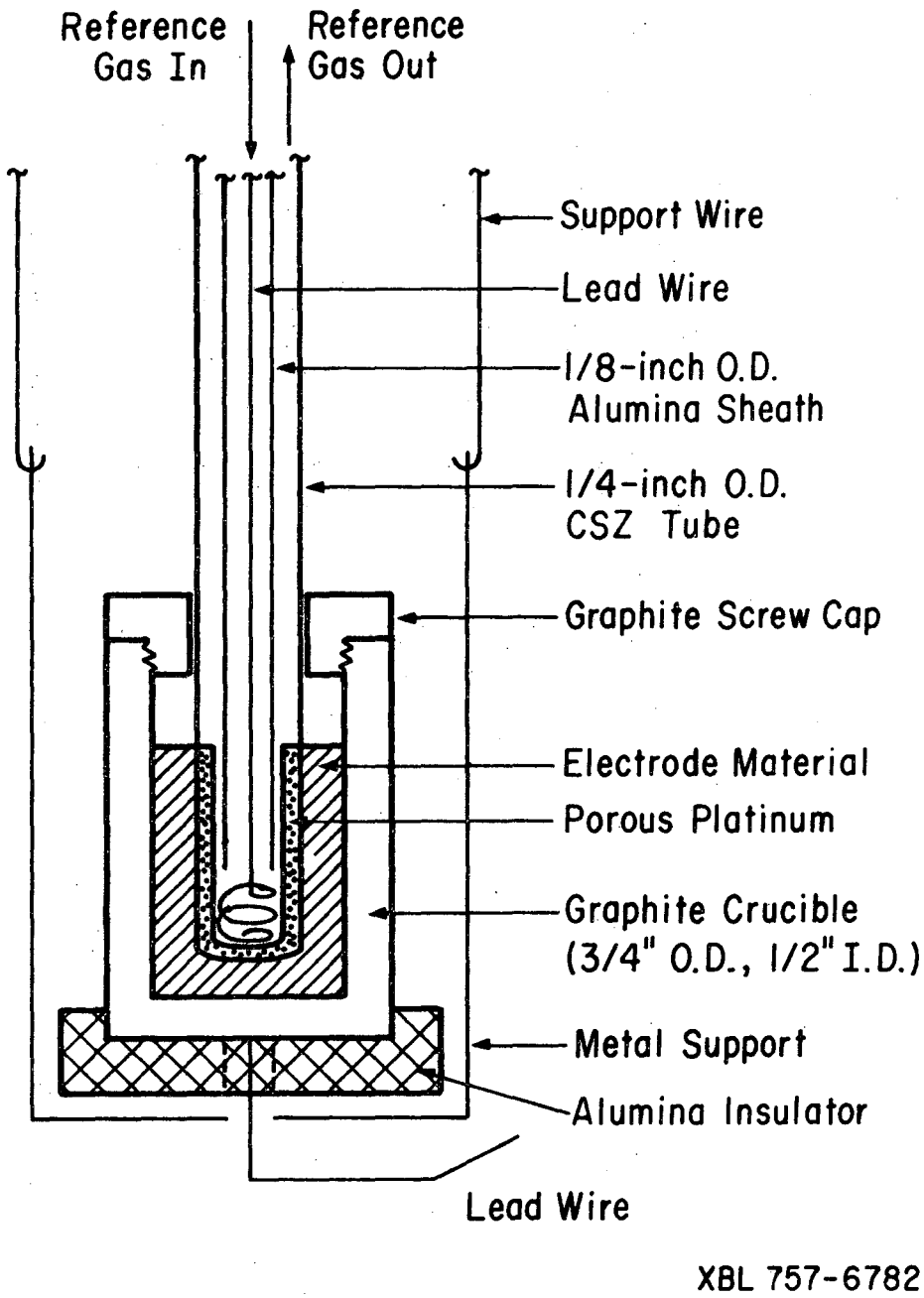
Reference Gas In
Reference Gas Out
Support Wire
Lead Wire
1/8-inch O.D. Alumina Sheath
1/4-inch O.D. CSZ Tube
Graphite Screw Cap
Electrode Material
Porous Platinum
Graphite Crucible (3/4" O.D., 1/2" I.D.)
Metal Support
Alumina Insulator
Lead Wire
XBL 757-6782

Fig. 5.

APPENDIX II

A. Materials

Listed in Table 1 are the chemicals, their source, and the purity used in this study. All materials were used as received except for the fluorides which were first dried. Handling and storage was done in a purified argon filled dry box. A diagram of the fluoride drying apparatus is shown in Fig. 1. The drying was accomplished with hot SF_4 at high pressure. The fluoride was placed on a platinum foil in the bottom of the high pressure vessel and filled with SF_4 gas. The temperature was brought to 350°C at which point the gas pressure was approximately 50 atm. The material was baked for 3 hours and the process repreated after purging with dried argon. The drying vessel was detachable so that material could be removed in the dry box.

Table 2

Material	Source	Purity
Ni	Atomergic Chemetals Co.	99.99 +
Mg	Orion Chemical Co.	99.9
Sb (1)	Orion Chemical Co.	99.9999
Sb (2)	Cominco American	High purity
In (1)	Orion Chemical Co.	99.999
In (2)	Cominco American	High purity
Ga	Cominco American	Semiconductor Grade
Al	Orion Chemical Co.	99.999
GaF_3	Alpha Products	99.999
InF_3 (1)	I.C.N.	99.5
InF_3 (2)	ROC/RIC	99.99
CaF_2 (1)	Alpha Products	99.99
AlF_3	Orion Chemical Co.	98.5
NiF_2 (1)	Appache Chemicals	99.5
MgF_2	Orion Chemical Co.	99.999
NiF_2 (2)	Apache Chemicals	from 99.999 Ni
CaF_2 (2)	Harshaw Chem. Corp.	Single Crystal
GaSb (1)	Alfa Products	99.99
GaSb (2)	Orion Chemical Co.	99.999
GaSb (3)	ROC/RIC	99.999 +
InSb	Orion Chemical Co.	99.999
$CO-CO_2-Ar$	Matheson Gas Products	Primary Standard
In_2O_3	Alfa Products	Ultrapure
Ga_2O_3	Alfa Products	99.99

LIST OF FIGURES

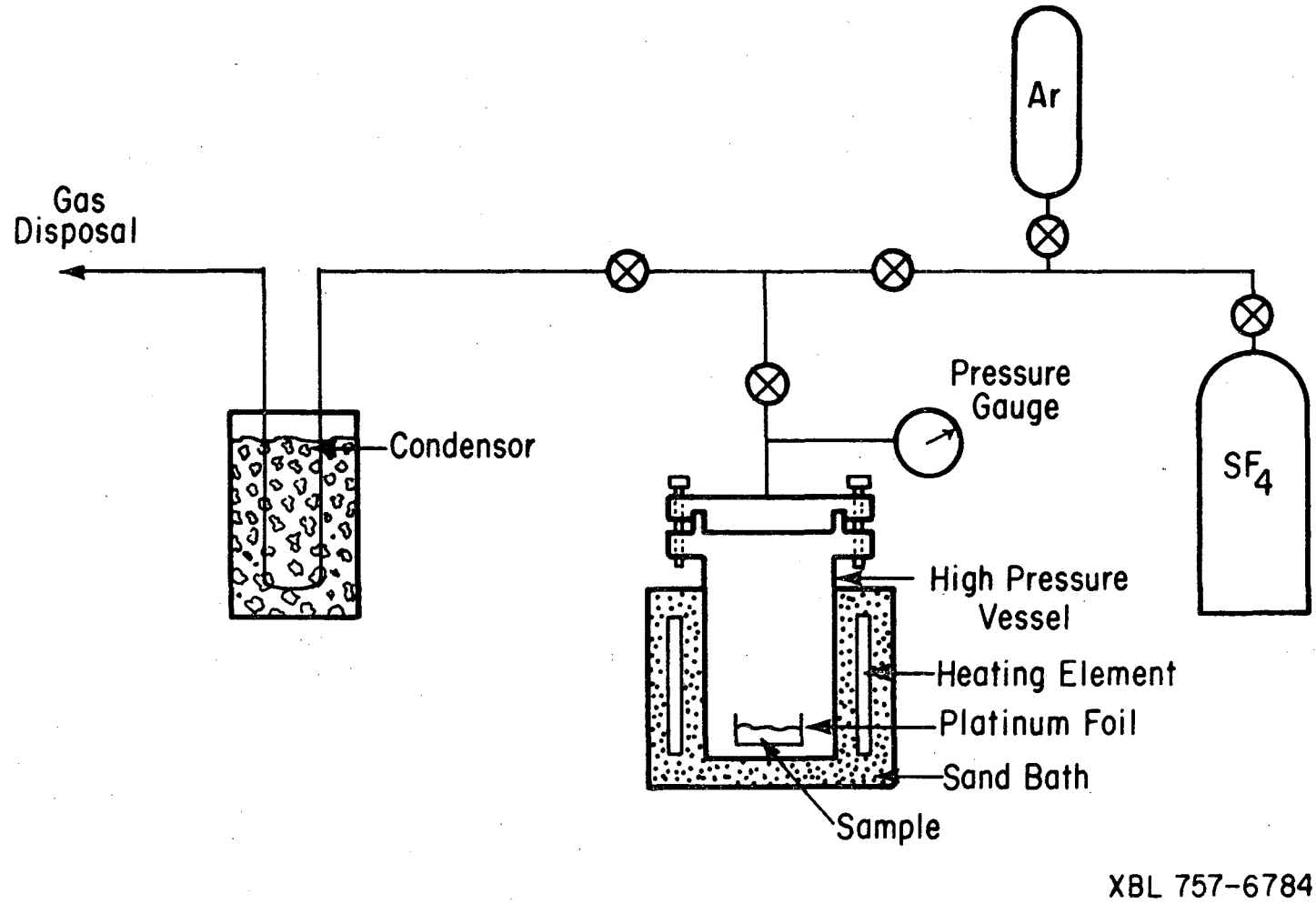
Ar
Gas
Disposal
Pressure
Gauge
Condensor
SF_4
High Pressure
Vessel
Heating Element
Platinum Foil
Sand Bath
Sample
XBL 757-6784

Fig. 1.

APPENDIX III. An Argon Purifier and Its Characterization

A. Introduction

Many research applications require an inert gas blanket or gas carrier of extremely high purity, particularly with respect to oxygen content. Specifically, in applications with solid oxide electrolytes an inert gas blanket having an oxygen partial pressure as small as 10^{-40} atm is required. The purifying device consisted of a two stage process, using a molecular sieve as an initial bulk getter and then hot Ti sponge to obtain the final purity. This design is similar to the purifier discussed by Klinedinst.[1] The results of Klinedinst exhibit a much higher oxygen content than would be expected from equilibrium considerations, which is thought to be a result of the use of the steel housing for the Ti sponge. Steel has a higher equilibrium oxygen partial pressure with respect to its oxide, and any oxide present on the steel can decompose and thus contaminate the gas exiting from the purifier. Results are presented for an improved design of a purifier where alumina, Al_2O_3, is used as the container material and also as the exhaust liner. The characterization was performed with a solid state galvanic cell, using calcia stabilized zirconia as a solid oxide electrolyte and a CO_2-CO mixture as a reference electrode while purified argon was the electrode of interest. Both the effects of flow rate and of the Ti sponge temperature were investigated.

B. Experimental

The purifying apparatus is depicted in Fig. 1. Tank argon was first passed through a molecular seive (Linde 4a) which was housed in a stainless steel cylinder (2.5 in. diam. x 12 in. height) and kept at ~78.5°C with a dry ice-acetone bath. The main advantage of this initial adsorber (mainly for water vapor) was that it served as a bulk remover which is very easily regenerated by evaculation at 300°C for three hours, thus increasing the ease of operation and enhancing its lifetime. The argon was further purified by flowing it over Ti metal sponge heated to 850°C as a peak temperature. The argon gas line was constructed of 1/4 inch stainless steel tubing with stainless steel Swagelock fittings throughout. The tubing inside the Ti chip furnace was 1/4 inch alumina tubing. This design eliminated the partial pressure of oxygen over steel at this elevated temperature. The purified argon was passed into the oxygen monitoring device.

The oxygen monitoring instrument consisted of an electrochemical oxygen concentration cell utilizing a slip cast high purity calcia stabilized zirconia, $Zr_{0.85}Ca_{0.15}O_{1.85}$, (CSZ) tube (Zircoa Corporation). A general schematic of the cell is shown in Apprendix I. The CSZ was in the form of the 1/4 inch O.D., closed end tube that passed through the center bore of the cell head. The electrical contacts consisted of a layer of porous platinum. These layers were prepared by the application of platinum paste (Englehard Industries) to the electrolyte surface, followed by firing of the electrolyte

to between 800 and 1000 C. Lead wires, also of platinum, were imbedded in the platinum paste before firing. The reference electrode was a gas mixture of CO_2 (25.29% ± .02%), CO (2.45% ± 0.2%) and the balance Ar. This primary standard gas mixture flowed into the cell through a T-joint located above the cell head and exited via a 1/8 inch O.D. alumina tube that extended nearly to the electrode surface, thus requiring the reference gas to flow over the porous platinum. The purified Ar entered the monitor system through a side bore on the cell head. The remaining experimental apparatus and procedures were as discussed in Appendix I.

C. Calculations

The monitoring galvanic cell can be represented schematically as

$$Pt|P(O_2,\text{Ar blanket})\|CSZ\|P(O_2,\ CO\text{-}CO_2)\ \ |Pt \qquad (1)$$

where $P(O_2,CO\text{-}CO_2)$ and $P(O_2,\text{Ar blanket})$ are the oxygen partial pressures in equilibrium with the reference gas mixture and the purified argon gas blanket, respectively. The equilibrium cell emf is related to the difference in oxygen pressure at two electrodes by the expression

$$E = \frac{RT}{4F} \ln \frac{P(O_2,CO+CO_2)}{P(O_2,\ \text{Ar blanket})} \qquad (2)$$

For temperatures in the range of 600 to 1000°C, the oxygen partial pressure must be lower than 10^{-3} atm. In order to remain in the ionic conduction domain for CSZ, the reference oxygen pressure is calculated

from the equilibrium constant for the reaction

$$CO(v) + \frac{1}{2} O_2(v) = CO_2(v) \qquad \text{I}$$

at the operating temperature. The equilibrium constants were obtained from the Gibbs free energy of formation of CO and CO_2 data given by Wicks and Block[2] as listed in Table 1. A linear least squares fit of the above data produced the following equation.

$$\Delta G^{o}(I) = (-67.43 \pm 0.12) + (0.0208 \pm 0.00012)T \text{ kcal}_{th} \text{mol}^{-1} \qquad (3)$$

This results in the partial pressure of oxygen in the reference gas is given by

$$P(O_2, CO\text{-}CO_2) = \left[\frac{P_{CO_2}}{P_{CO}}\right]^2 \exp[2\Delta G^{o}(I)/RT] \qquad (4)$$

The CO_2 to CO partial pressure ratio was determined by Matheson Gas Products to be 10.322 (±.092). Combining Eqs. (1) and (3) one obtains the following expression for the partial pressure of oxygen in the purified Ar stream

$$P(O_2, \text{ Ar blanket}) = (106.54 \pm 1.90)\exp\left[\frac{2\Delta G^{o}(I) - 92.24\ E}{RT}\right]. \qquad (5)$$

In order to prevent carbon from being deposited on the platinum electrodes as a result of the Boudouard equilibrium,[3,4]

TABLE 1

$\frac{T}{K}$	$\frac{-\Delta G^{o}_{f,CO}}{kcal_{th}\ mol^{-1}}$	$\frac{-\Delta G^{o}_{f,CO_2}}{kcal_{th}\ mol^{-1}}$	$\frac{-\Delta G^{o}_{I}}{kcal_{th}\ mol^{-1}}$
800	43.70	94.50	50.8
900	45.85	94.55	48.70
1000	47.95	94.60	46.65
1100	50.10	94.60	44.50
1200	52.15	94.65	42.50

Table 2. Experimental Results for Ti furnace at 860 C.

$\frac{E}{mV}$	$\frac{T}{K}$	$\frac{P_{(O_2,\ Ar\ blanket)}}{atm}$
	Flow Rate: 60 cc/min.	
176.0	668.6	5.4×10^{-39}
180.0	740.8	2.7×10^{-34}
185.9	813.1	1.8×10^{-30}
190.4	872.0	8.3×10^{-28}
194.5	912.0	3.2×10^{-26}
180.0	737.8	1.8×10^{-34}
185.9	816.6	2.7×10^{-30}
199.0	970.5	4.1×10^{-24}
	Flow Rate: 12 cc/min.	
150.1	733.2	6.2×10^{-34}
155.9	826.0	4.3×10^{-29}
159.4	852.5	6.0×10^{-28}
162.1	897.7	4.4×10^{-26}
166.5	953.4	4.8×10^{-24}
172.2	971.5	1.6×10^{-23}
178.9	1020.2	5.0×10^{-22}

$$2CO(v) = C(c) + CO_2(v) \qquad \text{II}$$

the gas flow was not initiated until the cell temperature reached 600 C.

D. Results

Characterization of the purifier's performance was carried out at two different operating temperatures of the Ti chip furnace, 860 and 390 C. At the higher temperature two different argon flow rates were examined as a function of the operating temperature of the monitoring device. Table 2 gives the observed emf's and calculated partial pressures as a function of temperature for the two flow rates. Figures 2 and 3 show how the ℓn(pressure O_2) varies with reciprical temperature for the flow rates of 12 and 60 cc/min., respectively. At the lower flow rate, 12 cc/min. P(O_2, Ar blanket) in atm was found to be

$$\ell n(P(O_2, \text{ Ar blanket})) = (21.24 \pm 0.42) - \left(\frac{71,554 \pm 372}{T}\right) \qquad (5)$$

A linear least squares fit for the higher flow rate, 60 cc/min., produced the following equation

$$\ell n(P(O_2, \text{ Ar blanket})) = (22.03 \pm .13) - \left(\frac{73,599 \pm 102}{T}\right) \qquad (6)$$

When the Ti chip furnace was set a 390°C a cell emf of +2.4 mV was observed with the monitor operating at 716.4°C. This is equivalent

to a calculated oxygen partial pressure of 1.94×10^{-19} atm. Tank argon was also passed into the monitoring system to determine the oxygen content of the source. At an operating temperature of 704 C a cell emf of -712.8 mV was recorded, corresponding to an equivalent oxygen content of 4.61×10^{-5} atm.

E. Discussion

The oxidation of titanium has been extensively investigated.[6-11] The oxidation usually involves simultaneous dissolution of oxygen in the metal and oxide scale formation. Generally the oxide found consisted of only rutile (TiO_2). The actual oxidation mechanism was complicated but approximate rate laws which have been experimentally determined. Up to a temperature of 300°C a logarithmic rate law is observed while a cubic rate law is obeyed in the temperature region 300-600°C. From 600°C to about 850°C a parabolic law has been found experimentally. Around 850°C a gradual shift in the rate occurs from the parabolic to a near linear one. This is probably due to the transformation of titanium from an α to β modification occurring at 882 C and thus changing the oxygen solubility. The effect of oxygen partial pressure on the oxidation rate has not received much attention. In particular no studies have been performed at less then $P_{O_2} = 10^{-5}$ atm (our inlet condition) with most studies being investigated in air. Because of this a theoretical analysis of the optimal Ti chip furnace temperature is not possible.

Operation of the Ti chip furnace at a much higher temperature obviously enhances the oxygen removal rate and the equilibrium P_{O_2}.

If equilibrium conditions are assumed to prevail between Ti and its most stable oxide (TiO_2) the oxygen partial pressures calculated[5] for the two furnace settings are 8.3×10^{-32} atm and 2.6×10^{-60} atm at 860 and 390°C, respectively. Thus at the lower furnace temperature the kinetics of titanium oxidation are obviously rate controlling. At the higher setting the observed partial pressure is in fair agreement with the equilibrium value though somewhat low. This could be explained by a temperature near the exist being somewhat lower than the main body of the purifier--a temperature of about 780°K would be required to match the partial pressures. The fact that the oxygen partial pressure was nearly equivalent for the two flow rates (mean residence times of 1.3 and 6.7 min. at 12 and 60 cc/min, respectively) at the higher temperature indicates the oxidation kinetics are no longer controlling. The experimental results show that the partial pressure was somewhat higher at the larger flow rate. This might be explained by the fact that the higher flow rate flushed the monitoring device more rapidly than at the lower flow rate and thus any foreign oxygen generation either in the purifier or monitor (such as small leaks, side reactions, etc.) could not accumulate as easily.

The monitor temperature was also varied in order to discern the controlling mechanism of oxygen generation. Since a temperature dependence was found, the oxygen content is controlled by some reaction. Equation (5) and (6) indicate that this reaction is probably the same reaction as at the reference electrode--the CO_2-CO-O_2

equilibrium. A possible of source of the carbon oxides is the platinum paste applied to the outside of CSZ tube since organic solvent were used. A gas sample was analysed in a mass spectrometer but the results indicated only Ar.

F. Conclusion

Operation of the Ti chip furnace near 850°C is sufficient for oxidation kinetic limitations to be overcome. The oxygen partial pressures achieved are more than adequate for successful operation of solid electrolyte galvanic cells. The use of an alumina housing produced a partial pressure of oxygen of nearly ten orders of magnitude lower than that obtainable with a stainless steel enclosure.

REFERENCE

1. K. A. Klinedinst, Thermodynamic and Kinetic Investigations of Metal Oxygen Systems Using Solid Oxide Electrolytes (Ph. D. dissertation) Stanford University, May 1972.
2. C. E. Wicks and F. E. Block, Bur. of Mines Bull. 605 (1963).
3. H. Peters and H. H. Möbius, Z. Physik. Chem. 209 298 (1958).
4. A. Borueka, Electrochemica Acta, 13, 295 (1968).
5. O. Kubaschewski and W. A. Dench, J. Inst. Metals 82, 87 (1953).
6. P. Kofstad, K. Hauffe and H. Kjöllesdal, Acta Chem. Scand. 12, 239 (1958).
7. J. Stringer, Acta Met. 8, 758 (1960).
8. L. G. Carpenter and W. N. Mair, J. Inst. Metals 8, 38 (1959-60).
9. P. Kofstad, J. Less-Common Metals, 12, 449 (1967),
10. C. J. Rosa, Met. Trans. 1, 2517 (1970).
11. D. Simon, B. Devillers and J. Bardolle, C. R. Acad. Sc. Paris, Ser. C 279, 99 (1974).

LIST OF FIGURES

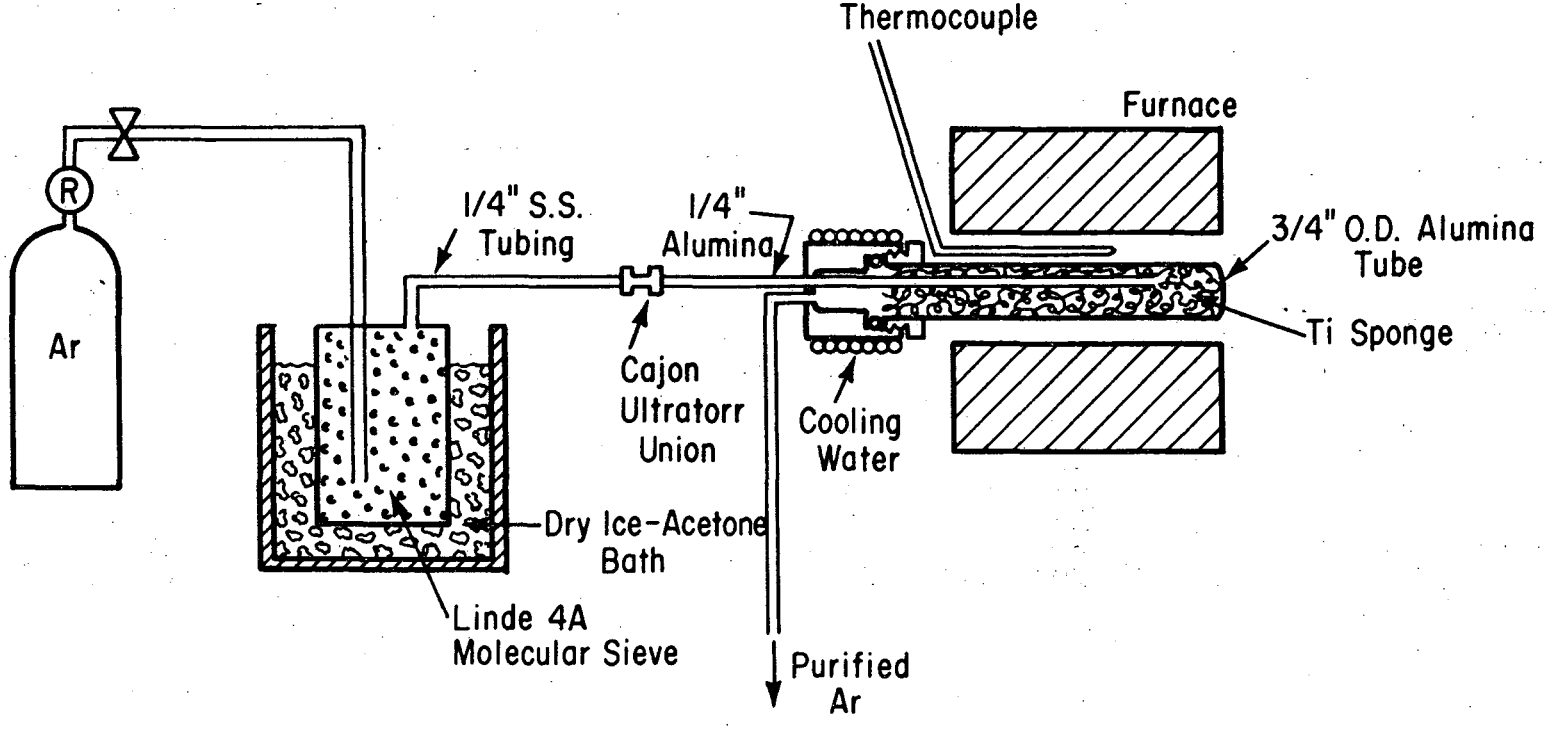

Fig. 1.

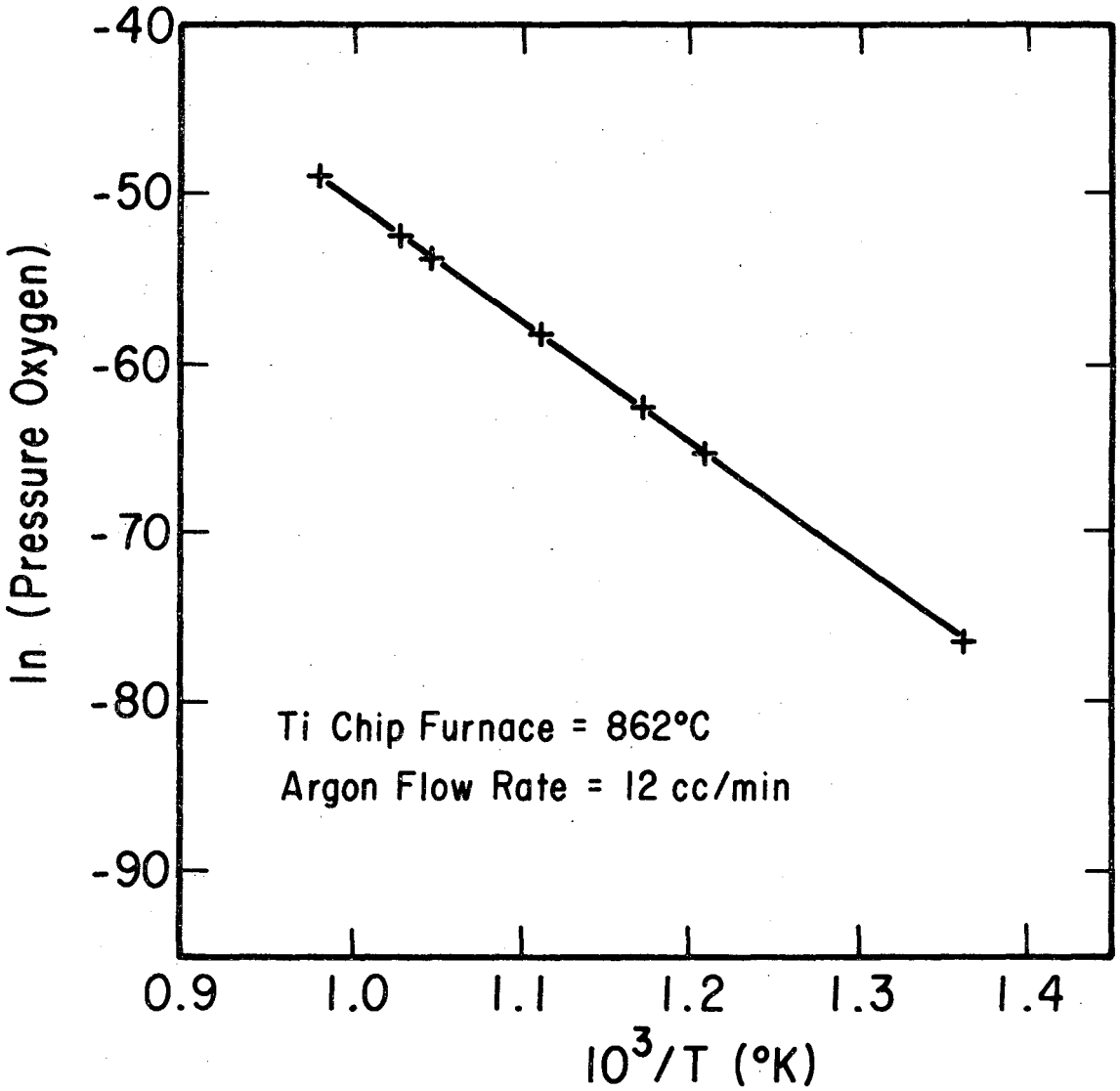

XBL 757-6779

Fig. 2.

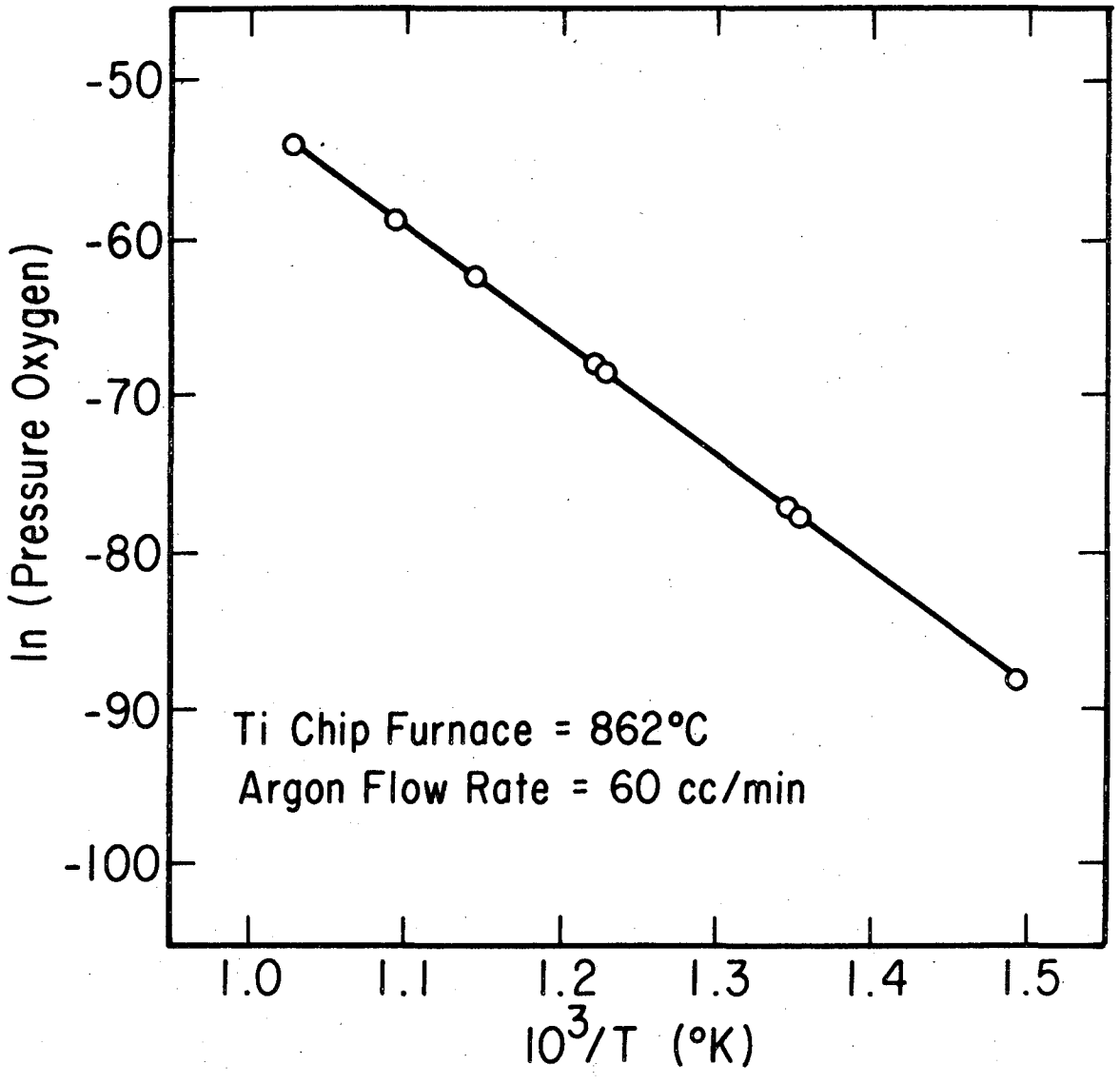

XBL 757-6778

Fig. 3.

TECHNICAL INFORMATION DIVISION
LAWRENCE BERKELEY LABORATORY
UNIVERSITY OF CALIFORNIA
BERKELEY, CALIFORNIA 94720